JAERI-Research
95-017

BULK SHIELDING EXPERIMENT ON A LARGE SS316/WATER ASSEMBLY BOMBARDED BY D-T NEUTRONS

VOLUME I : EXPERIMENT

March 1995

Chikara KONNO, Fujio MAEKAWA, Yukio OYAMA, Yujiro IKEDA
Yoshitomo UNO, Yuriy VERZILOV*, Masayuki WADA and Hiroshi MAEKAWA

日本原子力研究所
Japan Atomic Energy Research Institute

本レポートは，日本原子力研究所が不定期に公刊している研究報告書です。

入手の問合わせは，日本原子力研究所技術情報部情報資料課（〒319-11 茨城県那珂郡東海村）あて，お申し越しください。なお，このほかに財団法人原子力弘済会資料センター（〒319-11 茨城県那珂郡東海村日本原子力研究所内）で複写による実費頒布をおこなっております。

This report is issued irregularly.

Inquiries about availability of the reports should be addressed to Information Division, Department of Technical Information, Japan Atomic Energy Research Institute, Tokai-mura, Naka-gun, Ibaraki-ken 319-11, Japan.

編集兼発行　日本原子力研究所

印　　刷　㈱原子力資料サービス

Bulk Shielding Experiment on a Large SS316/Water Assembly Bombarded by D-T Neutrons Volume I: Experiment

Chikara KONNO, Fujio MAEKAWA, Yukio OYAMA, Yujiro IKEDA
Yoshitomo UNO, Yuriy VERZILOV * , Masayuki WADA and Hiroshi MAEKAWA

Department of Reactor Engineering
Tokai Research Establishment
Japan Atomic Energy Research Institute
Tokai-mura, Naka-gun, Ibaraki-ken

(Received February 8, 1995)

It is under consideration in the ITER/EDA that water will be flowed through stainless steel in the shielding blanket and vacuum vessel as coolant. A bulk shielding experiment on a large SS316/water assembly was performed by using the FNS D-T neutron source in Japan Atomic Energy Research Institute as the '94 ITER/EDA task(T-16). The objectives of this experiment are to obtain experimental data for the shielding performance of SS316/water shield, to verify the shielding design system of ITER and to deduce the shielding design margin finally. The experimental system, measuring procedures and the measured data are described in this report and the analysis of the experiment is given separately in the Volume II. The test region of the experimental assembly is a layered structure of SS316 and water(volume ratio is 4:1), which had a cylindrical shape of 1200 mm in diameter and 1372 mm in thickness. This test region was set at 300 mm from the D-T neutron source which was surrounded by a source reflector made of 200 mm-thick SS316. The data for i) neutron spectra in energy regions of MeV, keV and eV, ii) neutron activation reaction rates, iii)

This report was submitted to the Joint Central Team (JCT) of ITER.

* Research Fellow

fission rates, iv) gamma-ray spectra and v) gamma-ray heating rates were measured from the front surface to the depth of 914 mm in the test region. The experimental data which included few room-returned background were obtained even at the depth of 914 mm by adding water tanks or polyethylene blocks of about 160 mm in thickness around the rear part of the test region. The effect of water in SS316 on the shielding performance was examined from the comparison with the measured data of the previous SS316 bulk shielding experiments. It was found that SS316/water shield has shielding performance better by about 2 orders of magnitude than pure SS316 for neutrons less than 1 MeV and gamma-rays at the depth of 914mm.

Keyword: SS316/Water, Benchmark Experiment, Bulk Shielding, D-T Neutron,
ITER/EDA, Source Reflector, Neutron Spectrum,
Neutron Activation Reaction Rate, Fission Rate, Gamma-ray Spectrum,
Gamma-ray Heating Rate

Ｄ－Ｔ中性子による大型ＳＳ316/水体系におけるバルク遮蔽実験
第１部：実　験

日本原子力研究所東海究所原子炉工学部
今野　　力・前川　藤夫・大山　幸夫・池田裕二郎
宇野　喜智・Yuriy VERZILOV* ・和田　政行・前川　　洋

（1995年２月８日受理）

ＩＴＥＲ／ＥＤＡでは遮蔽ブランケットや真空容器内のステンレス中に冷却材として水を流すことが検討されている。'94 ＩＴＥＲ／ＥＤＡのタスク（Ｔ－16）として，大型ＳＳ３１６／水体系に対するバルク遮蔽実験を日本原子力研究所ＦＮＳのＤ－Ｔ中性子源を使用して行った。この実験の目的は，Ｄ－Ｔ中性子に対するＳＳ３１６／水遮蔽体の遮蔽性能に関する実験データを取得し，ＩＴＥＲの遮蔽設計計算システムを検証し，最終的に遮蔽設計裕度を導出することである。実験システム，測定手法及び実験結果をこのレポートで述べ，実験解析は，別に第２部で述べられている。実験体系のテスト領域は，ＳＳ３１６と水の層状構造（体積比４：１）で，直径1200mm，厚さ1372mmの円筒形状をしている。このテスト領域を厚さ200mm のＳＳ３１６でできた中性子反射体で囲まれたＤ－Ｔ中性子源から 300mmの位置に設置した。ｉ）MeV，keV，eVエネルギー領域の中性子スペクトル，ii）中性子放射化反応率，iii）核分裂率，iv）γ線スペクトル，v）γ線発熱率のデータを体系表面から体系内 914mmの深さまで測定した。約 160mmの厚さの水タンクあるいはポリエチレンブロックをテスト領域後部の周りに付け加えることにより，914mmの深さでも壁反射バックグラウンドの影響の小さい実験データを取得することができた。以前に行ったＳＳ３１６バルク遮蔽実験結果との比較から，ＳＳ３１６中の水の遮蔽性能に及ぼす効果について調べ，１MeV 以下の中性子とγ線に対して，深さ 914mmでＳＳ３１６／水はＳＳ３１６よりも２桁程度遮蔽性能が優れていることがわかった。

このレポートはITER/JCTに提出したものである。

東海研究所：〒319-11　茨城県那珂郡東海村白方字白根２－４

＊ リサーチフェロー

Contents

目　　次

List of Tables

List of Figures

1. Introduction

The major requirement for the shield of International Thermonuclear Experimental Reactor (ITER) is to reduce nuclear heating in super conducting magnet (SCM), displacement damage of copper stabilizer in SCM, fast neutron flux ($\geq$ 0.1 MeV) to Nb_3Sn super conductor, dose to electrical insulator, helium production in type 316 stainless steel (SS316) at shield/blanket region, and so on to less than the design limits[1]. Since the results of shielding design calculations include various uncertainties due to nuclear data, calculation codes, modeling, etc., they should be compared with the design limits by considering valid design margins. Larger design margins make the shielding design safer, but there is little space for thicker shield particularly in the inboard region. The construction cost for ITER will increase, even if there is no space limit. The objectives of fusion reactor shielding experiments are to obtain the appropriate experimental data related to the critical quantities such as helium production in the shield of ITER and to validate the calculation codes and nuclear data which will be used in the shielding design of ITER. The design margins as precise as possible will be deduced through various experimental analyses finally.

According to the recent design of ITER[2-4], two blanket options are proposed. One is a shielding/blanket reference design without tritium breeding, where a structural material is SS316 and a coolant is water. The other is a breeding blanket with an advanced blanket concept, where the blanket canisters are made of vanadium alloy (V5Cr5Ti) and natural liquid lithium is used as both coolant and tritium breeder. The shielding/blanket reference design will be probably adopted in the first phase (Basic Performance Phase) of ITER, while the advanced blanket concept will be used in the second phase (Extended Performance Phase) of ITER in order to supply a major part of the tritium required for ITER operation. The vacuum vessel of ITER has a double wall structure, the material candidates of which are Inconel 625 or SS316. The inside of its double walls will be filled with stainless steel balls for neutron shield and cooling water will be flowed through space among the stainless steel balls. As a result, the configuration of stainless steel and water is one of the most promising candidates used in the blanket and vacuum vessel of ITER. Therefore experimental data related to shielding performance of SS316/water configuration for D-T neutrons is urgently required for the shielding design of ITER.

A series of fusion reactor shielding experiments using the intense D-T neutron source FNS (Fusion Neutronics Source)[5] in Japan Atomic Energy Research Institute is in progress under ITER/EDA (Engineering Design Activities) R&D program. Bulk shielding experiments[6,7] on SS316 have been already performed in order to investigate the bulk shielding performance of SS316 for D-T neutrons. As the second shielding experiment, a bulk shielding experiment on SS316/water was performed under the '94 ITER/EDA R&D task (T-16 :

"Preparation of neutronic experiments and measuring technique"). The experimental assembly was designed based on the pre-analysis[8] and consisted of the test region and the source reflector. The test region had a cylindrical shape of 1200 mm in diameter and 1219 mm in thickness, which has a layered structure of SS316 and water. It is noticeable that not a water simulating material but water is used. Measurements were carried out from the front surface of the test region up to the depth of 914 mm, which was comparable to the thickness of the inboard shield/blanket and vacuum vessel on the midplane of ITER.

As described in the first paragraph, the critical quantities in the shield design of ITER are nuclear heating in SCM, displacement damage of copper stabilizer in SCM, fast neutron flux ($\geq$ 0.1 MeV) to Nb_3Sn super conductor, dose to electrical insulator, helium production from SS316 in shield/blanket, and so on. The main source of nuclear heating in SCM is gamma-rays produced by (n,γ) reactions with low energy neutrons. Neutrons in MeV region contribute to the most parts of displacement damage of copper stabilizer in SCM, fast neutron flux ($\geq$ 0.1 MeV) to Nb_3Sn super conductor and helium production in SS316 at shield/blanket. Dose rate in the electrical insulator is formed by both gamma-rays produced by (n,γ) reactions with low energy neutrons and neutrons above 1 MeV. Since neutron and gamma-ray fluxes over the whole energy are required in order to estimate the critical quantities, neutron and gamma-ray energy spectra were measured over the almost whole energy in this experiment. Neutron activation reaction rates and fission rates, which have sensitivity for neutrons of various energies, were also measured as the complemental data of the neutron spectrum. Moreover, the measurement of gamma-ray heating rate was carried out since gamma-ray heating rate has direct relation to nuclear heating in SCM.

This report focuses on the experimental procedures and the measured data of the bulk shielding experiment on SS316/water. The experimental arrangement is given in Chapter 2. Chapter 3 describes the measuring procedures and measured data. The experimental arrangement and measuring procedures are described briefly since they are similar to the previous ones[7]. The comparison between the previous SS316 and current SS316/water experiments is performed in Chapter 4 to examine the effect on the shielding performance of water in SS316. The detailed analyses of the experiments are given in the report of Volume II[9].

2. Experimental Arrangement

2.1 Neutron Source

The experiments were performed in the first target room of the Fusion Neutronics Source (FNS) facility[5] in Japan Atomic Energy Research Institute. The water cooled tritium-titanium target (about 3.7 x 10^{11} Bq) on copper backing was located at the point of 5.5 m from the nearest concrete walls (west and south) and 1.8 m high from the grating floor as shown in Fig. 2.1.1. A deuteron ion beam accelerated by 350 keV was bombarded to the tritium target to generate D-T neutrons. The maximum beam current was 2 mA, where the neutron yield was about 3 x 10^{11} n/sec. Short- and long-pulsed deuteron beams of about 1 μs and about 1 ms widths were also produced for neutron spectrum measurement in energy range of eV and the gamma-ray spectrum measurement, respectively. The total number of neutrons produced by D-T reaction was absolutely determined within ± 2 % by using the associated alpha-particle counting technique[10]. It was estimated[9, 11] to be smaller by about 3 % than that of neutrons emitted from the target, which also included neutrons generated by (n,2n) reactions in the materials of the target assembly. A long counter and a ^{232}Th fission counter were placed at the basement and under the beam drift tube, respectively, as the secondary neutron monitors. The neutron source spectrum emitted from the target is described in Ref. 11. It is notable that all the measured data in this report are normalized to one neutron produced by D-T reaction at the target, not one neutron emitted from the target.

2.2 Experimental Assembly

The experimental assembly was designed based on the pre-analysis[8] and consisted of the test region and source reflector as shown in Fig. 2.2.1. It was similar to the assembly #2 of the previous bulk shielding experiments on SS316[7]. The test region had a cylindrical shape of 1200 mm in diameter and 1372 mm in thickness, which was assembled by sandwiching several SS316 disks and water tank disks of 1200 mm in diameter. The thickness of the SS316 disk was 50.8 or 101.6 mm. The water tank disk was 50.8 mm in thickness and was made of 12 mm thick SS316. The space of 26.8 mm in thickness of the water tank was filled with demineralized pure water. The total volume ratio of water to SS316 was adjusted to be 1 : 4 in the region of 940 mm in thickness of the test region, which is proposed in the recent design[2-4] of ITER. The local volume ratio of water to SS316 decreased with the depth, which simulates the ITER shielding design. All the SS316 disks and water tanks were supported on the frame structure by two brims. Some disks of SS316 also had an experimental hole of 50 mm ϕ or 36 mm ϕ x 727 mm from the circumference to the center of the disk. The

structures of the SS316 disk with an experimental hole and water tank disk are shown in Fig. 2.2.2. Figure 2.2.3 is a photograph of the water tank disk, the appearance of which is very similar to the SS316 disk. The test region was located at 300 mm from the D-T neutron source as shown in Fig. 2.2.1. A source reflector of 200 mm thick SS316 was added to the test region in order to adjust neutron energy spectrum incident to the test region to that of a fusion reactor. This experimental assembly is formed to easily model in two-dimensional transport codes such as DOT 3.5[12], which are often used in the shielding design of ITER. The tritium target assembly was inserted into the cavity of the source reflector through a hole of 80 mm x 160 mm. The atomic number densities in the test region and source reflector are listed in Table 2.2.1. The experimental holes were located in the SS316 region of the depths of 127, 229, 330, 457, 610, 762 and 914 mm from the front surface of the test region as shown in Fig. 2.2.1. Detectors were inserted to the experimental holes using SS316 detector adapters. Figure 2.2.4 shows the photograph of detector adapters for neutron activation foils and thermoluminescence dosimeters. On the front surface of the test region, detectors were inserted through a hole of 22.5 mm x 22.5 mm made in the side wall of the source reflector. Experimental holes were filled with SS316 rods when the holes were not used. This experimental assembly was mounted on a supporting frame on two movable decks as shown in Fig. 2.2.5. One deck was 3440 mm x 1500 mm for the test region, the other was 3440 mm x 850 mm for the source reflector.

2.3 Additional Shield

Although the measurements were performed using this assembly at first, it was found from the comparison between the measurement and calculation that measured neutron data below 1 MeV and gamma-ray data in the test region deeper than 700 mm were affected by room-returned neutrons. As is described in Chapter 4, SS316/water combination has shielding performance for neutrons below 1 MeV better by 2 orders of magnitude than SS316 at the depth of 914 mm. Therefore it was considered that the foreground data of the current experiment became much smaller and that the influence of room returned background became relatively larger as a result.

The pre-analysis[8] was performed to determine an additional shield which reduced room-returned neutrons as much as possible. According to the pre-analysis, it is necessary to cover the test region with 150 mm thick polyethylene as shown in Fig. 2.2.6. Due to space restriction between the experimental assembly and supporting frame, polyethylene blocks or water tanks were added in complicated shape as shown in Fig. 2.2.7. Figure 2.2.8 is a photograph of the experimental assembly with additional shield, supporting frame and movable deck. The water tanks were made of 3 or 5 mm thick type 304 stainless steel and filled with

water. The effective thickness of water in the water tanks or the polyethylene blocks was about 150 mm. The thickness of the test region was shortened to 1219 mm in order to add a 160 mm thick water tank disk in the back of the test region. As examined in Appendix 1, this additional shield decreased the contribution of room-returned neutrons to less than 10 % of the foreground data even in the depth of 914 mm. The result in Appendix 2 suggests that the additional shield affects measured data for neutron and gamma-ray by only a few % along the central axis from the front surface of the test region to the depth of 914 mm. Therefore, only the data of the depths of 762 and 914 mm were measured again using the experimental assembly with the additional shield. On the other hand, the data measured using the experimental assembly without the additional shield were adopted for the region shallower than 700 mm. It is not necessary to consider the additional shield in the analysis of this experiment. It should be noted that the measured data related neutrons below 1 MeV and gamma-rays might include background less than 10 % at the depth of 914 mm.

3. Measurements and Results

Since the measuring procedures were almost the same as those applied to the previous SS316 experiments[7] and were described in detail in Ref. 7, they are given briefly here.

3.1 Neutron Spectrum

3.1.1 Neutron Spectrum in Energy Region of MeV

Neutron spectra above 2 MeV were measured by a 14 mm-diameter spherical NE213 liquid scintillator[13]. The measurements were carried out at the front surface of the SS316/water test region and at the depths of 127, 229, 330, 457, 610, 762 and 914 mm from the SS316/water test region front surface. The measuring time for each experimental run was 2000 seconds. The deuteron beam current was adjusted for the counting rate not to exceed 2000 cps because of dead time loss. Events of neutron were discriminated from those of gamma-rays by using the difference of rise time. A gain-stabilizer was applied for a stable measurement. The schematic diagram for the electronic circuit is shown in Fig. 3.1.1.1. Selected recoil proton spectrum was unfolded to neutron spectrum by the FORIST code[14] using the neutron response matrix previously determined.[15] The overall error was estimated to be ± 4 % for the neutron flux in the energy range above 10 MeV.

The measured neutron spectra are shown in Figs. 3.1.1.2 - 3.1.1.9, together with those measured by the proton recoil gas proportional counter and the slowing down time method which are to be described in Secs. 3.1.2 and 3.1.3. Table 3.1.1.1 summarizes the numerical data of the measured spectra with window functions which represent the energy resolution provided by the FORIST code. Since the measured neutron fluxes around 5 - 10 MeV tend to be deduced to be smaller in the case that 14 MeV neutrons are dominant as described in Ref. 7, the measured neutron flux from 5 to 10 MeV on the front surface might be estimated to be smaller. Strange oscillations appear below 10 MeV at the positions deeper than 457 mm. This is probably due to the incompleteness of neutron and gamma-ray discrimination. The errors in Table 3.1.1.1 do not include these effects. It is notable that the neutron spectra below 10 MeV on the front surface and at the positions deeper than 457 mm should be treated as tentative data.

3.1.2 Neutron Spectrum in Energy Region of keV

Neutron spectra in the energy range from a few keV to 1 MeV were measured by two types of small proton recoil gas proportional counters [16] (PRC), which were filled with hydrogen gas at 0.496 MPa (5.06 kgf/cm^2) with 1 percent methane and 50-50 mixture of hydrogen and argon gases at 0.610 MPa (6.22 kgf/cm^2), respectively. The both counter heads of PRC had a cylindrical shape, the outer diameter and effective length of which were 19 mm and 127 mm, respectively. These counters with the pre-amplifier were inserted into a hole of 21 mm x 21 mm one by one.

A continuous mode data acquisition technique[17] ,where supplied high voltage was constantly varied with a ramp shape during acquisition, was adopted to reduce time of measurement and data process. The block diagram of the data acquisition system is shown in Fig. 3.1.2.1. Output signals of the pre-amplifier were fed in parallel to an integrating amplifier (Y-amplifier) and a differentiating amplifier (X-amplifier). Since output of Y-amplifier was proportional to input pulse height and that of X-amplifier was proportional to the input pulse height and the reciprocal of the rise time of input pulse, the information of the rise time of the output of the pre-amplifier was obtained from the ratio of the outputs of X- and Y-amplifier. Supplied high voltage was monitored by a dividing resistance, which scaled down high voltage by about 1/500. The outputs of Y-, X-amplifier and the dividing resistor were digitized by one analog-to-digital converter using a multiplexer and logical circuits. The relative energy (in log-scale) of recoil proton was calculated on-line from the output of Y-amplifier and gas multiplication data which were reduced from the high voltage data. The X/Y ratio and the energy (in log-scale) were stored to a two-dimensional array (32 channels x 512 channels) during the measurement. In off-line data processing, neutron spectra were derived by differentiating the recoil proton energy spectra which were selected by using the rise time information.

The measurement was performed on the front surface of the SS316/water test region and at the depths of 127, 229, 330, 457, 610, 762 and 914 mm from the front surface of the SS316/water test region. The measured neutron spectra are shown in Figs. 3.1.1.2 - 3.1.1.9 together with those measured by the NE213 detector (see Sec. 3.1.1) and the slowing down time method to be described in Sec 3.1.3. The numerical data of the measured spectra are given in Table 3.1.2.1. The total experimental error for neutrons above 50 keV was estimated to be about 15 %.

3.1.3 Neutron Spectrum in Energy Region of eV

Slowing Down Time Method

The slowing down time method [18 - 20] was applied to measure neutron spectra in the energy region of eV. In principle the measuring method was the same as that adopted in the previous experiment.[7] Situations of the present measurement were, however, much different from the previous one in terms of the energy resolution.

Energy resolution of neutron spectrum measured with the slowing down time method is roughly calculated as the following formula.

$$FWHM(\%) = 235.5\sqrt{\frac{8}{3A}}, \qquad A: Mass\ number \qquad (3.1.3.1)$$

In the case of the previous experiment for the SS316 assemblies, the energy resolution is about 51 % since the mass number of SS316 is large (about 56). The energy resolution of the present measurement is expected to be much worse due to hydrogen atoms in the water layers (its mass number is one). Figure 3.1.3.1 shows the energy resolution of the spectra estimated with a Monte Carlo transport calculation with MCNP[21]. It is seen from the figure that the energy resolution is about 200 % in FWHM at the detector positions except 914 mm and much worse than the previous one of 50 - 60 %. Since the 914 mm position is far from the water layers, the resolution is better than that at the other detector positions. Due to the worse energy resolution, as to be described later, a difficulty appeared in the energy calibration, and larger uncertainty accompanied with the correction factors was included in the measured spectra.

Measurement

A BF_3 gas proportional counter, 14 mm in diameter, 99 mm in effective length and 0.39 MPa (900 mmHg) in pressure, was inserted in one of the detector holes of the assembly. Pulsed D-T neutrons were injected into the experimental assembly and time-dependent $^{10}B(n,\alpha)$ reaction rates were measured by the counter at the seven positions from 127 mm to 914 mm in depth. The repetition rate and the peak current of the deuteron pulses were 500 μs and 1 mA, respectively. The pulse widths were 1.0 μs for the 127, 229, 330, 457 and 610 mm positions and 1.7 μs for the 762 and 914 mm positions. Electronic circuit used in the measurement is shown in Fig. 3.1.3.2. Because of insufficient number of reaction events counted at the 914 mm position, the spectrum could not be obtained.

Energy Calibration

The resonance filter technique was applied for the energy calibration as similar to the

previous experiment[7] for the SS316 assemblies. The resonance filters used are listed in Table 3.1.3.1. Dips of the time spectrum of reaction rates measured with the resonance filters were apparently observed in the previous experiment. The dips, however, could not be clearly observed in the present experiment in spite of use of the thicker resonance filters. The reason was that the energy resolution of the spectrum in the present experiment was much worse than that in the previous one and the dips were spread into broader time ranges. Thus the energy calibration could be performed only with the gold filter, resonance energy of which was 4.9 eV. The experimentally obtained slowing down time for the gold filter is presented in Table 3.1.3.2 with estimated values by the MCNP calculation. The slowing down time could not be experimentally determined at the 762 mm and 914 mm positions because of lack of enough event counts. There are several groups of the slowing down time depending on the distances from the measurement position to the nearest water layer; 8.3 μs at the 127, 229 and 330 mm, 12.5 μs at the 457 and 610 mm and 14.8 μs at the 762 mm position according to the calculation. At the first three positions where the slowing down time was about 8.3 μs, since discrepancies between the calculated and the measured slowing down time are around 5 %, the error of 5 % was taken for these positions as a calibration error at 4.9 eV. Because the discrepancies are 6 and 10 % at the next two positions where the slowing down time is about 12.5 μs, and no experimental value is given for the 762 mm position, calibration errors of 10 % at 4.9 eV were assumed for the 457, 610 and 762 mm positions.

Data Processing

Procedures of the data processing are similar to those of the previous measurement except a procedure for thermal fluxes. The treatment for thermal flux is mentioned in the later section. The calibration curves were calculated by MCNP and were adjusted to reproduce the measured slowing time. The calibration curves, that is, relations between neutron mean energy $\bar{E}$ and slowing down time t, were used to convert the measured time-dependent reaction rates, $C(t)$, into energy-dependent reaction rates, $C(\bar{E})$. Neutron energy spectra $\phi(\bar{E})$ were derived by the formula, given by,

$$\phi(\bar{E}) = \frac{C(\bar{E})}{\sigma(\bar{E}) \cdot N \cdot Yn \cdot f_{ss}(\bar{E}) \cdot f_{\sigma}(\bar{E})} \quad , \qquad (3.1.3.2)$$

where,

$\phi(\bar{E})$: Energy spectrum [n / MeV / Source Neutron],

$C(\bar{E})$: Counts / MeV,

$\sigma(\bar{E})$: Cross section of the $^{10}B(n,\alpha)$ reaction taken from JENDL-3.1,

N: Number of effective B-10 atoms in the BF_3 counter.

Yn: Neutron yield,

$f_{ss}(\overline{E})$: Self-shielding correction factor of the counter,

$f_{\sigma}(\overline{E})$: Correction factor for the effective $^{10}B(n,\alpha)$ reaction cross section.

The uncertainties in the calibration curves used for the conversion are 5 or 10 % at 4.9 eV depending on the measurement positions. These uncertainties have a relation with magnitude of the measured spectra, and they are considered in the error estimation. Since the energy calibration can not be performed in an energy range higher than 4.9 eV, larger errors are assigned to the higher energy part of the measured spectra.

Magnitudes of the correction factor for the effective $^{10}B(n,\alpha)$ reaction cross section, $f_{\sigma}(\overline{E})$, depend on the energy resolution of the spectra. The factors range approximately between 1.3 and 1.5 for an energy range of 0.3 eV and 300 eV. The self-shielding correction for the counter is not so large since the minimum value of the factors, $f_{ss}(\overline{E})$, is 0.932 for thermal neutrons.

Estimation of Thermal Neutron Flux

Since neutrons can not slow down below thermal energy and then the mean energy of neutrons does not have the one to one correspondence to the slowing down time for the thermal energy, the slowing down time method can not be directly applied to measure neutron spectra in the thermal energy region. The $^{10}B(n,\alpha)$ reaction events observed after the time when mean neutron energy decreased to the upper limit of thermal energy, about 0.4 eV, are considered as ones caused by thermal neutrons. Hence neutron spectra in thermal energy region, typically having the Maxwell's distribution, can not be measured but total fluxes in the thermal energy, ϕ_{th}, can be deduced by the formula, given as,

$$\phi_{th} = \frac{C}{\sigma_{B-10}^{eff} \cdot N \cdot Yn \cdot f_{SS}^{th}}, \qquad (3.1.3.3)$$

where,

C: Counts after mean neutron energy reached to 0.322 eV,

σ_{B-10}^{eff}: Effective cross section of the $^{10}B(n,\alpha)$ reaction below 0.322 eV,

N: Number of effective B-10 atoms in the BF_3 counter,

Yn: Neutron yield,

f_{SS}^{th}: Self-shielding correction factor of the counter at the thermal energy.

In the present measurement, the upper energy of thermal energy region is determined to 0.322 eV, which is the upper energy limit of the 125 energy group structure used in the analyses[11] of the previous bulk shielding experiments. Slowing down time corresponding to the mean neutron energy of 0.322 eV is derived according to the MCNP calculation; 29.3 μs for the 127, 229 and 330 mm positions, 47 μs for the 457 and 610 mm positions and 52 μs

for the 762 mm positions.

Since the measurement positions are not inside the water layers but in the SS316 layers, energy distribution of the thermal fluxes at the measurement positions is much harder than the Maxwell's distribution at the room temperature. Hence the $^{10}B(n,\alpha)$ reaction cross section at the thermal energy, 3837 b, is not valid to estimate the fluxes, and we introduced an effective cross section. The effective cross sections, σ_{B-10}^{eff}, are deduced from the MCNP calculation. They are approximately 2400 b and 2200 b for the 127, 229 and 330 mm positions and the 457, 610 and 762 mm positions, respectively.

Energy Resolution

The measured spectra by the slowing down time method have the inherent energy resolution. Since it is impossible to determine experimentally the inherent resolutions, they are calculated with the MCNP code as previously shown in Fig. 3.1.3.1.

The time resolution in the measurement is another cause to broaden the energy resolution in addition to the inherent resolution. There are three main components in the time resolution; (i) fluctuation of timing signal from the BF_3 counter; 0.13 μs, (ii) neutron pulse width; 1.0 μs or 1.7 μs, and (iii) time width per channel of the multichannel analyzer; 0.476 μs. The time resolutions are converted to energy resolutions by multiplying $d\bar{E}/dt$ which was derivative of neutron mean energy $\bar{E}$ by time t.

Overall energy resolution is given as the sum of all the energy resolution. The energy resolution due to the time resolution is negligibly small comparing with the inherent energy resolution in the present experiment. The estimated overall energy resolutions are given in Table 3.1.3.3.

Error Estimation

Errors of the measured spectra are estimated as follows.

1.	Statistical error of counts	> 2 %
2.	Neutron yield	2 %
3.	Number of effective ^{10}B atoms	3 %
4.	Self shielding correction factor	negligible
5.	Correction factor for neutron energy broadening	3 ~ 5 %
6.	Error coming from energy calibration	> 5 %

The overall errors are 6 - 15 %, 14 - 36 % and 38 - 60 % for energy ranges of 1 - 10 eV, 10 - 100 eV and 100 - 300 eV, respectively. The errors for the thermal fluxes are about 11 %.

Results

The measured neutron spectra are presented in Table 3.1.3.3 and Figs. 3.1.1.2 - 3.1.1.9 with those measured by the NE213 and the PRC described in Secs. 3.1.1 and 3.1.2. The spectra are given in the unit of [n / lethargy / source neutron]. The lethargy width of the spectra except the thermal fluxes are 0.5756 as there are four measurement points in each decade. The energy range for the thermal fluxes is assumed to be as from 1.001×10^{-5} eV to 0.322 eV, thus, its lethargy width is 10.38. This lethargy width is necessary when one calculates total thermal fluxes.

3.2 Neutron Spectrum Index

3.2.1 Neutron Activation Reaction Rate

The reactions of $^{27}Al(n,\alpha)^{24}Na$, $^{32}S(n,p)^{32}P$, $^{93}Nb(n,2n)^{92m}Nb$, $^{115}In(n,n')^{115m}In$ and $^{197}Au(n,\gamma)^{198}Au$ reactions were selected as neutron activation dosimeters. Reaction rates for these reactions except the $^{32}S(n,p)^{32}P$ reaction were measured by counting γ-rays with Ge detectors. Reaction rate for the $^{32}S(n,p)^{32}P$ reaction was measured by counting β-rays with a Cherenkov radiation detector. Table 3.2.1.1 shows the data associated with the dosimetry reactions measured here. Figures 3.2.1.1 and 3.2.1.2 show cross sections of the dosimetry reactions, which are taken from JENDL Dosimetry File[22].

Measurement of Reaction Rates for γ-Activation

Neutron irradiation was performed twice. At the first time, natural metal foils of aluminum, niobium, indium and gold were placed on the front surface of the SS316/water test region and at the depths of 127, 229, 330 and 457 mm from the front surface of the SS316/water test region. The additional shield was not attached to the test region. The irradiation time was 9 hours and 19 minutes, and the total neutron yield was 6.07×10^{15}. At the second irradiation, the additional shield was added to the test region in order to measure reaction rates at the deeper positions of 610, 762 and 914 mm. The natural metal foils of fairly large size were irradiated for 10 hours with D-T neutrons and total neutron yield at the target was 8.71×10^{15}. The size of foils is given in Table 3.2.1.2. The neutron yield fluctuation was monitored every 10 seconds by using the multi-channel scaling (MCS) for the decay correction during irradiation.

After irradiation and appropriate cooling, γ-rays emitted from foils were measured with four germanium detectors. Reaction rate was derived from the γ-ray counts with necessary corrections. The decay data for the half-life and γ-ray branching ratio were taken from Ref. 23). The efficiency of Ge detectors for small foils was calibrated by a set of standard gamma-ray sources. The efficiency calibration of Ge detectors for large foils were performed as following. One large foil sandwiched by two small foils of the same metal of 10 mm ϕ x 1 mm (10 mm x 10 mm x 1 mm for In) was irradiated separately by D-T neutron. The reaction-rates of the small foils were determined absolutely by using the calibrated Ge detector. Gamma-rays from the large foil were measured by the same Ge detector and geometry that were adopted for large foils irradiated inside the SS316/water assembly. The efficiency of the Ge detector for the large foil was determined based on the fact that the reaction rate of the large foil is equal to the average of the two reaction rates of the small foils. The effect of self-shielding of the gamma-ray in the large foil and the influence of the

size of the large foil were corrected automatically in this method. The data up to the depth of 914 mm were obtained. The overall error for the most measured reaction rates ranged from 3 to 6 %. The measured activation reaction rates are shown in Fig. 3.2.1.3 with the reaction rate of $^{32}S(n,p)^{32}P$ reaction described in next sub-section and the fission rates described in Sec. 3.2.2. Table 3.2.1.3 summarizes the numerical data of the measured activation reaction rates.

Measurement of Reaction Rates for β-Activation

The samples were prepared by wrapping powder of dimethyl sulfone, $CH_3SO_2CH_3$, 99.9% purity, in the polyethylene packages made of 0.05 mm-thick film. Characteristics of the powder are given in Table 3.2.1.4. The quantity of the powder ranged from 0.3 to 30 grams depending on the position in the assembly. The dimensions of the samples and their position are given in Table 3.2.1.5. Special care was paid to the phosphorus content in the powder because two different reactions $^{32}S(n,p)^{32}P$ and $^{31}P(n,\gamma)^{32}P$ produce the same nuclide ^{32}P of interest. In order to estimate activities from ^{31}P impurities, the measurement of ^{32}P activity for samples with and without Cd cover was made and no difference between the two samples was observed. Thus it was concluded that there was no interference due to phosphorus contamination.

The samples were placed at several positions in the test region along the central axis of the assembly with the additional shield and irradiated for ten hours. The total D-T neutron yield at the target was 6.1×10^{15}. The irradiation history was recorded by using MCS for the decay correction during the irradiation.

After the irradiation, the ^{32}P activity was measured by using a Cherenkov radiation detector. The detector utilizes the principle of direct Cherenkov radiation counting of energetic β-rays in an aqueous medium. Cherenkov radiation is produced as a bluish light when β-particles of energy greater than 260 keV travel through a medium such as water. The maximal energy in the β-ray spectra of ^{32}P is 1.71 MeV. As no scintillator is required and chemical quenching is absent, sample preparation is extremely simple and the technique is ideal for the assay of ^{32}P in aqueous solution. Since Cherenkov radiation is formed by only a small proportion of the total energy losses, a liquid scintillation counting system (Oken LSC - 7100) capable for detecting very weak light pulses was used for this measurement.

In order to prepare the irradiated sample for counting, only one step dissolution procedure in an appropriate liquid medium is required. As the liquid medium, water was used because of the properties of low cost, non-volatility, non-toxicity and non-flammability. In order to eliminate the effect of the absorption of phosphorus - 32 onto vial walls, the 60 μg of inactive $NH_4PH_2O_2$ carrier was dissolved in the 15 ml of water before the dissolution of the sample. Aqueous solutions were assayed in 20 ml semitransparent teflon vials, which

were found to yield a higher counting efficiency than low background glass vials, presumably owing to diffusion of the directional Cherenkov emissions. For a few irradiated samples, the decays of activities were measured for seven half-lives and no other impurity activity than ^{32}P was observed.

Counting efficiency was obtained by adding 1 ml of standard solution of ^{32}P (2700 decay per minute, dpm) to a vial containing the solution of interest. Variations of solution volume gave an insignificant effect on counting efficiency in the range from 12 to 17 ml. Efficiency (ε) was calculated by the following equation:

$$\varepsilon\,(\%) = \frac{(N_1 - N_2) \times 100}{\text{number of phosphorus-32 decays per minute of the standard solution (dpm)}}$$

where, N_1 - number of counts per minute after addition of the standard solution,
N_2 - number of counts per minute before addition of the standard solution.

The counting efficiency for ^{32}P-decays was found to be 52.2 %. Although this is lower than the efficiency of liquid scintillation counting, the minimum detectable level of ^{32}P activity is much lower because the Cherenkov background activity is lower and the volume of the aqueous sample for counting is much larger.

The experimental errors in the $^{32}S(n,p)^{32}P$ reaction rate determination are summarized in Table 3.2.1.6. The overall error for the data at all the positions except one at the deepest one were less than 6%. The measured reaction rates are presented in Fig. 3.2.1.3 with reaction rates of other reactions of the γ-activation and fission rates described in Sec 3.2.2. The numerical data are given in Table 3.2.1.7.

3.2.2 Fission Rate

The neutron sensitivities of fission reactions of U-235 and U-238 are shown in Fig. 3.2.2.1. Fission rates of U-235 and U-238 were measured at the same time by two micro fission chambers of ^{235}U and ^{238}U tied. The chambers were 6.25 mm in outer diameter and 25.4 mm in active length. The effective numbers of the atoms were experimentally determined with accuracy of 2.8 %[24]. Amplified signals were discriminated from gamma-ray and noise signals. Signals for fission events were counted by scalers. Uranium atoms in the U-235 chamber contained 7 % of U-238, and those in the U-238 chamber did 0.044 % of U-235. The correction for these impurity uranium atoms was performed.

The obtained fission rates were presented in Fig. 3.2.1.3 with reaction rates described in Sec. 3.2.1. The numerical data were given in Table 3.2.2.1. The measured fission rate of U-238 at the depth of 914 mm should be considered to be tentative data, since the count of the U-238 chamber was only 11 and might include background counts due to gamma-rays.

3.2.3 $^{10}B(n,\alpha)$ Reaction Rate

The $^{10}B(n,\alpha)$ reaction has high sensitivity to low energy neutrons as shown in Fig. 3.2.3.1. The reaction rate of $^{10}B(n,\alpha)$ reaction is useful as an index for low energy neutrons. Since many detector signals due to neutrons of energy higher than 1 MeV were accumulated in only a few channels in the time dependent $^{10}B(n,\alpha)$ reaction rates described in Sec. 3.1.3, pile-up of the detector signals might occur for neutrons of energy higher than 1 MeV, which was out of energy range of interest in the spectrum measurement. Therefore the $^{10}B(n,\alpha)$ reaction rates were measured independently of the spectrum measurement in order to avoid the count loss due to pile-up.

The reaction events were detected by the BF_3 counter utilizing the continuous operation of the D-T neutron source. A part of the electronic circuit in Fig. 3.1.3.2 was used for the measurement. The deuteron beam current was adjusted between 0.5 μA and 1 mA depending on the measurement position to keep counting rates less than 400 cps. The reaction rates were derived from the measured counts taking account of the neutron yield, the number of effective ^{10}B atoms in the BF_3 counter and self-shielding correction factors. The overall self-shielding correction factors were estimated by considering the energy-dependent self-shielding correction factors and the calculated neutron spectra with MCNP. The maximum correction factor was 6 % in the case of the front surface of the experimental assembly. The overall errors, about 4 %, were dominated by the error of 3 %, associated with the number of effective ^{10}B atoms in the BF_3 counter. The measured reaction rate is presented in Table 3.2.3.1 and Fig. 3.2.1.3 with reaction rates of other reactions.

3.3 Gamma-Ray Spectrum

The BC537 (BICRON, USA) spectrometer[25], which consisted of a deuterated benzene base scintillator and a quartz glass container, was used to measure gamma-ray spectra. Outer dimensions of the counter were 48 mm in diameter and 262 mm in length. The scintillator was a sphere of 40 mm in diameter. The electronic circuit used in the measurement is shown in Fig. 3.3.1. The gain stabilizer was adopted. Two Delay Line Amplifiers (DLA), the gains of which were different by a factor of about 10, were used to obtain energy spectra of wider dynamic range. Neutron and gamma-ray signals were separated by Rise-Time-to-Pulse-Height-Convertors.

Prompt gamma-ray spectra were measured at four positions of 457, 610, 762 and 914 mm from the front surface of the test region. The accelerator was operated in the arc-pulse mode with the pulse width of 0.75 ms and repetition interval of 2.0 ms, in order to reject decay gamma-rays.[7] Contributions of decay gamma-rays can be regarded as constant during the short period of 2 ms because of the half-lives are usually longer than one second. Energy scale of measured pulse height spectra was calibrated with the Compton edge of 1.275 MeV gamma-rays from Na-22.

The measured pulse height spectra of gamma-ray events were unfolded by using the FORIST code[14] and the calculated response matrix with the MARTHA code[26] to derive energy spectra higher than about 0.25 MeV. The obtained gamma-ray spectra at four positions are shown in Fig. 3.3.2 and Table 3.3.1. Only statistical errors are included in the figure and table. The FORIST code also provides a window function W(E), which corresponds to the energy resolution of the unfolded spectrum in full width at half maximum in percentage. The overall errors are roughly about 10 %.

The contribution of target gamma-rays generated by neutron interactions with the structural materials of the target were negligibly small since the measurement were performed at the positions deeper than 400 mm.

3.4 Gamma-Ray Heating Rate

Gamma-ray heating rates, i.e., absorbed doses of gamma-rays in a medium, monotonously increase as a function of effective atomic numbers of the thermoluminescence dosimeters (TLD). The gamma-heating rates of SS316 (effective atomic number [Zeff] is 26.4) were measured by interpolating absorbed doses measured by two kinds of TLDs; Mg_2SiO_4, (Zeff=11.1) and Sr_2SiO_4 (Zeff=32.5). These TLDs were sealed in glass capsules of 2 mm in diameter and 12 mm in length and were calibrated by a cobalt-60 standard gamma-ray field. TLDs were annealed for 30 minutes at 500 °C before irradiation. Four samples of each TLD were packed in a thin aluminum foil and were installed in the SS316 test region. Neutron irradiations were performed three times. The irradiation data are summarized in Table 3.4.1. One week later after irradiation, thermoluminescence (TL) was read out by a TLD reader (KYOKKO 2500).

Average values and standard deviations of measured TL were calculated for each group of four TLDs and were converted to the unit of exposure dose of ^{60}Co equivalence. Neutron contribution on the TL was estimated by energy-integration of the products of the neutron response function and the neutron flux calculated by MCNP[21]. The neutron contributions were subtracted from the total TL response to derive pure gamma-ray responses. The gamma-ray heating rate due to gamma-rays emitted from the tritium target assembly was calculated by MCNP and was also subtracted from the total gamma-ray heating rate. Proportions of the target gamma-ray were 9.3 and 1.8 % at -1 and 127 mm, respectively. At the measuring positions deeper than 200 mm, contributions of target gamma-rays were less than 1 %.

The measured gamma-ray heating rates of SS316 are presented in Table 3.4.2 and Fig. 3.4.1. The overall errors range between 7 - 23 %.

4. Comparison with the Results of SS316 Experiment

The effects of water in SS316 on the shielding performance were demonstrated by comparing the present data with those of the assembly #2 in the previous bulk shielding experiments on SS316[7]. Figure 4.1 shows the ratios of the measured integrated neutron fluxes above 10 MeV and from 10 keV to 1 MeV, reaction rates of $^{27}Al(n,\alpha)^{24}Na$, $^{93}Nb(n,2n)^{92m}Nb$, $^{115}In(n,n')^{115m}In$ and $^{197}Au(n,\gamma)^{198}Au$, fission rate of ^{235}U and ^{238}U, and gamma-ray heating rate in the present experiment to those in the assembly #2 of the SS316 experiments along the center line of the test region. The integrated neutron fluxes above 10 MeV and from 10 keV to 1000 keV were obtained from the measured neutron spectra.

Since water does not attenuate 14 MeV neutrons so much as SS316, the ratios of the neutron flux above 10 MeV and the reaction rates of the high threshold reactions increase along the depth. As for the reaction rate of $^{197}Au(n,\gamma)^{198}Au$ and fission-rate of ^{235}U, the ratios at the front surface of the test region are about three since water increases low energy neutron flux. The ratios, however, decrease rapidly up to 0.01 at the depth of 914 mm. The ratio of the neutron flux from 10 keV to 1 MeV also decreases along the depth. It is concluded that the shielding performance of SS316/water is extremely high for neutrons lower than 1 MeV. The reaction-rate of $^{115}In(n,n')^{115m}In$, the threshold energy of which is 335 keV, almost dose not vary due to the balance of the increased higher energy neutrons and decreased lower energy neutrons. The ratio of the gamma-ray heating rate increases at the front region since gamma-rays produced via threshold reactions such as (n,2n) and (n,n') mainly with 14 MeV neutrons are dominant. On the other hand, it decreases eminently at the deeper positions than 300 mm since the main source of the gamma-heating is gamma-rays produced by (n,γ) reactions with low energy neutrons.

Figure 4.2 shows the measured neutron spectra at the depth of 914 mm of the present SS316/water assembly and the assembly #2 of the previous SS316 experiments. All the neutron fluxes above 10 MeV in the SS316/water are about three times as large as those in the SS316. This is consistent to the result in Fig. 4.1. On the other hand, the difference between the SS316/water and SS316 assemblies increases with decrease of neutron energy from 10 keV to 1 MeV. It is notable that the shielding performance of SS316/water becomes better with decrease of neutron energy for neutrons below 1 MeV than that of SS316.

5. Concluding Remarks

The bulk shielding experiment on SS316/water was performed by using the large SS316/water (volume ratio is 4 : 1) layered assembly of 1200 mm in diameter and 1372 mm in thickness as the second shielding experiment for ITER at FNS. The various experimental data for neutron and gamma-ray were obtained with the experimental errors of 5 - 25 % at the positions of 0 to 914 mm in depth, which is comparable to the thickness of the inboard shield/blanket and vacuum vessel on the midplane of ITER. By adding the extra shield, the fraction of background was reduced to less than 10 % even at the depth of 914 mm.

In-system neutron spectra in MeV region and reaction rates of threshold reactions such as ^{93}Nb(n,2n)^{92m}Nb, ^{115}In(n,n')^{115m}In were measured up to the depth of 914 mm. Neutron spectra in keV and eV regions and reaction rates of non threshold reactions such as ^{197}Au(n,γ)^{198}Au, ^{235}U(n,fission) were also measured. It is noticeable that the measurement of gamma-ray spectra and gamma-ray heating rates was performed.

It is found from the comparison of the measured data with those in the previous SS316 experiments that SS316/water has shielding performance for quantities related to neutrons less than 1 MeV, better by 2 orders of magnitude than SS316 . The result demonstrated experimentally that water is essential not only for coolant but also for shielding material.

These experimental data will be used as benchmark data for validation of the nuclear data and calculation codes used in nuclear design of fusion devices. The analysis of this experiment by JAERI is described in detail in the Volume II[9]. The analysis using Fusion Evaluated Nuclear Data Library, FENDL-1[27], will be carried out by the U. S. and other parties in the frame of ITER/EDA.

Acknowledgment

The authors gratefully acknowledge Drs. S. Matsuda and H. Takatsu, Department of ITER Project in JAERI/Naka, for their supports to this work. They also thank Messrs. C. Kutsukake, S. Tanaka, Y. Abe, M. Seki and J. kusano for their good operation of FNS accelerator.

5. Concluding Remarks

The bulk shielding experiment on SS316/water was performed by using the large SS316/water (volume ratio is 4 : 1) layered assembly of 1200 mm in diameter and 1372 mm in thickness as the second shielding experiment for ITER at FNS. The various experimental data for neutron and gamma-ray were obtained with the experimental errors of 5 - 25 % at the positions of 0 to 914 mm in depth, which is comparable to the thickness of the inboard shield/blanket and vacuum vessel on the midplane of ITER. By adding the extra shield, the fraction of background was reduced to less than 10 % even at the depth of 914 mm.

In-system neutron spectra in MeV region and reaction rates of threshold reactions such as ^{93}Nb(n,2n)^{92m}Nb, ^{115}In(n,n')^{115m}In were measured up to the depth of 914 mm. Neutron spectra in keV and eV regions and reaction rates of non threshold reactions such as ^{197}Au(n,γ)^{198}Au, ^{235}U(n,fission) were also measured. It is noticeable that the measurement of gamma-ray spectra and gamma-ray heating rates was performed.

It is found from the comparison of the measured data with those in the previous SS316 experiments that SS316/water has shielding performance for quantities related to neutrons less than 1 MeV, better by 2 orders of magnitude than SS316 . The result demonstrated experimentally that water is essential not only for coolant but also for shielding material.

These experimental data will be used as benchmark data for validation of the nuclear data and calculation codes used in nuclear design of fusion devices. The analysis of this experiment by JAERI is described in detail in the Volume II[9]. The analysis using Fusion Evaluated Nuclear Data Library, FENDL-1[27], will be carried out by the U. S. and other parties in the frame of ITER/EDA.

Acknowledgment

The authors gratefully acknowledge Drs. S. Matsuda and H. Takatsu, Department of ITER Project in JAERI/Naka, for their supports to this work. They also thank Messrs. C. Kutsukake, S. Tanaka, Y. Abe, M. Seki and J. kusano for their good operation of FNS accelerator.

References

1) ITER Blanket, Shield and Material Data Base, ITER Documentation Series, No. 29 (1991).
2) Ioki K., Johnson G., Shimizu K. and Willimson D. : "Design of ITER Vacuum Vessel," Proc. 3rd Symposium on Fusion Nuclear Technology, Los Angeles, California, USA, Jun. 27 - Jul. 1 1994, to be published in Fusion Engineering and Design.
3) Gohar Y., Parker R. and Rebut P.-H. : "ITER Blanket Designs," ibid.
4) Santoro R.T., Gohar Y., Parker R.R., Shatalov G., Sawan M.E. and Kharter Y. : "ITER Shielding Analysis," ibid.
5) Nakamura T., Maekawa H., Ikeda Y. and Oyama Y.: "A DT Neutron Source for Fusion Neutronics Experiments at the JAERI," Proc. Int. Ion Eng. Congress - ISIAT '83 & IAPT '83, Kyoto, Japan, Vol. 1, pp. 567-570 (1983).
6) Konno C., Maekawa F., Ikeda Y., Oyama Y., Kosako K. and Maekawa H.: "Bulk Shielding Experiments on Large SS316 Assemblies," Fusion Technol., 21, pp. 2169-2173 (1992).
7) Konno C., Maekawa F., Kosako K., Ikeda Y., Oyama Y. and Maekawa H.: "Bulk Shielding Experiments on Large SS316 Assemblies Bombarded by D-T Neutrons, Volume I : Experiment," JAERI-Research 94-043 (1994).
8) Konno C., Maekawa F., Iwai A., Kosako K., Ikeda Y., Oyama Y. and Maekawa H.: "Pre-analyses of SS316 and SS316/Water Bulk Shielding Experiments," JAERI-Tech 94-019 (1994).
9) Maekawa F., Konno C., Wada M., Oyama Y., Ikeda Y., Uno Y., Verzilov Y. and Maekawa H.: "Bulk Shielding Experiment on a Large SS316/Water Assembly Bombarded by D-T Neutrons, Volume II : Analysis," JAERI-Research 95-018 (1995).
10) Maekawa H., Ikeda Y., Oyama Y., Yamaguchi S. and Nakamura T.: "Neutron Yield Monitors for the Fusion Neutronics Source (FNS) -- for 80° Beam Line --," JAERI-M 83-219 (1983).
11) Maekawa F., Konno C., Kosako K., Ikeda Y., Oyama Y. and Maekawa H.: "Bulk Shielding Experiments on Large SS316 Assemblies Bombarded by D-T Neutrons, Volume II : Analysis," JAERI-Research 94-044 (1994).
12) Rhodes W.A. and Mynatt F.R. : "the DOT-III Two Dimensional Discrete Ordinates Transport Codes," ORNL-TM-4280 (1973).
13) Oyama Y., Tanaka S., Tsuda K., Ikeda Y. and Maekawa H.: "A small spherical NE213 scintillation detector for use in in-assembly fast neutron spectrum measurements", Nucl. Instr. and Meth., A256, pp. 333-338 (1987).
14) FORIST Spectrum Unfolding code: Radiation Shielding Information Center, Oak Ridge

National Laboratory, PSR-92 (1975).

15) Nakashima H.: "Study on Shielding Design Methods for Fusion Reactors Using Benchmark Experiments," pp. 20-45, JAERI-M 92-025 (1992, in Japanese).

16) Oyama Y., et al.: " Phase IIA and IIB Experiments of JAERI/USDOE Collaborative Program on Fusion Blanket Neutronics," JAERI-M 89-215 (1989).

17) Bennett E.F.: " A Continuous Mode Data Acquisition Technique for Proton Recoil Proportional Counter Neutron Spectrometers," ANL/FPP/TM-239 (1989).

18) Bergman A. A., et al.: Proc. 1st Int. Conf. on Peaceful Uses Atomic Energy, United Nations, 4, 135 (1955).

19) Maekawa F. and Oyama Y.: "Development of Measurement Technique for Neutron Spectrum in Energy Region of eV in Large Assemblies," JAERI-M 93-181, pp. 96 - 98, (1993).

20) Maekawa F., et al.: "Measurement of Low Energy Neutron Spectrum in Iron Assembly for Verification of Evaluated Nuclear Data," JAERI-Review 94-9, pp. 144 - 146, (1994).

21) Briesmeister J. F. (Ed.): "MCNP - A General Monte Carlo Code for Neutron and Photon Transport, Version 4," RSIC/CCC-200, Radiation Shielding Information Center (1991).

22) Nakazawa M., Kobayashi K., Iwasaki.S, Iguchi T., Sakurai K., Ikeda Y. and Nakagawa T. : "JENDL Dosimetry File," JAERI 1325 (1992).

23) Lederer C. M. and Shireley V.S.: Table of Isotopes, 7th edition (1978).

24) Maekawa H., Ikeda Y., Oyama Y., Yamaguchi S., Tsuda K., Fukumoto T., Kosako K., Yoshizawa M. and Nakamura T.: "Benchmark Experiments on a 60 cm-thick Graphite Cylindrical Assembly," JAERI-M 88-034 (1988).

25) Maekawa F. and Oyama Y.: "Techniques of Integral Experiment and Method for Validation of Evaluated Nuclear Data Libraries for Secondary Gamma-Ray Data under D-T Neutron Field," JAERI-M 94-19, pp. 369 - 379 (1994).

26) Saito K. and Moriuchi S.: "Monte Carlo Calculation of Accurate Response Functions for a NaI(Tl) Detector for Gamma rays," Nucl. Instrum. Meth. 185, pp. 299-308 (1981).

27) Ganesan S. and Muir D.W.: "FENDL Multigroup Libraries," IAEA-NDS-129 (1992).

Table 2.2.1 Atomic number densities of SS316 in the test region and source reflector.

Material	Test Region	Source Reflector
C	$7.1697X10^{-5}$ *	$1.9879X10^{-4}$
Si	$9.8440X10^{-4}$	$8.1608X10^{-4}$
P	$4.3162X10^{-5}$	$4.8895X10^{-5}$
S	$1.8780X10^{-6}$	$4.4677X10^{-6}$
Cr	$1.5476X10^{-2}$	$1.5025X10^{-2}$
Mn	$9.7963X10^{-4}$	$1.3561X10^{-3}$
Fe	$5.7589X10^{-2}$	$5.8332X10^{-2}$
Ni	$9.7128X10^{-3}$	$9.1456X10^{-3}$
Mo	$1.0503X10^{-3}$	$1.0254X10^{-3}$

* Unit is in [X 10^{24} atoms/cm^3]

Table 3.1.1.1 Neutron spectra at -10, 127, 228, 330, 457, 610, 762 and 914 mm from the front surface of the test region measured by the NE213 spectrometer.

	-10 mm			127 mm			229 mm			330 mm		
Neutron Energy [eV]	Flux [n/leth/ source]	Error	Window [%]	Flux [n/leth/ source]	Error	Window [%]	Flux [n/leth/ source]	Error	Wimdow [%]	Flux [n/leth/ source]	Error	Window [%]
2.69E+6	2.88E-5	5.50E-6	31.2	1.12E-5	1.92E-6	31.2	3.21E-6	5.43E-7	31.2	8.36E-7	1.36E-7	31.2
2.83E+6	2.89E-5	1.31E-6	30.5	1.08E-5	3.92E-7	30.5	3.01E-6	1.03E-7	30.5	7.80E-7	2.53E-8	30.5
2.98E+6	2.78E-5	1.45E-6	29.7	9.87E-6	3.90E-7	29.7	2.73E-6	9.89E-8	29.7	7.08E-7	2.44E-8	29.7
3.13E+6	2.58E-5	1.66E-6	29.0	8.96E-6	4.04E-7	29.0	2.48E-6	1.01E-7	29.0	6.43E-7	2.47E-8	29.0
3.29E+6	2.32E-5	1.72E-6	28.3	8.19E-6	4.05E-7	28.3	2.29E-6	1.00E-7	28.3	5.93E-7	2.43E-8	28.3
3.46E+6	2.01E-5	1.57E-6	27.6	7.63E-6	3.90E-7	27.6	2.17E-6	9.79E-8	27.6	5.60E-7	2.37E-8	27.6
3.63E+6	1.71E-5	1.34E-6	26.8	7.30E-6	3.64E-7	26.8	2.09E-6	9.21E-8	26.8	5.40E-7	2.26E-8	26.8
3.82E+6	1.44E-5	1.20E-6	26.1	7.13E-6	3.51E-7	26.1	2.03E-6	8.89E-8	26.1	5.26E-7	2.20E-8	26.1
4.02E+6	1.22E-5	1.24E-6	25.3	7.00E-6	3.55E-7	25.3	1.98E-6	8.93E-8	25.3	5.08E-7	2.20E-8	25.3
4.22E+6	1.05E-5	1.35E-6	24.5	6.77E-6	3.68E-7	24.5	1.88E-6	9.11E-8	24.5	4.84E-7	2.23E-8	24.5
4.44E+6	9.07E-6	1.42E-6	23.9	6.37E-6	3.76E-7	23.9	1.77E-6	9.21E-8	23.9	4.57E-7	2.24E-8	23.9
4.67E+6	7.58E-6	1.48E-6	23.3	5.84E-6	3.82E-7	23.3	1.65E-6	9.34E-8	23.3	4.27E-7	2.26E-8	23.3
4.91E+6	5.78E-6	1.57E-6	22.7	5.29E-6	3.95E-7	22.7	1.53E-6	9.61E-8	22.7	3.89E-7	2.33E-8	22.7
5.16E+6	3.74E-6	1.65E-6	22.2	4.73E-6	4.07E-7	22.2	1.37E-6	9.85E-8	22.2	3.37E-7	2.37E-8	22.2
5.42E+6	1.81E-6	1.79E-6	21.7	4.16E-6	4.26E-7	21.7	1.19E-6	1.02E-7	21.7	2.83E-7	2.45E-8	21.7
5.70E+6	3.72E-7	1.94E-6	21.1	3.66E-6	4.49E-7	21.1	1.03E-6	1.07E-7	21.1	2.50E-7	2.56E-8	21.1
5.99E+6	-6.66E-8	2.04E-6	20.6	3.35E-6	4.62E-7	20.6	9.16E-7	1.09E-7	20.6	2.54E-7	2.61E-8	20.6
6.30E+6	4.76E-7	2.34E-6	20.0	3.29E-6	4.99E-7	20.0	8.73E-7	1.17E-7	20.0	2.79E-7	2.78E-8	20.0
6.62E+6	1.03E-6	2.68E-6	19.5	3.47E-6	5.53E-7	19.5	9.19E-7	1.28E-7	19.5	2.93E-7	3.05E-8	19.5
6.96E+6	1.10E-6	2.78E-6	19.0	3.82E-6	5.68E-7	19.0	1.04E-6	1.32E-7	19.0	2.89E-7	3.12E-8	19.0
7.32E+6	1.81E-6	3.23E-6	18.5	4.23E-6	6.38E-7	18.5	1.17E-6	1.48E-7	18.5	2.90E-7	3.43E-8	18.5
7.69E+6	3.87E-6	3.83E-6	18.0	4.39E-6	7.32E-7	18.0	1.24E-6	1.67E-7	18.0	3.05E-7	3.88E-8	18.0
8.09E+6	5.21E-6	4.17E-6	17.6	4.07E-6	7.78E-7	17.6	1.24E-6	1.77E-7	17.6	3.08E-7	4.11E-8	17.6
8.50E+6	3.86E-6	4.82E-6	17.2	3.67E-6	8.74E-7	17.2	1.18E-6	1.96E-7	17.2	3.15E-7	4.48E-8	17.2
8.94E+6	2.02E-6	6.14E-6	16.8	3.90E-6	1.08E-6	16.8	1.11E-6	2.41E-7	16.8	3.41E-7	5.46E-8	16.8
9.40E+6	2.66E-6	6.82E-6	16.4	4.74E-6	1.18E-6	16.4	1.13E-6	2.61E-7	16.4	3.40E-7	5.94E-8	16.4
9.88E+6	4.65E-6	7.06E-6	15.9	5.26E-6	1.22E-6	15.9	1.28E-6	2.68E-7	15.9	3.27E-7	6.04E-8	15.9
1.04E+7	7.00E-6	8.01E-6	15.5	4.87E-6	1.36E-6	15.5	1.52E-6	3.00E-7	15.5	3.64E-7	6.73E-8	15.5
1.09E+7	9.63E-6	8.08E-6	15.1	4.08E-6	1.33E-6	15.1	1.45E-6	2.91E-7	15.1	3.92E-7	6.51E-8	15.1
1.15E+7	1.11E-5	8.20E-6	14.8	4.53E-6	1.32E-6	14.8	1.17E-6	2.86E-7	14.8	3.71E-7	6.35E-8	14.8
1.21E+7	1.72E-5	9.91E-6	14.5	7.25E-6	1.59E-6	14.5	1.47E-6	3.38E-7	14.5	4.50E-7	7.45E-8	14.5
1.27E+7	4.86E-5	1.08E-5	14.4	1.21E-5	1.81E-6	14.4	2.67E-6	3.89E-7	14.4	7.80E-7	8.67E-8	14.4
1.33E+7	1.80E-4	1.38E-5	14.4	2.86E-5	2.17E-6	14.4	6.33E-6	4.66E-7	14.4	1.64E-6	1.01E-7	14.4
1.40E+7	4.40E-4	1.66E-5	14.1	6.62E-5	2.81E-6	14.4	1.48E-5	6.03E-7	14.4	3.13E-6	1.34E-7	14.4
1.47E+7	5.67E-4	2.28E-5	14.1	8.77E-5	4.34E-6	14.4	1.96E-5	9.56E-7	14.4	3.75E-6	2.22E-7	14.4
1.55E+7	3.53E-4	9.75E-6	14.1	5.55E-5	1.79E-6	14.4	1.16E-5	3.84E-7	14.4	2.31E-6	8.72E-8	14.4
1.63E+7	1.24E-4	1.17E-5	12.8	1.81E-5	2.11E-6	14.4	2.89E-6	4.66E-7	14.4	7.81E-7	1.09E-7	14.4
1.71E+7	8.54E-5	7.54E-6	11.6	1.08E-5	1.58E-6	14.4	1.67E-6	3.48E-7	14.4	4.70E-7	8.24E-8	14.4
1.80E+7	5.67E-5	1.52E-6	10.5	9.17E-6	4.15E-7	14.4	1.80E-6	9.27E-8	14.4	4.00E-7	2.30E-8	14.4

Table 3.1.1.1 (Continued)

	457 mm			610 mm			762 mm			914 mm		
Neutron Energy [eV]	Flux [n/leth/ source]	Error	Window [%]	Flux [n/leth/ source]	Error	Window [%]	Flux [n/leth/ source]	Error	Wimdow [%]	Flux [n/leth/ source]	Error	Window [%]
2.10E+6	1.22E-07	5.90E-09	35.1	1.97E-08	7.24E-10	35.0	3.22E-09	1.08E-10	33.2	4.51E-10	1.39E-11	32.2
2.20E+6	1.41E-07	5.35E-09	34.3	1.97E-08	6.07E-10	34.1	3.43E-09	9.95E-11	31.0	4.49E-10	1.24E-11	30.4
2.32E+6	1.57E-07	5.33E-09	33.5	1.97E-08	5.83E-10	33.4	3.55E-09	9.62E-11	29.1	4.32E-10	1.16E-11	28.8
2.44E+6	1.67E-07	5.38E-09	32.8	1.92E-08	5.81E-10	32.6	3.49E-09	9.28E-11	27.8	4.05E-10	1.05E-11	28.5
2.56E+6	1.68E-07	5.50E-09	32.0	1.79E-08	5.76E-10	31.9	3.21E-09	9.01E-11	27.8	3.66E-10	1.00E-11	29.0
2.69E+6	1.62E-07	5.46E-09	31.2	1.59E-08	5.62E-10	31.2	2.76E-09	8.47E-11	28.2	3.16E-10	9.77E-12	29.2
2.83E+6	1.54E-07	5.26E-09	30.5	1.39E-08	5.46E-10	30.5	2.26E-09	7.85E-11	28.7	2.69E-10	8.77E-12	29.4
2.98E+6	1.51E-07	5.07E-09	29.7	1.28E-08	5.46E-10	29.7	1.83E-09	7.56E-11	29.1	2.42E-10	8.07E-12	29.5
3.13E+6	1.55E-07	5.09E-09	29.0	1.32E-08	5.60E-10	29.0	1.52E-09	6.93E-11	29.0	2.38E-10	7.94E-12	29.0
3.29E+6	1.60E-07	5.24E-09	28.3	1.51E-08	5.70E-10	27.9	1.37E-09	6.47E-11	28.3	2.37E-10	7.95E-12	28.3
3.46E+6	1.57E-07	5.27E-09	27.6	1.77E-08	5.61E-10	26.9	1.36E-09	6.37E-11	27.6	2.22E-10	7.65E-12	27.6
3.63E+6	1.43E-07	5.06E-09	26.8	1.95E-08	5.61E-10	26.2	1.41E-09	6.33E-11	26.8	1.93E-10	7.27E-12	26.8
3.82E+6	1.24E-07	4.81E-09	26.1	1.93E-08	5.67E-10	25.4	1.48E-09	6.29E-11	26.1	1.69E-10	7.09E-12	26.1
4.02E+6	1.10E-07	4.72E-09	25.3	1.69E-08	5.43E-10	24.6	1.56E-09	6.29E-11	25.3	1.57E-10	7.27E-12	25.3
4.22E+6	1.02E-07	4.77E-09	24.5	1.37E-08	4.97E-10	24.3	1.65E-09	6.30E-11	24.5	1.54E-10	7.60E-12	24.5
4.44E+6	1.01E-07	4.82E-09	23.9	1.16E-08	4.71E-10	23.9	1.76E-09	6.34E-11	23.9	1.54E-10	7.95E-12	23.9
4.67E+6	1.05E-07	4.89E-09	23.3	1.08E-08	4.65E-10	23.3	1.86E-09	6.29E-11	23.3	1.57E-10	8.23E-12	23.3
4.91E+6	1.11E-07	5.00E-09	22.7	1.04E-08	4.68E-10	22.7	1.89E-09	6.22E-11	22.7	1.58E-10	8.54E-12	22.7
5.16E+6	1.15E-07	5.00E-09	22.2	9.77E-09	4.65E-10	22.2	1.77E-09	6.08E-11	22.2	1.50E-10	8.82E-12	22.2
5.42E+6	1.12E-07	4.99E-09	21.7	8.85E-09	4.63E-10	21.7	1.55E-09	5.84E-11	21.7	1.28E-10	9.21E-12	21.7
5.70E+6	1.02E-07	5.05E-09	21.1	7.93E-09	4.71E-10	21.1	1.32E-09	5.65E-11	21.1	1.01E-10	9.47E-12	21.1
5.99E+6	8.78E-08	4.99E-09	20.6	7.15E-09	4.76E-10	20.6	1.17E-09	5.50E-11	20.6	8.31E-11	9.58E-12	20.6
6.30E+6	7.59E-08	4.96E-09	20.0	6.69E-09	4.83E-10	20.0	1.07E-09	5.60E-11	20.0	8.04E-11	1.02E-11	20.0
6.62E+6	7.15E-08	5.23E-09	19.5	6.69E-09	5.09E-10	19.5	9.67E-10	5.88E-11	19.5	8.17E-11	1.11E-11	19.5
6.96E+6	7.08E-08	5.35E-09	19.0	6.61E-09	5.25E-10	19.0	8.38E-10	5.97E-11	19.0	7.34E-11	1.14E-11	19.0
7.32E+6	6.79E-08	5.76E-09	18.5	5.79E-09	5.72E-10	18.5	6.76E-10	6.62E-11	18.5	5.36E-11	1.28E-11	18.5
7.69E+6	6.44E-08	6.32E-09	18.0	4.81E-09	6.41E-10	18.0	5.82E-10	7.47E-11	18.0	3.93E-11	1.44E-11	18.0
8.09E+6	6.38E-08	6.57E-09	17.6	4.56E-09	6.82E-10	17.6	5.97E-10	7.95E-11	17.6	4.62E-11	1.54E-11	17.6
8.50E+6	6.36E-08	7.19E-09	17.2	5.10E-09	7.41E-10	17.2	5.49E-10	8.48E-11	17.2	6.35E-11	1.59E-11	17.2
8.94E+6	5.94E-08	8.68E-09	16.8	5.93E-09	9.03E-10	16.8	4.45E-10	1.01E-10	16.8	6.98E-11	1.83E-11	16.8
9.40E+6	5.45E-08	9.29E-09	16.4	6.35E-09	9.94E-10	16.4	5.46E-10	1.11E-10	16.4	6.05E-11	2.08E-11	16.4
9.88E+6	5.66E-08	9.48E-09	15.9	6.69E-09	1.02E-09	15.9	7.91E-10	1.14E-10	15.9	5.35E-11	2.10E-11	15.9
1.04E+7	6.63E-08	1.06E-08	15.5	7.69E-09	1.12E-09	15.5	8.72E-10	1.25E-10	15.5	6.49E-11	2.26E-11	15.5
1.09E+7	7.44E-08	1.02E-08	15.1	8.83E-09	1.12E-09	15.1	9.04E-10	1.28E-10	15.1	9.05E-11	2.40E-11	15.1
1.15E+7	8.64E-08	9.53E-09	14.8	9.95E-09	1.14E-09	14.8	1.15E-09	1.35E-10	14.8	1.24E-10	2.56E-11	14.8
1.21E+7	1.18E-07	1.13E-08	14.5	1.36E-08	1.37E-09	14.5	1.70E-09	1.58E-10	14.5	1.97E-10	2.80E-11	14.5
1.27E+7	1.99E-07	1.33E-08	14.4	2.51E-08	1.59E-09	14.4	2.97E-09	1.74E-10	14.4	3.22E-10	2.87E-11	14.4
1.33E+7	3.75E-07	1.50E-08	14.4	4.37E-08	1.82E-09	14.4	4.74E-09	1.99E-10	14.4	4.35E-10	3.30E-11	14.4
1.40E+7	5.29E-07	2.10E-08	14.4	4.88E-08	2.57E-09	14.4	4.97E-09	2.66E-10	14.4	4.01E-10	3.92E-11	14.4
1.47E+7	4.56E-07	3.57E-08	14.4	3.19E-08	4.07E-09	14.4	3.03E-09	3.94E-10	14.4	2.22E-10	4.14E-11	14.4
1.55E+7	2.08E-07	1.34E-08	14.4	1.49E-08	1.51E-09	14.4	1.11E-09	1.55E-10	14.4	7.08E-11	2.03E-11	14.4
1.63E+7	4.52E-08	1.80E-08	14.4	7.23E-09	2.11E-09	14.4	3.58E-10	1.92E-10	14.4	4.32E-12	1.99E-11	14.4
1.71E+7	2.36E-08	1.34E-08	14.4	4.26E-09	1.53E-09	14.4	2.09E-10	1.43E-10	14.4			
1.80E+7	2.54E-08	3.67E-09	14.4	2.45E-09	4.17E-10	14.4	9.79E-11	4.05E-11	14.4			

Table 3.1.2.1 Neutron spectra at -10, 127, 229, 330,457, 610, 762 and 914 mm from the front surface of the test region measured by the proton-recoil gas proportional counters.

-10 mm			127 mm			229 mm			330 mm		
Neutron Energy [eV]	Flux [n/leth/ source]	Absolute Error	Neutron Energy [eV]	Flux [n/leth/ source]	Absolute Error	Neutron Energy [eV]	Flux [n/leth/ source]	Absolute Error	Neutron Energy [eV]	Flux [n/leth/ source]	Absolute Error
3.13E+3	9.87E-6	3.23E-6	3.04E+3	3.03E-6	1.92E-6	3.04E+3	2.52E-6	7.12E-7	3.13E+3	6.73E-7	2.08E-7
3.27E+3	6.84E-6	3.10E-6	3.18E+3	6.99E-6	1.82E-6	3.18E+3	1.80E-6	6.71E-7	3.27E+3	5.72E-7	1.99E-7
3.41E+3	5.68E-6	2.96E-6	3.31E+3	4.13E-6	1.72E-6	3.31E+3	1.88E-6	6.27E-7	3.41E+3	6.50E-7	1.89E-7
3.56E+3	7.43E-6	2.86E-6	3.46E+3	4.82E-6	1.64E-6	3.46E+3	2.38E-6	6.03E-7	3.56E+3	4.95E-7	1.83E-7
3.72E+3	1.05E-5	2.72E-6	3.61E+3	5.45E-6	1.57E-6	3.61E+3	1.27E-6	5.80E-7	3.72E+3	8.22E-7	1.74E-7
3.88E+3	9.41E-6	2.65E-6	3.77E+3	3.76E-6	1.49E-6	3.77E+3	1.64E-6	5.57E-7	3.88E+3	5.86E-7	1.68E-7
4.05E+3	5.77E-6	2.53E-6	3.94E+3	4.99E-6	1.45E-6	3.94E+3	2.43E-6	5.39E-7	4.05E+3	5.04E-7	1.61E-7
4.23E+3	8.23E-6	2.49E-6	4.11E+3	3.73E-6	1.39E-6	4.11E+3	1.10E-6	5.20E-7	4.23E+3	6.06E-7	1.57E-7
4.42E+3	2.05E-6	2.42E-6	4.29E+3	2.12E-6	1.36E-6	4.29E+3	1.10E-6	5.05E-7	4.42E+3	5.77E-7	1.52E-7
4.62E+3	5.22E-6	2.39E-6	4.49E+3	3.47E-6	1.33E-6	4.49E+3	1.31E-6	5.01E-7	4.62E+3	5.05E-7	1.49E-7
4.83E+3	7.83E-6	2.36E-6	4.69E+3	6.34E-6	1.29E-6	4.69E+3	1.29E-6	4.86E-7	4.83E+3	5.34E-7	1.44E-7
5.04E+3	6.08E-6	2.31E-6	4.90E+3	4.40E-6	1.24E-6	4.90E+3	1.65E-6	4.78E-7	5.04E+3	4.49E-7	1.42E-7
5.27E+3	5.36E-6	2.25E-6	5.12E+3	2.86E-6	1.22E-6	5.12E+3	2.18E-6	4.63E-7	5.27E+3	5.23E-7	1.39E-7
5.51E+3	7.76E-6	2.24E-6	5.35E+3	2.54E-6	1.19E-6	5.35E+3	2.30E-6	4.50E-7	5.51E+3	6.55E-7	1.36E-7
5.76E+3	8.63E-6	2.19E-6	5.59E+3	3.88E-6	1.17E-6	5.59E+3	8.17E-7	4.42E-7	5.76E+3	5.08E-7	1.35E-7
6.02E+3	1.19E-5	2.14E-6	5.85E+3	3.76E-6	1.16E-6	5.85E+3	1.73E-6	4.33E-7	6.02E+3	5.31E-7	1.31E-7
6.29E+3	4.95E-6	2.12E-6	6.11E+3	3.74E-6	1.12E-6	6.11E+3	1.64E-6	4.31E-7	6.29E+3	6.97E-7	1.29E-7
6.58E+3	4.16E-6	2.08E-6	6.39E+3	4.23E-6	1.11E-6	6.39E+3	1.86E-6	4.17E-7	6.58E+3	5.95E-7	1.27E-7
6.88E+3	9.30E-6	2.07E-6	6.68E+3	3.06E-6	1.09E-6	6.68E+3	2.24E-6	4.15E-7	6.88E+3	5.78E-7	1.24E-7
7.20E+3	8.12E-6	2.04E-6	6.99E+3	5.18E-6	1.07E-6	6.99E+3	8.65E-7	4.06E-7	7.20E+3	4.60E-7	1.23E-7
7.53E+3	6.38E-6	2.00E-6	7.31E+3	2.33E-6	1.06E-6	7.31E+3	1.10E-6	4.02E-7	7.53E+3	3.36E-7	1.22E-7
7.88E+3	6.07E-6	2.00E-6	7.65E+3	2.50E-6	1.04E-6	7.65E+3	1.60E-6	3.97E-7	7.88E+3	4.08E-7	1.20E-7
8.24E+3	4.97E-6	1.99E-6	8.00E+3	3.09E-6	1.05E-6	8.00E+3	7.83E-7	3.95E-7	8.24E+3	4.67E-7	1.20E-7
8.62E+3	9.12E-6	2.00E-6	8.37E+3	1.97E-6	1.04E-6	8.37E+3	1.88E-6	3.93E-7	8.62E+3	4.43E-7	1.20E-7
9.02E+3	1.00E-5	2.01E-6	8.75E+3	5.07E-6	1.05E-6	8.75E+3	1.88E-6	3.94E-7	9.02E+3	7.37E-7	1.21E-7
9.44E+3	8.65E-6	2.02E-6	9.16E+3	3.80E-6	1.05E-6	9.16E+3	1.94E-6	3.96E-7	9.44E+3	8.17E-7	1.21E-7
9.88E+3	1.11E-5	2.02E-6	9.59E+3	3.80E-6	1.04E-6	9.59E+3	1.90E-6	3.94E-7	9.88E+3	7.32E-7	1.20E-7
1.03E+4	1.19E-5	2.02E-6	1.00E+4	6.90E-6	1.04E-6	1.00E+4	1.91E-6	3.96E-7	1.03E+4	7.84E-7	1.20E-7
1.08E+4	1.08E-5	2.02E-6	1.05E+4	6.41E-6	1.03E-6	1.05E+4	2.17E-6	3.96E-7	1.08E+4	7.78E-7	1.19E-7
1.13E+4	1.07E-5	2.02E-6	1.10E+4	4.44E-6	1.03E-6	1.10E+4	2.35E-6	3.95E-7	1.13E+4	7.41E-7	1.19E-7
1.19E+4	9.93E-6	2.03E-6	1.15E+4	4.62E-6	1.02E-6	1.15E+4	2.29E-6	3.93E-7	1.19E+4	9.06E-7	1.18E-7
1.24E+4	1.13E-5	2.03E-6	1.20E+4	5.51E-6	1.02E-6	1.20E+4	2.07E-6	3.94E-7	1.24E+4	7.39E-7	1.19E-7
1.30E+4	1.30E-5	2.04E-6	1.26E+4	4.86E-6	1.02E-6	1.26E+4	2.41E-6	3.91E-7	1.30E+4	6.86E-7	1.18E-7
1.36E+4	8.69E-6	2.04E-6	1.32E+4	4.19E-6	1.02E-6	1.32E+4	2.42E-6	3.94E-7	1.36E+4	8.06E-7	1.18E-7
1.42E+4	7.33E-6	2.05E-6	1.38E+4	3.37E-6	1.03E-6	1.38E+4	1.79E-6	3.91E-7	1.42E+4	4.10E-7	1.19E-7
1.49E+4	8.72E-6	2.08E-6	1.45E+4	3.73E-6	1.03E-6	1.45E+4	1.98E-6	3.94E-7	1.49E+4	5.26E-7	1.19E-7
1.56E+4	8.34E-6	2.09E-6	1.51E+4	4.95E-6	1.04E-6	1.51E+4	1.32E-6	3.96E-7	1.56E+4	6.74E-7	1.19E-7
1.63E+4	9.75E-6	2.11E-6	1.58E+4	3.63E-6	1.04E-6	1.58E+4	1.15E-6	4.01E-7	1.63E+4	5.10E-7	1.21E-7
1.71E+4	1.11E-5	2.13E-6	1.66E+4	3.37E-6	1.05E-6	1.66E+4	1.35E-6	4.05E-7	1.71E+4	4.30E-7	1.21E-7
1.79E+4	7.42E-6	2.14E-6	1.74E+4	3.13E-6	1.06E-6	1.74E+4	2.29E-6	4.08E-7	1.79E+4	6.42E-7	1.22E-7
1.88E+4	8.14E-6	2.16E-6	1.82E+4	3.70E-6	1.06E-6	1.82E+4	1.71E-6	4.10E-7	1.88E+4	6.75E-7	1.23E-7
1.97E+4	1.14E-5	2.18E-6	1.91E+4	5.03E-6	1.08E-6	1.91E+4	1.84E-6	4.12E-7	1.97E+4	7.18E-7	1.23E-7
2.06E+4	1.21E-5	2.20E-6	2.00E+4	4.23E-6	1.08E-6	2.00E+4	2.44E-6	4.16E-7	2.06E+4	7.43E-7	1.24E-7
2.16E+4	1.42E-5	2.20E-6	2.09E+4	4.70E-6	1.09E-6	2.09E+4	2.09E-6	4.15E-7	2.16E+4	8.67E-7	1.25E-7
2.26E+4	1.64E-5	2.20E-6	2.19E+4	5.86E-6	1.09E-6	2.19E+4	2.24E-6	4.19E-7	2.26E+4	1.06E-6	1.23E-7
2.36E+4	1.98E-5	2.20E-6	2.29E+4	6.85E-6	1.09E-6	2.29E+4	2.95E-6	4.16E-7	2.36E+4	1.26E-6	1.23E-7
2.48E+4	1.92E-5	2.19E-6	2.40E+4	7.85E-6	1.08E-6	2.40E+4	3.98E-6	4.15E-7	2.48E+4	1.14E-6	1.21E-7
2.59E+4	1.59E-5	2.19E-6	2.51E+4	7.48E-6	1.08E-6	2.51E+4	4.10E-6	4.11E-7	2.59E+4	1.09E-6	1.20E-7
2.72E+4	1.42E-5	2.19E-6	2.63E+4	6.62E-6	1.07E-6	2.63E+4	2.32E-6	4.10E-7	2.72E+4	7.47E-7	1.20E-7
2.85E+4	7.36E-6	2.22E-6	2.76E+4	3.68E-6	1.08E-6	2.76E+4	1.97E-6	4.09E-7	2.85E+4	5.87E-7	1.21E-7
2.98E+4	5.52E-6	2.25E-6	2.89E+4	3.45E-6	1.09E-6	2.89E+4	1.52E-6	4.16E-7	2.98E+4	2.59E-7	1.23E-7
3.12E+4	6.91E-6	2.30E-6	3.03E+4	2.92E-6	1.10E-6	3.03E+4	1.25E-6	4.20E-7	3.12E+4	2.89E-7	1.25E-7
3.27E+4	8.32E-6	2.33E-6	3.17E+4	1.52E-6	1.12E-6	3.17E+4	1.45E-6	4.26E-7	3.27E+4	4.95E-7	1.27E-7
3.43E+4	1.22E-5	2.38E-6	3.32E+4	4.75E-6	1.13E-6	3.32E+4	1.94E-6	4.32E-7	3.43E+4	6.62E-7	1.29E-7
3.59E+4	9.25E-6	2.40E-6	3.48E+4	4.40E-6	1.15E-6	3.48E+4	1.61E-6	4.38E-7	3.59E+4	5.98E-7	1.31E-7
3.76E+4	1.28E-5	2.44E-6	3.65E+4	2.95E-6	1.16E-6	3.65E+4	1.52E-6	4.42E-7	3.76E+4	7.09E-7	1.32E-7
3.94E+4	1.02E-5	2.47E-6	3.82E+4	6.95E-6	1.18E-6	3.82E+4	1.89E-6	4.54E-7	3.94E+4	7.27E-7	1.33E-7
4.13E+4	1.31E-5	2.50E-6	4.00E+4	4.97E-6	1.19E-6	4.00E+4	2.60E-6	4.54E-7	4.13E+4	8.35E-7	1.34E-7
4.32E+4	1.81E-5	2.53E-6	4.19E+4	3.80E-6	1.21E-6	4.19E+4	2.61E-6	4.63E-7	4.32E+4	8.02E-7	1.36E-7
4.53E+4	1.91E-5	2.54E-6	4.39E+4	4.96E-6	1.22E-6	4.39E+4	2.77E-6	4.62E-7	4.53E+4	9.49E-7	1.37E-7
4.75E+4	1.78E-5	2.56E-6	4.60E+4	6.74E-6	1.24E-6	4.60E+4	2.57E-6	4.72E-7	4.75E+4	1.12E-6	1.38E-7
4.97E+4	1.36E-5	2.60E-6	4.82E+4	7.90E-6	1.23E-6	4.82E+4	2.63E-6	4.71E-7	4.97E+4	7.68E-7	1.39E-7
5.21E+4	1.44E-5	2.63E-6	5.05E+4	6.42E-6	1.25E-6	5.05E+4	3.29E-6	4.78E-7	5.21E+4	8.31E-7	1.40E-7
5.46E+4	1.78E-5	2.68E-6	5.29E+4	4.72E-6	1.26E-6	5.29E+4	2.22E-6	4.81E-7	5.46E+4	8.86E-7	1.41E-7
5.72E+4	1.63E-5	2.70E-6	5.54E+4	5.26E-6	1.28E-6	5.54E+4	2.58E-6	4.87E-7	5.72E+4	8.81E-7	1.44E-7
5.99E+4	1.97E-5	2.73E-6	5.81E+4	7.12E-6	1.30E-6	5.81E+4	3.26E-6	4.91E-7	5.99E+4	1.14E-6	1.44E-7

Table 3.1.2.1 (Continued-1)

-10 mm			127 mm			229 mm			330 mm		
Neutron Energy [eV]	Flux [n/leth/ source]	Absolute Error	Neutron Energy [eV]	Flux [n/leth/ source]	Absolute Error	Neutron Energy [eV]	Flux [n/leth/ source]	Absolute Error	Neutron Energy [eV]	Flux [n/leth/ source]	Absolute Error
6.28E+4	1.76E-5	2.77E-6	6.08E+4	5.89E-6	1.31E-6	6.08E+4	2.99E-6	4.97E-7	6.28E+4	1.05E-6	1.46E-7
6.58E+4	1.99E-5	2.79E-6	6.38E+4	5.97E-6	1.33E-6	6.38E+4	2.97E-6	5.01E-7	6.58E+4	9.03E-7	1.47E-7
6.89E+4	2.31E-5	2.82E-6	6.68E+4	7.35E-6	1.35E-6	6.68E+4	3.17E-6	5.06E-7	6.89E+4	1.19E-6	1.48E-7
7.22E+4	2.16E-5	2.86E-6	7.00E+4	6.96E-6	1.37E-6	7.00E+4	3.51E-6	5.12E-7	7.22E+4	1.17E-6	1.49E-7
7.57E+4	2.25E-5	2.88E-6	7.33E+4	7.35E-6	1.38E-6	7.33E+4	3.54E-6	5.16E-7	7.57E+4	1.21E-6	1.51E-7
7.93E+4	3.03E-5	2.91E-6	7.68E+4	1.08E-5	1.40E-6	7.68E+4	3.80E-6	5.23E-7	7.93E+4	1.33E-6	1.52E-7
8.31E+4	2.38E-5	2.94E-6	8.05E+4	1.18E-5	1.39E-6	8.05E+4	3.96E-6	5.25E-7	8.31E+4	1.12E-6	1.53E-7
8.70E+4	1.96E-5	2.97E-6	8.44E+4	5.34E-6	1.41E-6	8.44E+4	4.42E-6	5.29E-7	8.70E+4	1.34E-6	1.55E-7
9.12E+4	2.35E-5	3.01E-6	8.84E+4	4.96E-6	1.42E-6	8.84E+4	3.17E-6	5.33E-7	9.12E+4	1.03E-6	1.56E-7
9.56E+4	1.61E-5	3.06E-6	9.26E+4	6.39E-6	1.46E-6	9.26E+4	2.86E-6	5.43E-7	9.56E+4	9.33E-7	1.59E-7
1.00E+5	2.35E-5	3.10E-6	9.71E+4	5.89E-6	1.49E-6	9.71E+4	3.07E-6	5.49E-7	1.00E+5	1.25E-6	1.60E-7
1.05E+5	2.67E-5	3.16E-6	1.02E+5	9.00E-6	1.51E-6	1.02E+5	3.29E-6	5.60E-7	1.05E+5	7.94E-7	1.63E-7
1.10E+5	3.05E-5	3.19E-6	1.07E+5	9.01E-6	1.54E-6	1.07E+5	3.07E-6	5.69E-7	1.10E+5	1.17E-6	1.66E-7
1.15E+5	2.99E-5	3.22E-6	1.12E+5	9.80E-6	1.55E-6	1.12E+5	3.97E-6	5.79E-7	1.15E+5	1.43E-6	1.68E-7
1.21E+5	3.33E-5	3.25E-6	1.17E+5	1.02E-5	1.58E-6	1.17E+5	4.52E-6	5.88E-7	1.21E+5	1.65E-6	1.70E-7
1.26E+5	3.93E-5	3.31E-6	1.23E+5	9.54E-6	1.60E-6	1.23E+5	4.95E-6	5.96E-7	1.26E+5	1.66E-6	1.73E-7
1.33E+5	3.61E-5	3.39E-6	1.28E+5	1.31E-5	1.64E-6	1.28E+5	5.89E-6	6.08E-7	1.33E+5	1.91E-6	1.77E-7
1.39E+5	2.84E-5	3.49E-6	1.35E+5	1.30E-5	1.68E-6	1.35E+5	4.92E-6	6.23E-7	1.39E+5	1.50E-6	1.82E-7
1.46E+5	1.95E-5	3.61E-6	1.41E+5	1.09E-5	1.74E-6	1.41E+5	4.47E-6	6.43E-7	1.46E+5	1.37E-6	1.87E-7
1.53E+5	3.15E-5	3.73E-6	1.48E+5	7.06E-6	1.79E-6	1.48E+5	4.79E-6	6.60E-7	1.53E+5	1.41E-6	1.94E-7
1.60E+5	3.62E-5	3.85E-6	1.55E+5	1.11E-5	1.85E-6	1.55E+5	4.98E-6	6.84E-7	1.60E+5	1.68E-6	1.99E-7
1.67E+5	3.66E-5	3.98E-6	1.62E+5	1.26E-5	1.92E-6	1.62E+5	5.02E-6	6.99E-7	1.67E+5	1.67E-6	2.06E-7
1.76E+5	3.42E-5	4.11E-6	1.70E+5	1.37E-5	1.98E-6	1.70E+5	5.75E-6	7.21E-7	1.76E+5	1.65E-6	2.11E-7
1.84E+5	3.00E-5	4.26E-6	1.78E+5	1.01E-5	2.06E-6	1.78E+5	5.61E-6	7.48E-7	1.84E+5	1.47E-6	2.19E-7
1.93E+5	3.32E-5	4.41E-6	1.87E+5	9.95E-6	2.13E-6	1.87E+5	3.76E-6	7.76E-7	1.91E+5	1.27E-6	1.87E-7
2.02E+5	3.43E-5	4.62E-6	1.96E+5	1.03E-5	2.23E-6	1.96E+5	5.20E-6	8.07E-7	2.00E+5	1.33E-6	1.87E-7
2.06E+5	3.38E-5	3.61E-6	2.05E+5	8.87E-6	2.34E-6	2.00E+5	5.29E-6	5.63E-7	2.10E+5	1.31E-6	1.87E-7
2.16E+5	2.66E-5	3.58E-6	2.13E+5	9.94E-6	1.48E-6	2.10E+5	4.68E-6	5.58E-7	2.20E+5	1.82E-6	1.86E-7
2.27E+5	3.50E-5	3.60E-6	2.23E+5	1.28E-5	1.46E-6	2.20E+5	4.37E-6	5.58E-7	2.30E+5	1.95E-6	1.83E-7
2.37E+5	4.62E-5	3.57E-6	2.34E+5	1.33E-5	1.46E-6	2.30E+5	6.02E-6	5.52E-7	2.41E+5	1.70E-6	1.83E-7
2.49E+5	4.04E-5	3.54E-6	2.45E+5	1.27E-5	1.46E-6	2.41E+5	6.06E-6	5.51E-7	2.53E+5	1.72E-6	1.81E-7
2.61E+5	3.93E-5	3.52E-6	2.57E+5	1.44E-5	1.46E-6	2.53E+5	5.74E-6	5.47E-7	2.65E+5	2.03E-6	1.80E-7
2.73E+5	4.83E-5	3.51E-6	2.69E+5	1.41E-5	1.46E-6	2.65E+5	6.97E-6	5.47E-7	2.77E+5	2.28E-6	1.79E-7
2.86E+5	5.27E-5	3.47E-6	2.82E+5	1.73E-5	1.46E-6	2.77E+5	7.35E-6	5.40E-7	2.91E+5	2.06E-6	1.77E-7
3.00E+5	5.14E-5	3.45E-6	2.95E+5	1.78E-5	1.44E-6	2.91E+5	6.55E-6	5.35E-7	3.05E+5	2.06E-6	1.76E-7
3.14E+5	4.49E-5	3.41E-6	3.10E+5	1.79E-5	1.44E-6	3.05E+5	7.17E-6	5.33E-7	3.19E+5	2.43E-6	1.76E-7
3.29E+5	5.06E-5	3.44E-6	3.24E+5	1.91E-5	1.44E-6	3.19E+5	7.45E-6	5.32E-7	3.35E+5	2.64E-6	1.75E-7
3.45E+5	5.73E-5	3.45E-6	3.40E+5	1.94E-5	1.45E-6	3.35E+5	7.56E-6	5.34E-7	3.51E+5	2.33E-6	1.75E-7
3.62E+5	4.67E-5	3.46E-6	3.56E+5	2.01E-5	1.45E-6	3.51E+5	8.40E-6	5.35E-7	3.67E+5	1.87E-6	1.76E-7
3.79E+5	4.44E-5	3.48E-6	3.73E+5	1.62E-5	1.46E-6	3.67E+5	7.54E-6	5.37E-7	3.85E+5	1.84E-6	1.77E-7
3.97E+5	4.58E-5	3.53E-6	3.91E+5	1.45E-5	1.48E-6	3.85E+5	6.29E-6	5.38E-7	4.04E+5	2.06E-6	1.79E-7
4.16E+5	4.20E-5	3.55E-6	4.10E+5	1.56E-5	1.51E-6	4.04E+5	6.79E-6	5.46E-7	4.23E+5	1.93E-6	1.80E-7
4.36E+5	3.49E-5	3.61E-6	4.30E+5	1.53E-5	1.53E-6	4.23E+5	6.02E-6	5.48E-7	4.43E+5	1.91E-6	1.82E-7
4.57E+5	4.17E-5	3.70E-6	4.50E+5	1.61E-5	1.56E-6	4.43E+5	5.72E-6	5.59E-7	4.64E+5	2.24E-6	1.86E-7
4.79E+5	4.79E-5	3.81E-6	4.72E+5	1.77E-5	1.61E-6	4.64E+5	7.20E-6	5.71E-7	4.87E+5	2.38E-6	1.90E-7
5.02E+5	5.69E-5	3.91E-6	4.94E+5	2.25E-5	1.65E-6	4.87E+5	8.36E-6	5.87E-7	5.10E+5	2.73E-6	1.95E-7
5.26E+5	5.57E-5	4.03E-6	5.18E+5	2.22E-5	1.69E-6	5.10E+5	8.78E-6	5.99E-7	5.35E+5	2.47E-6	1.98E-7
5.52E+5	6.24E-5	4.09E-6	5.43E+5	2.17E-5	1.73E-6	5.35E+5	9.40E-6	6.10E-7	5.60E+5	2.79E-6	2.02E-7
5.78E+5	7.52E-5	4.17E-6	5.69E+5	2.61E-5	1.78E-6	5.60E+5	1.00E-5	6.24E-7	5.87E+5	3.54E-6	2.02E-7
6.06E+5	7.33E-5	4.23E-6	5.96E+5	2.95E-5	1.80E-6	5.87E+5	1.11E-5	6.24E-7	6.15E+5	3.33E-6	2.04E-7
6.35E+5	6.84E-5	4.27E-6	6.25E+5	2.86E-5	1.84E-6	6.15E+5	1.14E-5	6.34E-7	6.45E+5	2.90E-6	2.03E-7
6.65E+5	5.72E-5	4.36E-6	6.55E+5	2.61E-5	1.85E-6	6.45E+5	1.06E-5	6.37E-7	6.76E+5	2.81E-6	2.06E-7
6.97E+5	6.10E-5	4.46E-6	6.86E+5	2.54E-5	1.90E-6	6.76E+5	9.17E-6	6.42E-7	7.08E+5	2.40E-6	2.07E-7
7.31E+5	5.52E-5	4.56E-6	7.19E+5	2.55E-5	1.92E-6	7.08E+5	8.37E-6	6.54E-7	7.42E+5	2.18E-6	2.10E-7
7.66E+5	5.18E-5	4.67E-6	7.54E+5	2.53E-5	1.96E-6	7.42E+5	8.85E-6	6.60E-7	7.78E+5	2.60E-6	2.12E-7
8.02E+5	6.42E-5	4.80E-6	7.90E+5	2.42E-5	2.00E-6	7.78E+5	9.18E-6	6.73E-7	8.15E+5	2.13E-6	2.16E-7
8.41E+5	5.88E-5	4.86E-6	8.28E+5	2.19E-5	2.06E-6	8.15E+5	7.63E-6	6.81E-7	8.54E+5	2.30E-6	2.18E-7
8.81E+5	6.08E-5	4.99E-6	8.68E+5	2.56E-5	2.08E-6	8.54E+5	8.50E-6	6.98E-7	8.95E+5	2.24E-6	2.23E-7
9.23E+5	6.02E-5	5.07E-6	9.09E+5	2.57E-5	2.12E-6	8.95E+5	8.42E-6	7.04E-7	9.38E+5	2.19E-6	2.24E-7
9.68E+5	6.70E-5	5.17E-6	9.53E+5	2.85E-5	2.15E-6	9.38E+5	8.89E-6	7.13E-7	9.83E+5	2.51E-6	2.26E-7
1.01E+6	6.72E-5	5.26E-6	9.98E+5	2.73E-5	2.17E-6	9.83E+5	8.03E-6	7.15E-7	1.03E+6	2.49E-6	2.28E-7
			1.05E+6	2.81E-5	2.16E-6	1.03E+6	9.55E-6	7.20E-7			

Table 3.1.2.1 (Continued-2)

457 mm			610 mm			762 mm			914 mm		
Neutron Energy [eV]	Flux [n/leth/ source]	Absolute Error	Neutron Energy [eV]	Flux [n/leth/ source]	Absolute Error	Neutron Energy [eV]	Flux [n/leth/ source]	Absolute Error	Neutron Energy [eV]	Flux [n/leth/ source]	Absolute Error
3.04E+3	1.53E-7	4.79E-8	3.09E+3	2.91E-8	9.42E-9	1.01E+4	-3.20E-09	2.05E-09	9.83E+3	2.99E-09	1.30E-09
3.18E+3	1.78E-7	4.50E-8	3.22E+3	1.59E-8	9.07E-9	1.06E+4	-4.60E-09	1.99E-09	1.03E+4	4.35E-09	1.25E-09
3.31E+3	1.71E-7	4.30E-8	3.36E+3	3.62E-8	8.58E-9	1.11E+4	-4.07E-09	2.03E-09	1.08E+4	2.19E-09	1.22E-09
3.46E+3	1.36E-7	4.08E-8	3.51E+3	3.92E-8	8.20E-9	1.16E+4	-1.58E-10	2.00E-09	1.13E+4	2.18E-09	1.17E-09
3.61E+3	1.18E-7	3.90E-8	3.66E+3	1.44E-8	7.82E-9	1.22E+4	-7.27E-09	2.02E-09	1.18E+4	1.51E-09	1.15E-09
3.77E+3	1.78E-7	3.74E-8	3.82E+3	2.62E-8	7.55E-9	1.27E+4	2.36E-09	1.98E-09	1.24E+4	4.75E-09	1.13E-09
3.94E+3	1.55E-7	3.63E-8	3.99E+3	2.64E-8	7.37E-9	1.33E+4	7.45E-09	2.04E-09	1.29E+4	3.48E-09	1.09E-09
4.11E+3	1.00E-7	3.49E-8	4.17E+3	1.72E-8	7.13E-9	1.40E+4	-2.65E-09	1.98E-09	1.35E+4	3.00E-09	1.07E-09
4.29E+3	6.55E-8	3.44E-8	4.36E+3	2.43E-8	6.97E-9	1.46E+4	1.33E-09	1.98E-09	1.42E+4	3.42E-09	1.06E-09
4.49E+3	8.72E-8	3.35E-8	4.55E+3	2.84E-8	6.80E-9	1.53E+4	-4.78E-09	1.98E-09	1.48E+4	-1.10E-09	1.05E-09
4.69E+3	1.03E-7	3.30E-8	4.75E+3	2.96E-8	6.53E-9	1.60E+4	2.77E-09	1.90E-09	1.55E+4	1.88E-10	1.04E-09
4.90E+3	1.25E-7	3.21E-8	4.97E+3	1.42E-8	6.50E-9	1.68E+4	3.19E-09	2.02E-09	1.63E+4	4.07E-09	1.04E-09
5.12E+3	1.58E-7	3.15E-8	5.19E+3	1.54E-8	6.33E-9	1.76E+4	-5.15E-09	1.94E-09	1.70E+4	4.10E-09	1.02E-09
5.35E+3	7.34E-8	3.09E-8	5.43E+3	2.40E-8	6.29E-9	1.84E+4	8.79E-09	1.99E-09	1.78E+4	3.28E-09	1.02E-09
5.59E+3	1.21E-7	3.02E-8	5.67E+3	2.21E-8	6.15E-9	1.93E+4	1.03E-08	1.95E-09	1.87E+4	4.71E-09	9.92E-10
5.85E+3	1.25E-7	3.00E-8	5.93E+3	2.30E-8	6.02E-9	2.02E+4	3.45E-09	1.94E-09	1.96E+4	5.48E-09	9.83E-10
6.11E+3	6.85E-8	2.95E-8	6.20E+3	1.76E-8	6.00E-9	2.11E+4	8.86E-09	1.85E-09	2.05E+4	5.71E-09	9.66E-10
6.39E+3	1.06E-7	2.92E-8	6.48E+3	2.37E-8	5.88E-9	2.21E+4	1.46E-08	1.87E-09	2.15E+4	7.89E-09	9.41E-10
6.68E+3	1.18E-7	2.89E-8	6.78E+3	2.34E-8	5.81E-9	2.32E+4	4.35E-09	1.81E-09	2.25E+4	8.07E-09	9.21E-10
6.99E+3	1.06E-7	2.85E-8	7.09E+3	1.10E-8	5.81E-9	2.43E+4	9.10E-09	1.75E-09	2.35E+4	8.26E-09	9.03E-10
7.31E+3	1.18E-7	2.84E-8	7.42E+3	1.82E-8	5.75E-9	2.54E+4	1.59E-08	1.75E-09	2.46E+4	9.76E-09	8.67E-10
7.65E+3	7.16E-8	2.81E-8	7.76E+3	2.37E-8	5.72E-9	2.66E+4	1.95E-09	1.70E-09	2.58E+4	7.19E-09	8.57E-10
8.00E+3	6.23E-8	2.81E-8	8.12E+3	2.12E-8	5.65E-9	2.79E+4	8.22E-10	1.69E-09	2.70E+4	4.14E-09	8.37E-10
8.37E+3	1.30E-7	2.80E-8	8.49E+3	2.11E-8	5.69E-9	2.92E+4	-1.83E-10	1.78E-09	2.83E+4	2.27E-09	8.41E-10
8.75E+3	1.68E-7	2.80E-8	8.89E+3	3.01E-8	5.69E-9	3.06E+4	1.96E-09	1.79E-09	2.97E+4	1.24E-09	8.60E-10
9.16E+3	1.71E-7	2.81E-8	9.30E+3	3.36E-8	5.69E-9	3.21E+4	-2.01E-09	1.88E-09	3.11E+4	9.91E-10	8.80E-10
9.59E+3	1.78E-7	2.81E-8	9.73E+3	3.30E-8	5.71E-9	3.36E+4	-1.57E-09	1.91E-09	3.26E+4	2.69E-09	8.99E-10
1.00E+4	1.74E-7	2.83E-8	1.02E+4	3.30E-8	5.74E-9	3.52E+4	4.95E-09	1.98E-09	3.41E+4	5.18E-09	9.13E-10
1.05E+4	1.63E-7	2.82E-8	1.07E+4	3.95E-8	5.73E-9	3.68E+4	3.50E-09	2.01E-09	3.57E+4	2.99E-09	9.19E-10
1.10E+4	1.70E-7	2.83E-8	1.12E+4	3.35E-8	5.75E-9	3.86E+4	4.94E-09	2.05E-09	3.74E+4	6.11E-09	9.34E-10
1.15E+4	2.04E-7	2.83E-8	1.17E+4	3.17E-8	5.74E-9	4.04E+4	5.52E-09	2.09E-09	3.92E+4	5.49E-09	9.38E-10
1.20E+4	1.81E-7	2.83E-8	1.22E+4	3.97E-8	5.73E-9	4.24E+4	8.56E-09	2.10E-09	4.11E+4	5.46E-09	9.48E-10
1.26E+4	1.04E-7	2.84E-8	1.28E+4	2.51E-8	5.78E-9	4.44E+4	1.28E-08	2.14E-09	4.30E+4	7.49E-09	9.54E-10
1.32E+4	1.40E-7	2.87E-8	1.34E+4	3.17E-8	5.80E-9	4.65E+4	6.17E-09	2.16E-09	4.51E+4	6.83E-09	9.60E-10
1.38E+4	1.82E-7	2.88E-8	1.40E+4	3.50E-8	5.85E-9	4.87E+4	7.34E-09	2.18E-09	4.72E+4	6.33E-09	9.68E-10
1.45E+4	1.51E-7	2.91E-8	1.47E+4	2.52E-8	5.86E-9	5.10E+4	1.02E-08	2.22E-09	4.95E+4	5.99E-09	9.76E-10
1.51E+4	1.29E-7	2.91E-8	1.54E+4	2.40E-8	5.93E-9	5.35E+4	9.46E-09	2.25E-09	5.18E+4	5.98E-09	9.79E-10
1.58E+4	1.40E-7	2.96E-8	1.61E+4	2.40E-8	6.00E-9	5.60E+4	1.26E-08	2.28E-09	5.43E+4	7.80E-09	9.92E-10
1.66E+4	1.12E-7	2.98E-8	1.69E+4	2.85E-8	6.03E-9	5.87E+4	9.84E-09	2.31E-09	5.69E+4	7.55E-09	9.93E-10
1.74E+4	1.82E-7	3.01E-8	1.76E+4	3.13E-8	6.09E-9	6.15E+4	1.13E-08	2.33E-09	5.96E+4	7.15E-09	1.00E-09
1.82E+4	1.93E-7	3.02E-8	1.85E+4	3.35E-8	6.15E-9	6.44E+4	1.45E-08	2.36E-09	6.25E+4	7.01E-09	1.01E-09
1.91E+4	1.61E-7	3.03E-8	1.94E+4	4.19E-8	6.16E-9	6.75E+4	1.76E-08	2.35E-09	6.55E+4	8.54E-09	1.01E-09
2.00E+4	2.41E-7	3.06E-8	2.03E+4	4.39E-8	6.19E-9	7.07E+4	1.56E-08	2.37E-09	6.86E+4	1.03E-08	1.01E-09
2.09E+4	2.35E-7	3.06E-8	2.12E+4	5.44E-8	6.17E-9	7.41E+4	1.89E-08	2.38E-09	7.19E+4	1.02E-08	1.02E-09
2.19E+4	3.00E-7	3.06E-8	2.22E+4	5.93E-8	6.17E-9	7.77E+4	1.57E-08	2.39E-09	7.53E+4	1.04E-08	1.01E-09
2.29E+4	3.09E-7	3.04E-8	2.33E+4	5.86E-8	6.10E-9	8.14E+4	1.45E-08	2.40E-09	7.89E+4	9.43E-09	1.02E-09
2.40E+4	3.65E-7	3.01E-8	2.44E+4	7.83E-8	6.04E-9	8.53E+4	1.38E-08	2.43E-09	8.27E+4	6.01E-09	1.02E-09
2.51E+4	3.52E-7	2.98E-8	2.55E+4	6.23E-8	5.97E-9	8.94E+4	1.52E-08	2.44E-09	8.66E+4	7.84E-09	1.03E-09
2.63E+4	2.62E-7	2.95E-8	2.68E+4	5.04E-8	5.93E-9	9.36E+4	1.06E-08	2.49E-09	9.08E+4	7.18E-09	1.04E-09
2.76E+4	1.88E-7	2.99E-8	2.80E+4	3.33E-8	5.96E-9	9.81E+4	1.51E-08	2.48E-09	9.51E+4	6.29E-09	1.05E-09
2.89E+4	9.37E-8	3.00E-8	2.94E+4	1.35E-8	6.04E-9	1.03E+5	2.05E-08	2.51E-09	9.96E+4	8.83E-09	1.06E-09
3.03E+4	7.44E-8	3.06E-8	3.07E+4	1.28E-8	6.18E-9	1.08E+5	1.59E-08	2.55E-09	1.04E+5	1.02E-08	1.07E-09
3.17E+4	7.98E-8	3.13E-8	3.22E+4	1.69E-8	6.29E-9	1.13E+5	1.85E-08	2.54E-09	1.09E+5	1.28E-08	1.07E-09
3.32E+4	1.49E-7	3.17E-8	3.37E+4	2.48E-8	6.40E-9	1.18E+5	2.95E-08	2.55E-09	1.15E+5	1.34E-08	1.06E-09
3.48E+4	1.71E-7	3.21E-8	3.53E+4	3.76E-8	6.49E-9	1.24E+5	2.79E-08	2.54E-09	1.20E+5	1.49E-08	1.05E-09
3.65E+4	1.84E-7	3.27E-8	3.70E+4	3.52E-8	6.59E-9	1.30E+5	2.08E-08	2.52E-09	1.26E+5	1.29E-08	1.04E-09
3.82E+4	1.97E-7	3.29E-8	3.88E+4	4.26E-8	6.64E-9	1.36E+5	2.05E-08	2.53E-09	1.32E+5	1.02E-08	1.02E-09
4.00E+4	2.27E-7	3.35E-8	4.06E+4	4.06E-8	6.71E-9	1.43E+5	1.48E-08	2.56E-09	1.38E+5	9.28E-09	1.03E-09
4.19E+4	2.34E-7	3.35E-8	4.26E+4	5.07E-8	6.78E-9	1.49E+5	1.87E-08	2.57E-09	1.45E+5	7.72E-09	1.03E-09
4.39E+4	2.56E-7	3.40E-8	4.46E+4	5.55E-8	6.80E-9	1.57E+5	2.43E-08	2.59E-09	1.52E+5	9.55E-09	1.04E-09
4.60E+4	2.78E-7	3.43E-8	4.67E+4	5.68E-8	6.83E-9	1.64E+5	2.19E-08	2.60E-09	1.59E+5	9.98E-09	1.04E-09
4.82E+4	2.55E-7	3.45E-8	4.90E+4	4.64E-8	6.90E-9	1.72E+5	2.16E-08	2.59E-09	1.67E+5	1.06E-08	1.04E-09
5.05E+4	2.75E-7	3.48E-8	5.13E+4	4.25E-8	6.95E-9	1.80E+5	1.85E-08	2.63E-09	1.75E+5	1.02E-08	1.04E-09
5.29E+4	2.00E-7	3.53E-8	5.37E+4	5.43E-8	7.04E-9	1.89E+5	1.47E-08	2.66E-09	1.83E+5	7.32E-09	1.04E-09
5.54E+4	2.09E-7	3.58E-8	5.63E+4	4.88E-8	7.08E-9	1.98E+5	2.12E-08	2.67E-09	1.92E+5	8.50E-09	1.05E-09
5.81E+4	2.72E-7	3.62E-8	5.90E+4	5.10E-8	7.19E-9	2.07E+5	2.26E-08	2.70E-09	2.01E+5	9.95E-09	1.06E-09

Table 3.1.2.1 (Continued-3)

457 mm			610 mm			762 mm			914 mm		
Neutron Energy [eV]	Flux [n/leth/ source]	Absolute Error	Neutron Energy [eV]	Flux [n/leth/ source]	Absolute Error	Neutron Energy [eV]	Flux [n/leth/ source]	Absolute Error	Neutron Energy [eV]	Flux [n/leth/ source]	Absolute Error
6.08E+4	3.27E-7	3.65E-8	6.18E+4	6.17E-8	7.22E-9	2.17E+5	2.24E-08	2.71E-09	2.11E+5	8.84E-09	1.06E-09
6.38E+4	3.25E-7	3.69E-8	6.48E+4	6.43E-8	7.31E-9	2.28E+5	2.11E-08	2.71E-09	2.21E+5	9.59E-09	1.06E-09
6.68E+4	3.17E-7	3.72E-8	6.78E+4	6.06E-8	7.34E-9	2.39E+5	2.65E-08	2.71E-09	2.31E+5	1.13E-08	1.06E-09
7.00E+4	3.52E-7	3.76E-8	7.11E+4	5.87E-8	7.43E-9	2.50E+5	2.41E-08	2.72E-09	2.42E+5	1.13E-08	1.05E-09
7.33E+4	3.48E-7	3.77E-8	7.45E+4	5.76E-8	7.50E-9	2.62E+5	2.37E-08	2.72E-09	2.54E+5	1.32E-08	1.05E-09
7.68E+4	4.00E-7	3.81E-8	7.80E+4	7.27E-8	7.52E-9	2.75E+5	2.77E-08	2.72E-09	2.66E+5	1.24E-08	1.02E-09
8.05E+4	3.19E-7	3.83E-8	8.18E+4	8.45E-8	7.61E-9	2.88E+5	3.55E-08	2.73E-09	2.79E+5	1.38E-08	1.01E-09
8.44E+4	2.70E-7	3.91E-8	8.57E+4	6.67E-8	7.58E-9	3.02E+5	2.44E-08	2.74E-09	2.92E+5	1.31E-08	1.00E-09
8.84E+4	2.91E-7	3.94E-8	8.98E+4	5.43E-8	7.70E-9	3.16E+5	2.64E-08	2.77E-09	3.06E+5	1.12E-08	9.84E-10
9.26E+4	3.19E-7	4.00E-8	9.41E+4	5.39E-8	7.79E-9	3.31E+5	2.73E-08	2.78E-09	3.21E+5	1.04E-08	9.94E-10
9.71E+4	2.83E-7	4.06E-8	9.86E+4	4.99E-8	7.91E-9	3.47E+5	2.63E-08	2.81E-09	3.36E+5	1.01E-08	9.83E-10
1.02E+5	3.32E-7	4.11E-8	1.03E+5	6.46E-8	8.03E-9	3.64E+5	2.15E-08	2.86E-09	3.53E+5	9.03E-09	9.87E-10
1.07E+5	3.68E-7	4.21E-8	1.08E+5	6.65E-8	8.17E-9	3.81E+5	1.87E-08	2.89E-09	3.69E+5	6.51E-09	9.99E-10
1.12E+5	3.55E-7	4.22E-8	1.13E+5	6.47E-8	8.22E-9	3.99E+5	1.69E-08	3.01E-09	3.87E+5	7.34E-09	1.01E-09
1.17E+5	4.67E-7	4.30E-8	1.19E+5	9.75E-8	8.34E-9	4.19E+5	2.18E-08	3.06E-09	4.06E+5	8.95E-09	1.00E-09
1.23E+5	5.44E-7	4.33E-8	1.25E+5	1.05E-7	8.40E-9	4.39E+5	2.68E-08	3.08E-09	4.25E+5	6.78E-09	1.03E-09
1.28E+5	6.33E-7	4.39E-8	1.31E+5	1.08E-7	8.57E-9	4.60E+5	2.32E-08	3.16E-09	4.46E+5	7.00E-09	1.03E-09
1.35E+5	5.41E-7	4.49E-8	1.37E+5	9.27E-8	8.72E-9	4.82E+5	2.06E-08	3.14E-09	4.67E+5	7.19E-09	1.04E-09
1.41E+5	4.50E-7	4.60E-8	1.43E+5	7.91E-8	8.93E-9	5.05E+5	2.50E-08	3.22E-09	4.89E+5	8.00E-09	1.03E-09
1.48E+5	3.25E-7	4.74E-8	1.50E+5	9.14E-8	9.16E-9	5.29E+5	2.10E-08	3.25E-09	5.13E+5	7.50E-09	1.04E-09
1.55E+5	4.55E-7	4.91E-8	1.57E+5	6.97E-8	9.44E-9	5.54E+5	1.77E-08	3.26E-09	5.37E+5	7.43E-09	1.03E-09
1.62E+5	5.04E-7	5.08E-8	1.65E+5	8.51E-8	9.73E-9	5.81E+5	2.48E-08	3.35E-09	5.63E+5	7.06E-09	1.03E-09
1.70E+5	5.54E-7	5.21E-8	1.73E+5	9.20E-8	1.01E-8	6.09E+5	3.34E-08	3.28E-09	5.90E+5	7.87E-09	9.89E-10
1.78E+5	4.98E-7	5.39E-8	1.81E+5	8.56E-8	1.04E-8	6.38E+5	2.43E-08	3.17E-09	6.18E+5	8.41E-09	9.67E-10
1.87E+5	4.07E-7	5.54E-8	1.90E+5	8.22E-8	1.07E-8	6.69E+5	1.69E-08	3.19E-09	6.48E+5	4.54E-09	9.12E-10
1.94E+5	4.60E-7	4.14E-8	1.99E+5	7.72E-8	1.11E-8	7.01E+5	1.61E-08	3.14E-09	6.79E+5	5.00E-09	9.08E-10
2.03E+5	5.22E-7	4.12E-8	2.03E+5	7.68E-8	6.92E-9	7.34E+5	1.41E-08	3.21E-09	7.12E+5	3.70E-09	8.99E-10
2.13E+5	4.26E-7	4.10E-8	2.13E+5	7.76E-8	6.89E-9	7.70E+5	1.48E-08	3.25E-09	7.46E+5	2.80E-09	8.96E-10
2.23E+5	5.03E-7	4.06E-8	2.23E+5	8.81E-8	6.83E-9	8.07E+5	1.12E-08	3.25E-09	7.82E+5	2.85E-09	8.96E-10
2.34E+5	5.34E-7	4.05E-8	2.34E+5	9.78E-8	6.75E-9	8.45E+5	1.26E-08	3.37E-09	8.19E+5	3.02E-09	9.06E-10
2.45E+5	5.62E-7	3.99E-8	2.45E+5	9.64E-8	6.67E-9	8.86E+5	1.13E-08	3.38E-09	8.59E+5	3.26E-09	9.11E-10
2.57E+5	6.68E-7	3.97E-8	2.57E+5	1.10E-7	6.62E-9	9.28E+5	1.08E-08	3.74E-09	9.00E+5	1.12E-09	9.46E-10
2.69E+5	6.79E-7	3.90E-8	2.69E+5	1.26E-7	6.48E-9	9.73E+5	1.11E-08	3.53E-09	9.43E+5	1.99E-09	9.18E-10
2.82E+5	6.49E-7	3.87E-8	2.82E+5	1.25E-7	6.38E-9	1.02E+6	8.04E-09	4.18E-09	9.88E+5	2.81E-09	9.76E-10
2.95E+5	6.72E-7	3.82E-8	2.95E+5	1.10E-7	6.23E-9				1.04E+6	1.10E-09	9.92E-10
3.10E+5	6.57E-7	3.79E-8	3.10E+5	1.03E-7	6.20E-9						
3.24E+5	8.19E-7	3.75E-8	3.24E+5	1.06E-7	6.14E-9						
3.40E+5	7.33E-7	3.73E-8	3.40E+5	1.20E-7	6.12E-9						
3.56E+5	6.18E-7	3.72E-8	3.56E+5	9.99E-8	6.09E-9						
3.73E+5	4.73E-7	3.75E-8	3.73E+5	9.00E-8	6.10E-9						
3.91E+5	4.61E-7	3.78E-8	3.91E+5	9.15E-8	6.14E-9						
4.10E+5	6.13E-7	3.82E-8	4.10E+5	9.34E-8	6.13E-9						
4.30E+5	6.47E-7	3.83E-8	4.30E+5	9.67E-8	6.17E-9						
4.50E+5	7.24E-7	3.85E-8	4.50E+5	1.11E-7	6.18E-9						
4.72E+5	7.13E-7	3.88E-8	4.72E+5	1.18E-7	6.26E-9						
4.94E+5	6.92E-7	3.95E-8	4.94E+5	1.12E-7	6.32E-9						
5.18E+5	7.64E-7	4.00E-8	5.18E+5	1.22E-7	6.33E-9						
5.43E+5	8.00E-7	4.03E-8	5.43E+5	1.36E-7	6.37E-9						
5.69E+5	9.00E-7	4.05E-8	5.69E+5	1.47E-7	6.30E-9						
5.96E+5	9.25E-7	4.02E-8	5.96E+5	1.40E-7	6.25E-9						
6.25E+5	8.30E-7	4.00E-8	6.25E+5	1.21E-7	6.11E-9						
6.55E+5	7.35E-7	3.97E-8	6.55E+5	1.04E-7	6.11E-9						
6.86E+5	7.06E-7	3.99E-8	6.86E+5	8.90E-8	6.02E-9						
7.19E+5	5.40E-7	3.99E-8	7.19E+5	8.44E-8	6.09E-9						
7.54E+5	5.33E-7	4.06E-8	7.54E+5	8.72E-8	6.06E-9						
7.90E+5	5.90E-7	4.08E-8	7.90E+5	7.12E-8	6.08E-9						
8.28E+5	5.58E-7	4.13E-8	8.28E+5	7.95E-8	6.12E-9						
8.68E+5	5.52E-7	4.12E-8	8.68E+5	8.05E-8	6.08E-9						
9.09E+5	5.98E-7	4.16E-8	9.09E+5	6.64E-8	6.09E-9						
9.53E+5	4.86E-7	4.10E-8	9.53E+5	6.36E-8	6.02E-9						
9.98E+5	5.03E-7	4.14E-8	9.98E+5	6.62E-8	6.07E-9						
1.05E+6	5.39E-7	4.06E-8	1.05E+6	7.40E-8	5.92E-9						

Table 3.1.3.1 Properties of resonance filters used in the slowing down time method.

Material	Resonance Energy [eV]	Thickness [mm]	Form
In	1.46	0.5	Foil
W	4.15	0.2	Foil
Au	4.906	0.2	Foil
Co	132.	0.4	Foil
Mn	336.	1.8, 60 % density	Powder

Table 3.1.3.2 Comparison of measured and calculated slowing down time.

Position [mm]	Filter	Energy [eV]	Expt. [μs]	Calc. [μs]	C/E
127	Au	4.906	8.5	8.3	0.98
229	Au	4.906	8.4	8.3	0.99
330	Au	4.906	8.9	8.3	1.07
457	Au	4.906	11.4	12.5	1.10
610	Au	4.906	11.8	12.5	1.06
762	Au	4.906	-	14.8	-

Table 3.1.3.3 Neutron spectra at 127, 229, 330, 457, 610 and 762 mm from the front surface of the test region measured by the slowing down time method.

	127 mm			229 mm			330 mm		
Neutron Energy [eV]	Flux [n/leth/ source]	Absolute Error	FWHM [%]	Flux [n/leth/ source]	Absolute Error	FWHM [%]	Flux [n/leth/ source]	Absolute Error	FWHM [%]
thermal	2.69E-07	3.06E-08	——	1.31E-07	1.40E-08	——	5.41E-08	5.62E-09	——
4.22E-01	1.06E-06	6.72E-08	294.6	5.90E-07	3.73E-08	256.4	2.03E-07	1.30E-08	278.9
7.50E-01	1.80E-06	1.19E-07	272.1	7.42E-07	4.93E-08	241.2	2.59E-07	1.72E-08	233.4
1.33E+00	1.82E-06	1.30E-07	320.6	9.04E-07	6.43E-08	242.4	3.25E-07	2.31E-08	237.3
2.37E+00	2.89E-06	2.27E-07	425.4	1.36E-06	1.09E-07	227.4	4.76E-07	3.85E-08	230.4
4.22E+00	2.93E-06	2.70E-07	353.4	1.30E-06	1.21E-07	237.7	4.61E-07	4.33E-08	241.0
7.50E+00	3.10E-06	3.59E-07	236.0	1.44E-06	1.63E-07	233.2	5.11E-07	5.85E-08	230.8
1.33E+01	3.14E-06	4.46E-07	267.5	1.45E-06	2.07E-07	246.7	4.88E-07	7.05E-08	243.0
2.37E+01	2.96E-06	5.43E-07	255.4	1.42E-06	2.59E-07	241.2	4.49E-07	8.02E-08	246.6
4.22E+01	3.39E-06	7.89E-07	275.4	1.52E-06	3.52E-07	249.0	5.72E-07	1.32E-07	241.6
7.50E+01	2.89E-06	8.25E-07	554.1	1.64E-06	4.90E-07	261.7	5.19E-07	1.57E-07	264.7
1.33E+02	3.29E-06	1.24E-06	625.9	1.48E-06	5.82E-07	287.8	4.92E-07	1.95E-07	288.3
2.37E+02	3.54E-06	1.60E-06	1126.1	1.02E-06	5.23E-07	348.3	4.31E-07	2.22E-07	320.6

	457 mm			610 mm			762 mm		
Neutron Energy [eV]	Flux [n/leth/ source]	Absolute Error	FWHM [%]	Flux [n/leth/ source]	Absolute Error	FWHM [%]	Flux [n/leth/ source]	Absolute Error	FWHM [%]
thermal	2.83E-09	2.91E-10	——	5.88E-10	6.06E-11	——	8.29E-11	8.54E-12	——
4.22E-01	2.56E-08	1.58E-09	200.4	4.83E-09	3.88E-10	203.4	6.91E-10	7.35E-11	213.1
7.50E-01	4.51E-08	2.89E-09	183.1	7.90E-09	6.26E-10	184.8	1.40E-09	1.32E-10	197.7
1.33E+00	4.94E-08	3.55E-09	172.8	1.21E-08	1.01E-09	178.1	2.08E-09	1.98E-10	173.8
2.37E+00	8.93E-08	7.37E-09	171.2	1.54E-08	1.44E-09	172.3	3.43E-09	3.40E-10	174.8
4.22E+00	8.50E-08	8.65E-09	180.3	1.81E-08	2.00E-09	177.6	3.02E-09	3.61E-10	187.5
7.50E+00	1.05E-07	1.31E-08	176.7	1.89E-08	2.63E-09	176.6	3.20E-09	4.63E-10	187.3
1.33E+01	1.09E-07	1.79E-08	186.1	2.11E-08	3.57E-09	186.3	3.99E-09	6.79E-10	192.3
2.37E+01	1.12E-07	2.32E-08	186.2	2.35E-08	5.02E-09	189.9	4.57E-09	9.48E-10	198.3
4.22E+01	1.15E-07	3.09E-08	186.1	2.46E-08	6.77E-09	184.7	4.78E-09	1.24E-09	199.1
7.50E+01	1.25E-07	4.45E-08	189.4	2.86E-08	1.00E-08	185.7	5.85E-09	1.90E-09	200.4
1.33E+02	1.43E-07	6.64E-08	211.7	2.88E-08	1.32E-08	207.9	4.86E-09	2.03E-09	248.3
2.37E+02	1.44E-07	8.57E-08	229.1	2.98E-08	1.76E-08	233.4	4.97E-09	2.61E-09	262.4

Table 3.2.1.1 Properties of dosimetry reactions.

(a) γ-Activation

Reactions	Half-Life	Abundance [%]	γ-ray Energy [keV]	γ-ray Branching [%]	Threshold Energy [MeV]
$^{27}Al(n,\alpha)^{24}Na$	15.02 h	100.0	1368.6	100.0	5
$^{93}Nb(n,2n)^{92m}Nb$	10.15 d	100.0	934.5	99.0	9
$^{115}In(n,n')^{115m}In$	4.486 h	95.7	336.3	45.8	0.34
$^{197}Au(n,\gamma)^{198}Au$	2.694 d	100.0	411.8	95.5	--------

(b) β-Activation

Reactions	Half-Life	Abundance [%]	Max. Energy of β-ray [keV]	β-ray Branching [%]	Threshold Energy [MeV]
$^{32}S(n,p)^{32}P$	14.29 d	95.00	1710	100.0	2

Table 3.2.1.2 Size of natural metal foils used in γ-activation.

Position [mm]	Al	Nb	In	Au
Front Surface	10 ϕ x 1	10 ϕ x 1	10 x 10 x 1	10 x 10 x 0.001
127	10 ϕ x 1	10 ϕ x 1	10 x 10 x 1	10 x 10 x 0.001
229	10 ϕ x 1	10 ϕ x 1	10 x 10 x 1	10 x 10 x 0.001
330	10 ϕ x 1	10 ϕ x 1	10 x 10 x 1	10 x 10 x 0.001
457	10 ϕ x 1	20 ϕ x 1	15 x 15 x 1	10 x 10 x 0.001
610	45 x 45 x 3	45 x 45 x 2	45 x 45 x 1.5	45 x 45 x 0.001
762	45 x 45 x 9	45 x 45 x 6	45 x 45 x 3	45 x 45 x 0.001
914	45 x 45 x 9	45 x 45 x 8	45 x 45 x 4	45 x 45 x 0.001

(Unit : mm)

Table 3.2.1.3 Measured neutron activation reaction rates in γ-activation.

Distance from the front surface of the test region [mm]	$^{27}Al(n,\alpha)^{24}Na$ Reaction Rate [1/source]	Absolute Error	$^{93}Nb(n,2n)^{92m}Nb$ Reaction Rate [1/source]	Absolute Error	$^{115}In(n,n')^{115m}In$ Reaction Rate [1/source]	Absolute Error	$^{197}Au(n,\gamma)^{198}Au$ Reaction Rate [1/source]	Absolute Error
-1	1.10E-29	3.32E-31	4.45E-29	1.33E-30	1.88E-29	5.44E-31	5.32E-28	1.61E-29
127	1.88E-30	6.05E-32	6.97E-30	2.18E-31	8.08E-30	2.37E-31	4.55E-28	1.39E-29
229	4.19E-31	1.48E-32	1.52E-30	5.10E-32	2.41E-30	7.23E-32	2.18E-28	6.84E-30
330	9.53E-32	3.42E-33	3.39E-31	1.07E-32	6.27E-31	2.10E-32	7.76E-29	2.52E-30
457	————	————	5.04E-32	2.54E-33	1.16E-31	4.76E-33	1.41E-29	4.58E-31
610	1.36E-33	4.40E-35	4.74E-33	1.45E-34	1.27E-32	4.13E-34	2.83E-30	1.19E-31
762	1.36E-34	5.73E-36	4.75E-34	1.59E-35	1.40E-33	5.20E-35	4.68E-31	2.39E-32
914	1.06E-35	8.51E-37	4.11E-35	2.92E-36	2.19E-34	1.07E-35	7.80E-32	4.13E-33

Table 3.2.1.4 Some characteristics of dimethyl sulfone, $CH_3SO_2CH_3$.

Purity (%)	Density (g/cm^3) theoretical	Density (g/cm^3) experiment* (apparent)	Sulfur density (x10^{21} atoms/g)	Solubility (g/100 ml H_2O)
99.9	1.17	0.77	6.398	20.4

Sulfur isotopic content		
^{32}S - 95.0%;	^{33}S - 0.76%;	^{34}S - 4.22%

* The sample was made from powder without pressing.

Table 3.2.1.5 Characteristics of the sulfur samples and their position in the assembly.

Position (mm)	Dimentions (mm^3)	Weight (g)
-0.5	21 x 21 x 1	0.341
126	99 x 34 x 1.5	3.60
228	99 x 34 x 1.5	3.62
329	99 x 34 x 1.5	3.61
457	99 x 49 x 4	15.1
610	99 x 49 x 4	15.0
762	99 x 49 x 4	15.1
914	99 x 49 x 8	30.2

Table 3.2.1.6 Experimental errors for $^{32}S(n,p)^{32}P$ reaction rate.

Source	Systematic error (%)	Random error (%)
Neutron yield	2	0.1
Sample position	negligible	0.5
β-ray counting statistics	-	0.1 - 6
β- ray detector efficiency	2.5*	negligible
Half -life	0.14	-
Sample weight	negligible	0.5
^{32}S atom number	2	-

* Accuracy of standard solution

Table 3.2.1.7 Measured $^{32}S(n,p)^{32}P$ reaction rate.

Distance from the front surface of the test region [mm]	Reaction Rate [1/source]	Absolute Error
-1	2.69E-29	1.02E-30
127	6.26E-30	2.38E-31
229	1.53E-30	5.81E-32
330	3.66E-31	1.39E-32
457	5.74E-32	2.18E-33
610	6.06E-33	2.55E-34
762	6.99E-34	4.12E-35
914	1.43E-34	5.46E-35

Table 3.2.2.1 Measured fission rates.

Distance from the front surface of the test region [mm]	^{235}U(n,fission) Fission Rate [1/source]	Absolute Error	^{238}U(n,fission) Fission Rate [1/source]	Absolute Error
-4	4.77E-27	1.74E-28	1.38E-28	5.12E-30
127	2.40E-27	8.78E-29	2.92E-29	1.13E-30
229	9.92E-28	3.62E-29	6.97E-30	2.90E-31
330	3.63E-28	1.33E-29	1.67E-30	7.87E-32
457	4.39E-29	1.61E-30	2.84E-31	1.75E-32
610	8.84E-30	3.25E-31	3.32E-32	2.96E-33
762	1.55E-30	5.98E-32	3.86E-33	1.01E-33
914	3.21E-31	1.38E-32	1.38E-33	4.63E-34

Table 3.2.3.1 Measured ^{10}B(n,α) reaction rate.

Distance from the front surface of the test region [mm]	Reaction Rate [1/source]	Absolute Error
-7	2.99E-26	1.30E-27
127	1.60E-26	6.86E-28
229	6.60E-27	2.69E-28
330	2.41E-27	9.60E-29
457	2.49E-28	9.58E-30
610	4.79E-29	1.80E-30
762	8.34E-30	3.08E-31
914	9.80E-31	3.80E-32

Table 3.3.1 Gamma-ray spectra at 457, 610, 762 and 914 mm from the front surface of the test region measured by the BC537 spectrometer.

	457 mm			610 mm			762 mm			914 mm		
Gamma-ray Energy [MeV]	Flux [n/leth/ source]	Absolute Error	Window [%]	Flux [n/leth/ source]	Absolute Error	Window [%]	Flux [n/leth/ source]	Absolute Error	Wimdow [%]	Flux [n/leth/ source]	Absolute Error	Window [%]
2.51E-1	3.88E-07	8.31E-08	30.9	7.09E-08	1.32E-08	30.9	1.12E-08	2.20E-09	30.9	1.39E-09	2.57E-10	30.9
2.63E-1	4.73E-07	6.91E-08	30.4	8.26E-08	1.11E-08	30.4	1.33E-08	1.83E-09	30.3	1.62E-09	2.14E-10	30.4
2.75E-1	5.35E-07	4.46E-08	29.8	8.89E-08	7.17E-09	29.9	1.46E-08	1.18E-09	29.8	1.74E-09	1.39E-10	29.9
2.88E-1	5.63E-07	2.58E-08	29.5	8.96E-08	4.11E-09	29.6	1.50E-08	6.78E-10	29.5	1.74E-09	7.89E-11	29.6
3.02E-1	5.61E-07	2.63E-08	29.2	8.68E-08	4.11E-09	29.3	1.46E-08	6.86E-10	29.2	1.66E-09	7.87E-11	29.3
3.16E-1	5.42E-07	2.82E-08	28.8	8.33E-08	4.43E-09	29.0	1.39E-08	7.34E-10	28.9	1.57E-09	8.46E-11	29.0
3.31E-1	5.19E-07	2.68E-08	28.7	8.07E-08	4.24E-09	28.9	1.33E-08	7.00E-10	28.9	1.51E-09	8.05E-11	29.0
3.47E-1	5.01E-07	2.52E-08	28.7	7.89E-08	3.99E-09	28.8	1.29E-08	6.56E-10	28.8	1.47E-09	7.57E-11	28.9
3.63E-1	4.90E-07	2.45E-08	28.4	7.78E-08	3.87E-09	28.5	1.27E-08	6.37E-10	28.6	1.45E-09	7.38E-11	28.6
3.80E-1	4.89E-07	2.52E-08	28.0	7.79E-08	4.00E-09	28.0	1.27E-08	6.63E-10	28.1	1.44E-09	7.64E-11	28.2
3.98E-1	5.02E-07	2.63E-08	27.1	8.00E-08	4.21E-09	27.1	1.30E-08	6.97E-10	27.3	1.47E-09	7.99E-11	27.5
4.17E-1	5.39E-07	2.75E-08	26.0	8.59E-08	4.41E-09	26.0	1.39E-08	7.33E-10	26.2	1.57E-09	8.24E-11	26.5
4.37E-1	6.06E-07	2.83E-08	24.8	9.71E-08	4.55E-09	24.7	1.59E-08	7.52E-10	24.8	1.76E-09	8.43E-11	25.2
4.57E-1	6.95E-07	3.02E-08	23.6	1.13E-07	4.87E-09	23.4	1.89E-08	8.23E-10	23.3	2.07E-09	9.53E-11	23.7
4.79E-1	7.75E-07	3.51E-08	22.7	1.28E-07	5.74E-09	22.5	2.19E-08	9.94E-10	22.1	2.42E-09	1.13E-10	22.4
5.01E-1	7.99E-07	3.56E-08	22.7	1.32E-07	5.79E-09	22.5	2.33E-08	9.83E-10	21.9	2.66E-09	1.09E-10	22.0
5.25E-1	7.41E-07	3.11E-08	23.5	1.21E-07	5.03E-09	23.2	2.18E-08	8.79E-10	22.5	2.63E-09	1.06E-10	22.2
5.49E-1	6.18E-07	3.23E-08	24.4	1.01E-07	5.28E-09	24.1	1.79E-08	9.45E-10	23.5	2.29E-09	1.16E-10	23.1
5.75E-1	4.80E-07	2.85E-08	25.4	8.06E-08	4.62E-09	25.2	1.32E-08	7.79E-10	24.7	1.78E-09	9.37E-11	24.3
6.03E-1	3.81E-07	2.41E-08	26.2	6.61E-08	3.93E-09	26.1	9.72E-09	6.57E-10	25.9	1.34E-09	8.31E-11	25.5
6.31E-1	3.43E-07	2.29E-08	26.5	5.86E-08	3.67E-09	26.5	8.26E-09	6.16E-10	26.4	1.11E-09	7.60E-11	26.0
6.61E-1	3.55E-07	2.03E-08	25.9	5.68E-08	3.14E-09	26.2	8.44E-09	5.09E-10	26.0	1.08E-09	6.10E-11	25.8
6.92E-1	3.91E-07	2.03E-08	25.1	5.88E-08	3.06E-09	25.5	9.38E-09	4.95E-10	25.2	1.16E-09	5.92E-11	24.9
7.24E-1	4.34E-07	2.11E-08	24.0	6.29E-08	3.13E-09	24.6	1.05E-08	5.08E-10	24.2	1.28E-09	6.02E-11	23.8
7.59E-1	4.79E-07	2.22E-08	22.7	6.81E-08	3.27E-09	23.4	1.16E-08	5.30E-10	23.1	1.38E-09	6.16E-11	22.8
7.94E-1	5.25E-07	2.40E-08	21.7	7.48E-08	3.44E-09	22.3	1.23E-08	5.66E-10	22.1	1.43E-09	6.44E-11	22.1
8.32E-1	5.59E-07	2.41E-08	21.3	8.14E-08	3.52E-09	21.7	1.27E-08	5.66E-10	21.8	1.42E-09	6.42E-11	22.2
8.71E-1	5.55E-07	2.50E-08	21.5	8.40E-08	3.80E-09	21.5	1.23E-08	5.72E-10	22.1	1.34E-09	6.23E-11	22.6
9.12E-1	5.01E-07	2.49E-08	22.4	7.84E-08	3.74E-09	22.1	1.13E-08	5.74E-10	22.9	1.21E-09	6.25E-11	23.5
9.55E-1	4.15E-07	2.04E-08	23.5	6.64E-08	3.19E-09	23.1	9.84E-09	4.92E-10	23.8	1.05E-09	5.39E-11	24.4
1.00E+0	3.41E-07	1.89E-08	24.6	5.50E-08	2.97E-09	24.1	8.45E-09	4.52E-10	24.7	9.17E-10	4.86E-11	25.1
1.05E+0	3.03E-07	1.71E-08	25.1	4.89E-08	2.68E-09	24.9	7.57E-09	4.18E-10	25.3	8.44E-10	4.61E-11	25.5
1.10E+0	2.99E-07	1.63E-08	25.1	4.75E-08	2.57E-09	25.4	7.24E-09	3.99E-10	25.6	8.21E-10	4.41E-11	25.7
1.15E+0	3.15E-07	1.61E-08	24.4	4.79E-08	2.44E-09	25.4	7.28E-09	3.85E-10	25.5	8.26E-10	4.30E-11	25.6
1.20E+0	3.38E-07	1.64E-08	23.5	4.87E-08	2.39E-09	25.1	7.54E-09	3.80E-10	25.2	8.44E-10	4.26E-11	25.5
1.26E+0	3.60E-07	1.73E-08	22.5	4.96E-08	2.41E-09	24.7	7.92E-09	3.87E-10	24.8	8.68E-10	4.33E-11	25.3
1.32E+0	3.73E-07	1.80E-08	21.6	5.06E-08	2.45E-09	24.2	8.28E-09	3.98E-10	24.5	8.92E-10	4.42E-11	25.0
1.38E+0	3.74E-07	1.84E-08	21.1	5.15E-08	2.49E-09	23.7	8.45E-09	4.05E-10	24.2	9.11E-10	4.48E-11	24.6
1.45E+0	3.69E-07	1.83E-08	20.9	5.23E-08	2.52E-09	23.1	8.37E-09	4.03E-10	24.0	9.27E-10	4.52E-11	24.2
1.51E+0	3.62E-07	1.80E-08	21.1	5.29E-08	2.54E-09	22.8	8.19E-09	3.96E-10	24.0	9.45E-10	4.55E-11	23.9
1.59E+0	3.51E-07	1.75E-08	21.5	5.31E-08	2.55E-09	22.6	8.07E-09	3.93E-10	24.1	9.63E-10	4.58E-11	23.6
1.66E+0	3.35E-07	1.69E-08	22.2	5.27E-08	2.57E-09	22.9	8.06E-09	3.95E-10	24.2	9.76E-10	4.66E-11	23.5
1.74E+0	3.17E-07	1.65E-08	22.9	5.16E-08	2.56E-09	23.4	8.10E-09	4.00E-10	24.4	9.76E-10	4.73E-11	23.8
1.82E+0	3.05E-07	1.58E-08	23.5	4.97E-08	2.53E-09	24.0	8.12E-09	4.03E-10	24.6	9.55E-10	4.75E-11	24.2
1.91E+0	2.99E-07	1.55E-08	23.6	4.79E-08	2.49E-09	24.4	8.05E-09	4.04E-10	24.7	9.18E-10	4.70E-11	24.7
2.00E+0	2.99E-07	1.51E-08	23.5	4.73E-08	2.44E-09	24.4	7.94E-09	4.01E-10	24.8	8.85E-10	4.61E-11	25.2
2.09E+0	3.06E-07	1.51E-08	23.3	4.84E-08	2.42E-09	24.2	7.90E-09	3.99E-10	24.7	8.73E-10	4.53E-11	25.5
2.19E+0	3.14E-07	1.53E-08	23.0	5.04E-08	2.47E-09	23.9	8.02E-09	4.04E-10	24.5	8.85E-10	4.57E-11	25.5
2.29E+0	3.16E-07	1.53E-08	23.2	5.15E-08	2.50E-09	23.8	8.24E-09	4.08E-10	24.5	9.10E-10	4.63E-11	25.2
2.40E+0	3.08E-07	1.50E-08	23.7	5.07E-08	2.47E-09	24.1	8.40E-09	4.09E-10	24.6	9.44E-10	4.68E-11	24.8
2.51E+0	2.93E-07	1.48E-08	24.3	4.83E-08	2.45E-09	24.5	8.36E-09	4.14E-10	24.8	9.80E-10	4.78E-11	24.3
2.63E+0	2.82E-07	1.47E-08	25.0	4.62E-08	2.46E-09	25.1	8.13E-09	4.17E-10	25.1	1.01E-09	4.91E-11	23.9
2.75E+0	2.77E-07	1.44E-08	25.5	4.52E-08	2.44E-09	25.5	7.85E-09	4.15E-10	25.5	1.03E-09	5.00E-11	23.8
2.88E+0	2.79E-07	1.41E-08	25.7	4.51E-08	2.41E-09	25.7	7.68E-09	4.12E-10	25.7	1.03E-09	5.01E-11	24.2

Table 3.3.1 (Continued)

	457 mm			610 mm			762 mm			914 mm		
Gamma-ray Energy [eV]	Flux [n/leth/ source]	Absolute Error	Window [%]	Flux [n/leth/ source]	Absolute Error	Window [%]	Flux [n/leth/ source]	Absolute Error	Wimdow [%]	Flux [n/leth/ source]	Absolute Error	Window [%]
3.02E+0	2.86E-07	1.43E-08	25.7	4.54E-08	2.45E-09	25.7	7.65E-09	4.19E-10	25.7	1.00E-09	5.03E-11	24.6
3.16E+0	2.95E-07	1.52E-08	25.7	4.60E-08	2.61E-09	25.7	7.69E-09	4.46E-10	25.7	9.71E-10	5.24E-11	25.1
3.31E+0	3.01E-07	1.66E-08	25.7	4.70E-08	2.85E-09	25.7	7.75E-09	4.88E-10	25.7	9.58E-10	5.61E-11	25.5
3.47E+0	3.04E-07	1.73E-08	25.7	4.81E-08	2.97E-09	25.7	7.86E-09	5.12E-10	25.7	9.73E-10	5.82E-11	25.7
3.63E+0	3.03E-07	1.63E-08	25.7	4.98E-08	2.83E-09	25.7	8.07E-09	4.90E-10	25.7	1.01E-09	5.50E-11	25.7
3.80E+0	3.02E-07	1.67E-08	25.7	5.21E-08	2.91E-09	25.7	8.52E-09	5.01E-10	25.7	1.03E-09	5.52E-11	25.7
3.98E+0	3.04E-07	2.29E-08	25.7	5.44E-08	3.91E-09	25.7	9.20E-09	6.78E-10	25.7	1.03E-09	7.45E-11	25.7
4.17E+0	3.06E-07	2.86E-08	25.7	5.52E-08	4.87E-09	25.7	9.78E-09	8.49E-10	25.7	1.02E-09	9.39E-11	25.7
4.36E+0	3.06E-07	2.66E-08	25.7	5.39E-08	4.60E-09	25.7	9.76E-09	8.02E-10	25.7	1.01E-09	8.95E-11	25.7
4.57E+0	3.02E-07	2.10E-08	25.7	5.18E-08	3.67E-09	25.7	9.07E-09	6.36E-10	25.7	1.05E-09	7.38E-11	25.7
4.79E+0	2.95E-07	2.04E-08	25.7	5.12E-08	3.67E-09	25.7	8.37E-09	6.34E-10	25.7	1.13E-09	7.53E-11	25.7
5.01E+0	2.90E-07	2.17E-08	25.7	5.32E-08	4.03E-09	25.7	8.55E-09	7.04E-10	25.7	1.17E-09	7.74E-11	25.7
5.25E+0	2.94E-07	2.57E-08	25.7	5.62E-08	4.43E-09	25.7	9.68E-09	7.91E-10	25.7	1.13E-09	7.97E-11	25.7
5.49E+0	3.08E-07	2.81E-08	25.7	5.74E-08	4.70E-09	25.7	1.08E-08	8.46E-10	25.7	1.05E-09	8.31E-11	25.7
5.75E+0	3.22E-07	2.52E-08	25.7	5.64E-08	4.39E-09	25.7	1.07E-08	7.86E-10	25.7	9.97E-10	7.17E-11	25.7
6.03E+0	3.23E-07	2.61E-08	25.7	5.52E-08	4.18E-09	25.7	9.73E-09	7.60E-10	25.7	1.03E-09	5.69E-11	25.4
6.31E+0	3.13E-07	2.54E-08	25.7	5.56E-08	3.79E-09	25.5	8.88E-09	7.06E-10	25.7	1.10E-09	5.04E-11	24.1
6.61E+0	3.09E-07	2.10E-08	25.5	5.77E-08	3.25E-09	24.4	8.95E-09	5.98E-10	24.7	1.15E-09	5.46E-11	22.4
6.92E+0	3.29E-07	2.03E-08	24.0	6.30E-08	3.19E-09	22.5	1.01E-08	5.66E-10	22.7	1.24E-09	6.45E-11	20.6
7.24E+0	3.80E-07	2.07E-08	21.9	7.47E-08	3.61E-09	20.1	1.26E-08	6.28E-10	20.3	1.42E-09	7.93E-11	19.2
7.59E+0	4.50E-07	2.05E-08	19.7	9.06E-08	4.05E-09	17.6	1.58E-08	6.94E-10	17.9	1.59E-09	8.16E-11	19.2
7.94E+0	5.00E-07	2.06E-08	17.5	9.93E-08	3.92E-09	15.7	1.73E-08	6.78E-10	15.9	1.60E-09	8.47E-11	20.4
8.32E+0	4.89E-07	2.13E-08	16.2	9.05E-08	3.82E-09	15.4	1.55E-08	6.71E-10	15.8	1.41E-09	8.68E-11	22.1
8.71E+0	4.19E-07	1.92E-08	17.1	6.92E-08	3.26E-09	17.3	1.20E-08	5.62E-10	17.7	1.13E-09	9.95E-11	23.9
9.12E+0	3.33E-07	1.62E-08	19.1	4.92E-08	2.60E-09	19.8	9.00E-09	4.61E-10	20.1	8.45E-10	1.21E-10	25.4
9.55E+0	2.52E-07	1.39E-08	21.4	3.52E-08	2.16E-09	22.3	6.80E-09	4.81E-10	22.5	5.99E-10	1.30E-10	25.7
1.00E+1	1.72E-07	1.19E-08	23.5	2.40E-08	1.71E-09	24.5	4.84E-09	4.93E-10	24.5	3.95E-10	1.20E-10	25.7
1.05E+1	1.00E-07	9.74E-09	25.2	1.54E-08	1.29E-09	25.7	3.05E-09	4.25E-10	25.7	2.35E-10	7.38E-11	25.7
1.10E+1	5.19E-08	7.19E-09	25.7	9.34E-09	9.08E-10	25.7	1.66E-09	2.67E-10	25.7	1.27E-10	7.35E-11	25.7
1.15E+1	2.64E-08	4.69E-09	25.7	5.36E-09	6.05E-10	25.7	8.03E-10	1.18E-10	25.7	6.98E-11	1.16E-10	25.7
1.20E+1	1.48E-08	3.61E-09	25.7	2.88E-09	4.09E-10	25.7	3.69E-10	2.38E-10	25.7	4.60E-11	1.34E-10	25.7
1.26E+1	8.77E-09	3.69E-09	25.7	1.47E-09	3.03E-10	25.7	1.66E-10	2.80E-10	25.7	3.41E-11	1.18E-10	25.7
1.32E+1	4.67E-09	3.11E-09	25.7	7.06E-10	2.13E-10	25.7	6.95E-11	2.22E-10	25.7	2.25E-11	7.58E-11	25.7
1.38E+1	2.00E-09	1.89E-09	25.7	2.95E-10	1.20E-10	25.7	2.44E-11	1.24E-10	25.7	1.15E-11	3.62E-11	25.7
1.44E+1	6.46E-10	8.03E-10	25.7	9.86E-11	4.92E-11	25.7	6.69E-12	4.87E-11	25.7	4.30E-12	1.26E-11	25.7
1.51E+1	1.51E-10	2.33E-10	25.7	2.44E-11	1.41E-11	25.7	1.35E-12	1.33E-11	25.7	1.13E-12	3.28E-12	25.7

Table 3.4.1 Neutron irradiation data for TLD.

Irradiation No	TLD Position [mm]	Irradiation Time [minutes]	Neutron Yield [n/sec]	Additional Shield
#1	-1, 127, 229, 330	10	1.56×10^{14}	without
#2	457, 610	285	4.89×10^{15}	without
#3	762, 914	600	8.65×10^{15}	with

Table 3.4.2 Measured gamma-ray heating rates of SS316 by the TLD.

Distance from the front surface of the test region [mm]	Gamma-ray Heating Rate [Gy/Source Neutron]	Absolute Error
-1	1.12E-15	2.60E-16
127	5.27E-16	4.15E-17
229	1.90E-16	2.78E-17
330	5.62E-17	6.63E-18
457	9.26E-18	8.24E-19
610	1.58E-18	1.09E-19
762	2.57E-19	2.58E-20
914	3.02E-20	6.35E-21

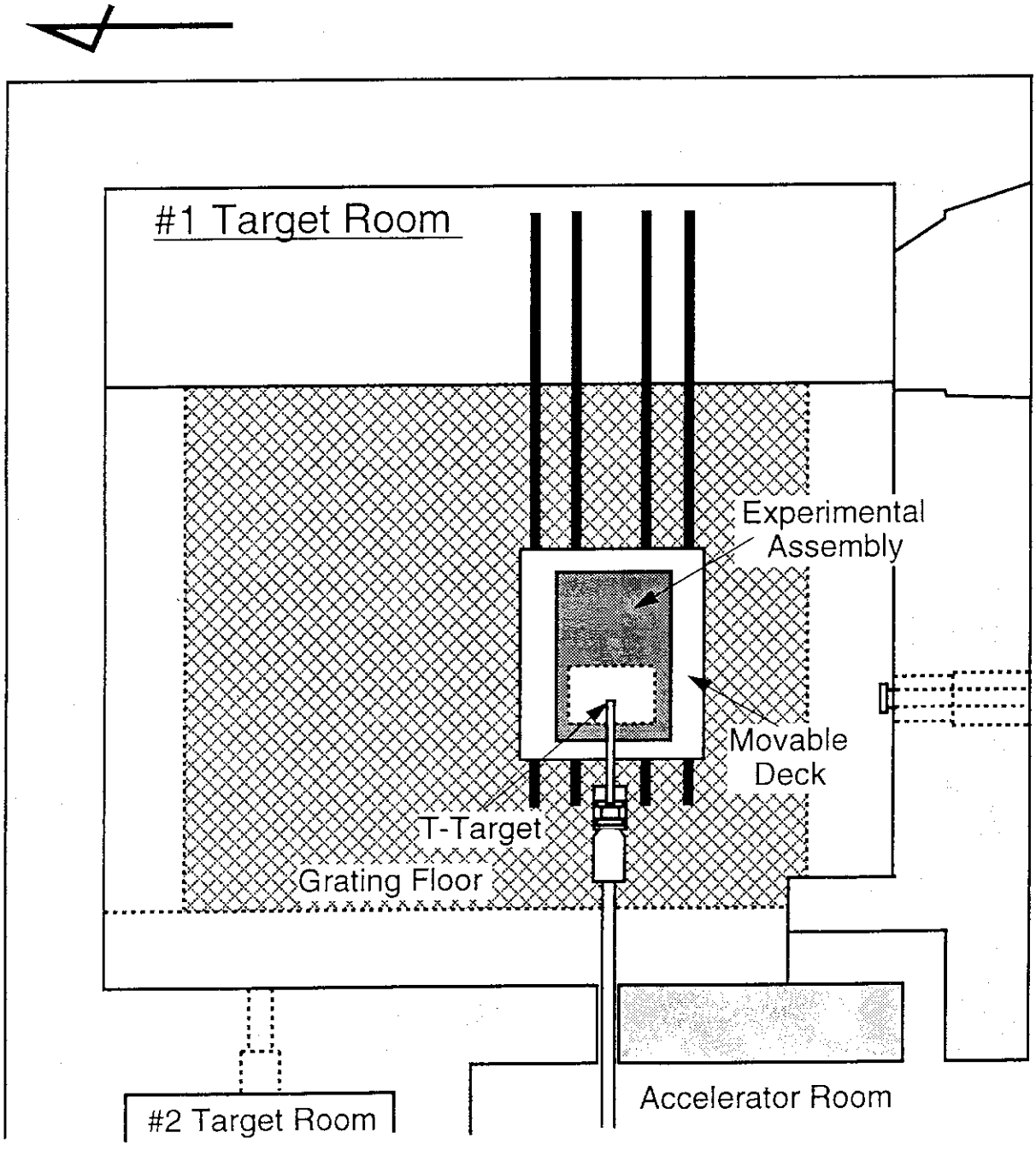

Fig. 2.1.1 Layout of the FNS first target room.

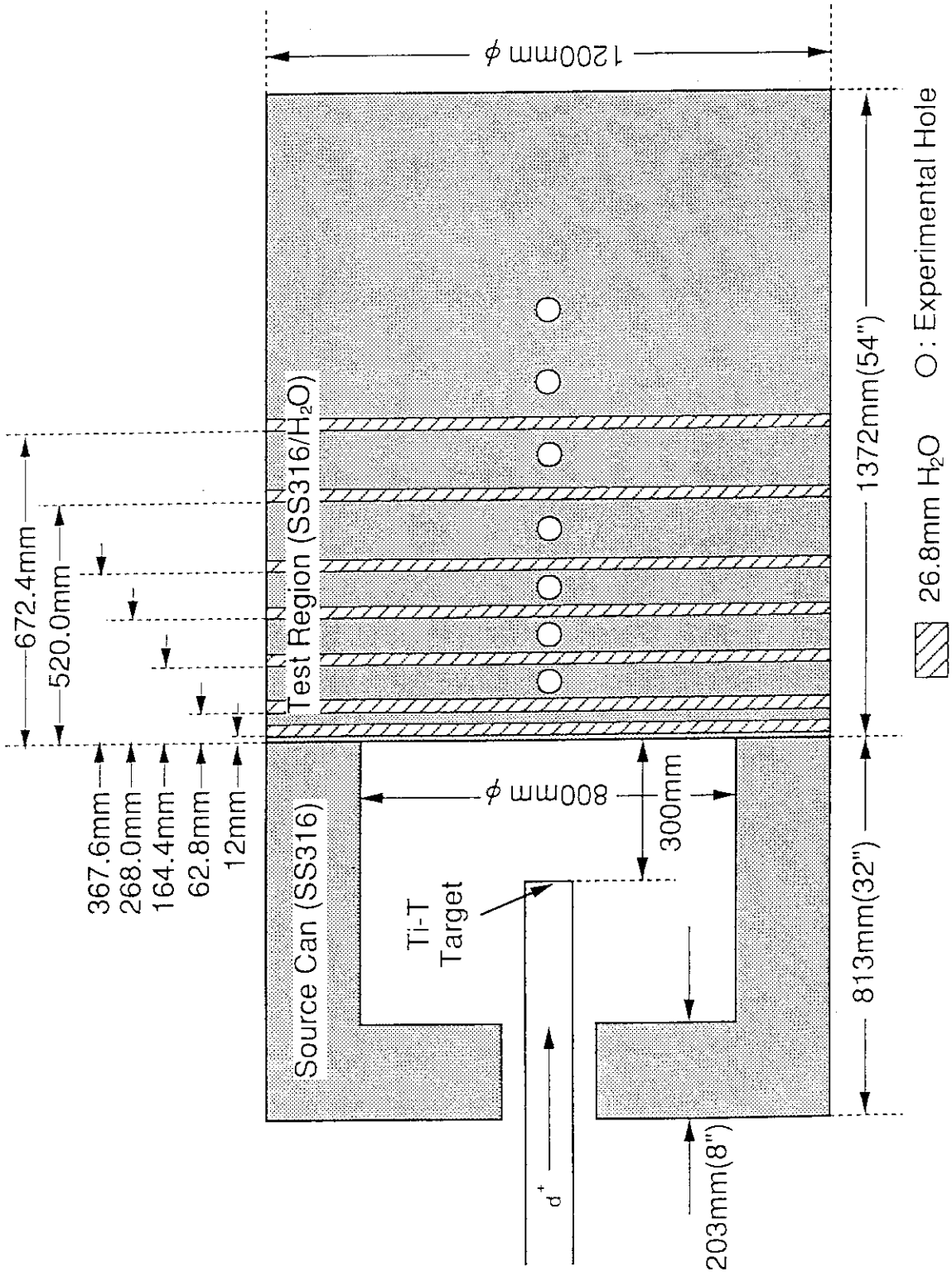

Fig. 2.2.1 Experimental assembly.

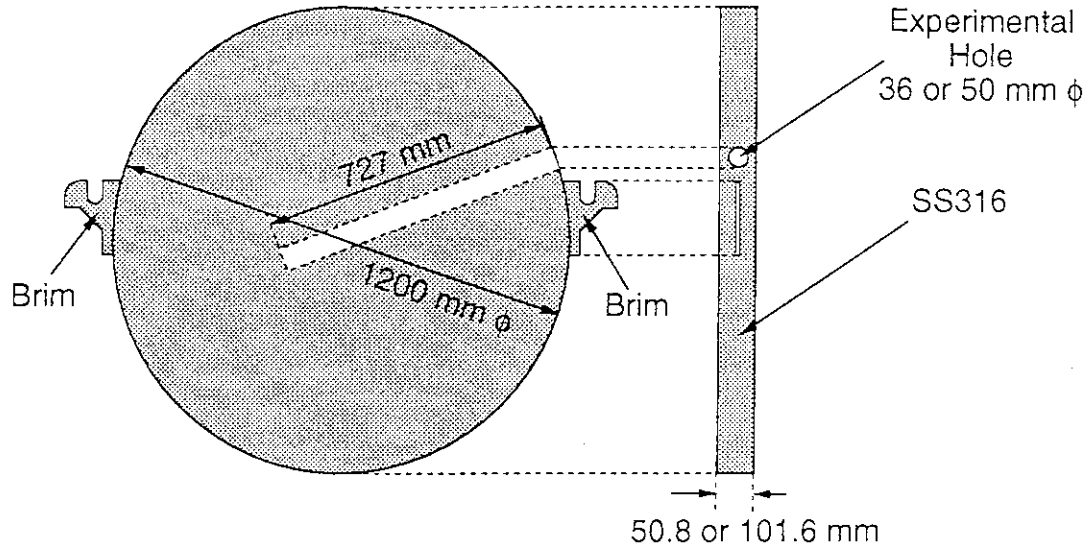

(a) SS316 disk with experimental hole

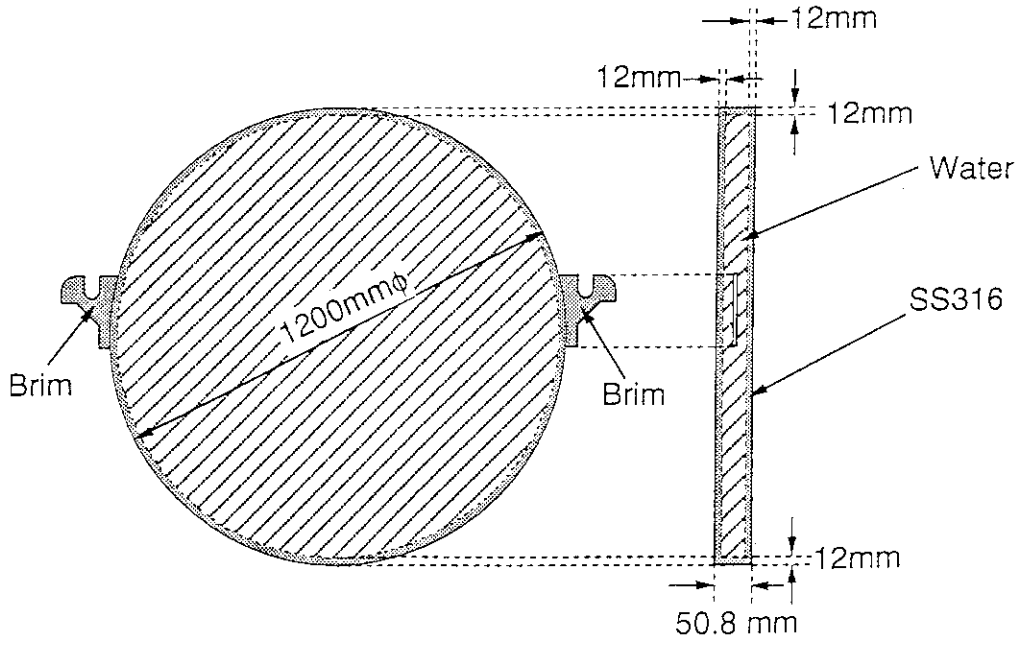

(b) Water tank disk

Fig. 2.2.2 Structure of SS316 disk with an experimental hole and water tank disk.

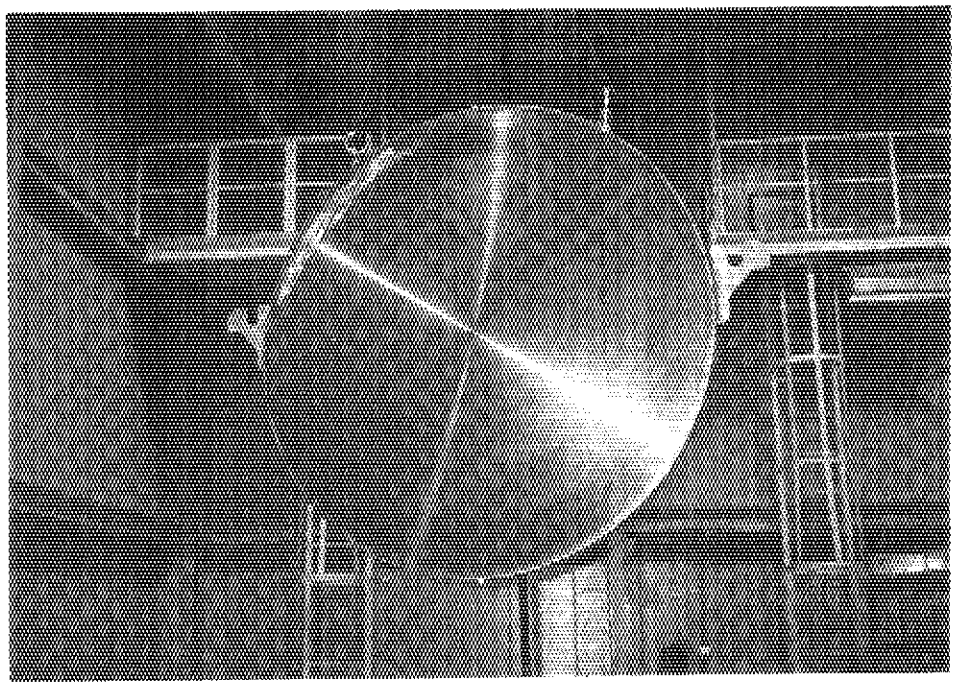

Fig. 2.2.3 Photograph of the water tank disk.

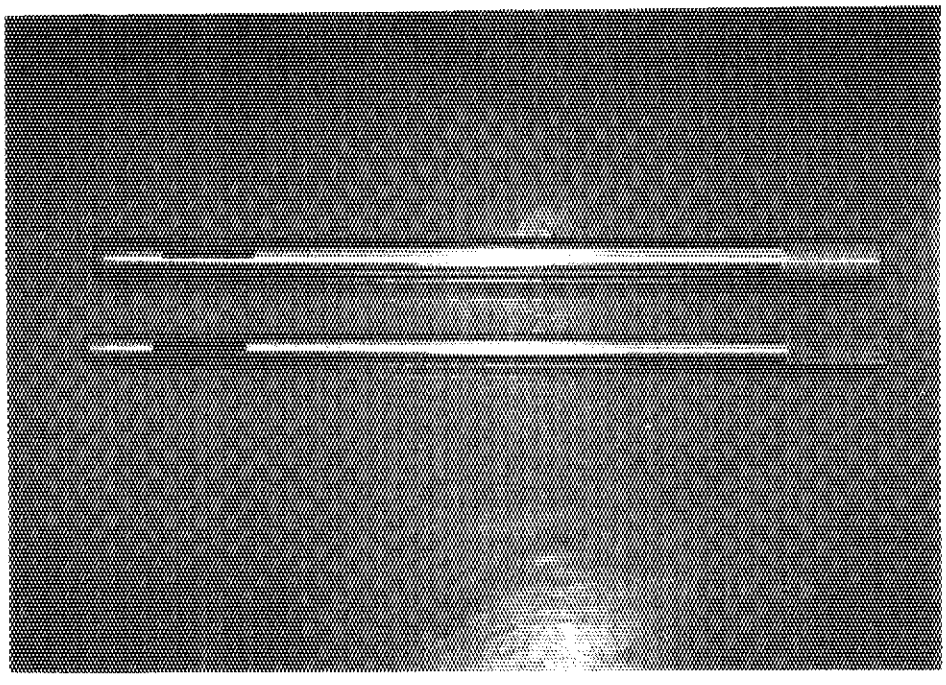

Fig. 2.2.4 Photograph of the detector adapters for neutron activation foils and thermoluminescence dosimeters.

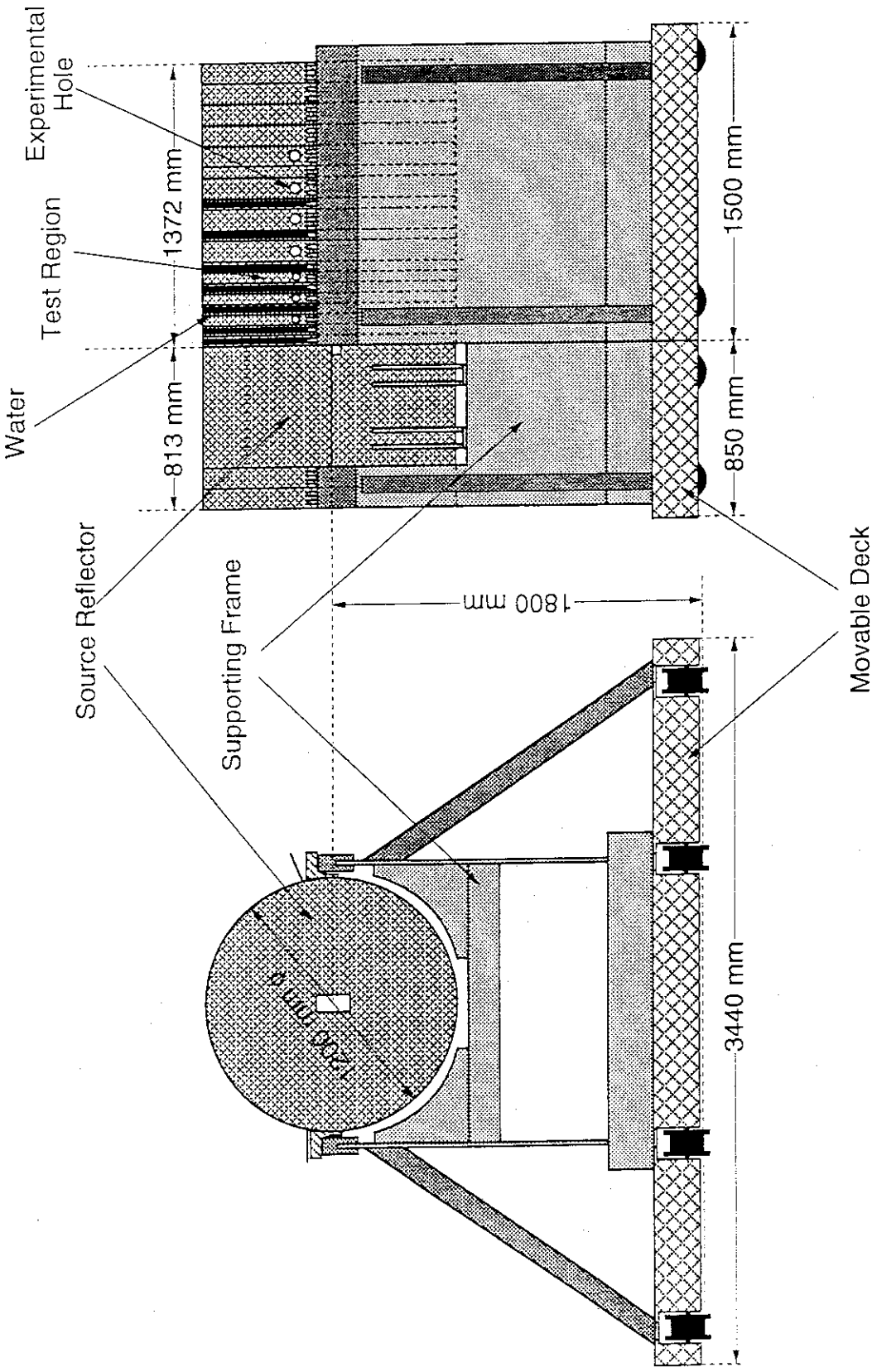

Fig. 2.2.5 Overview of the experimental assembly, supporting frame and movable deck.

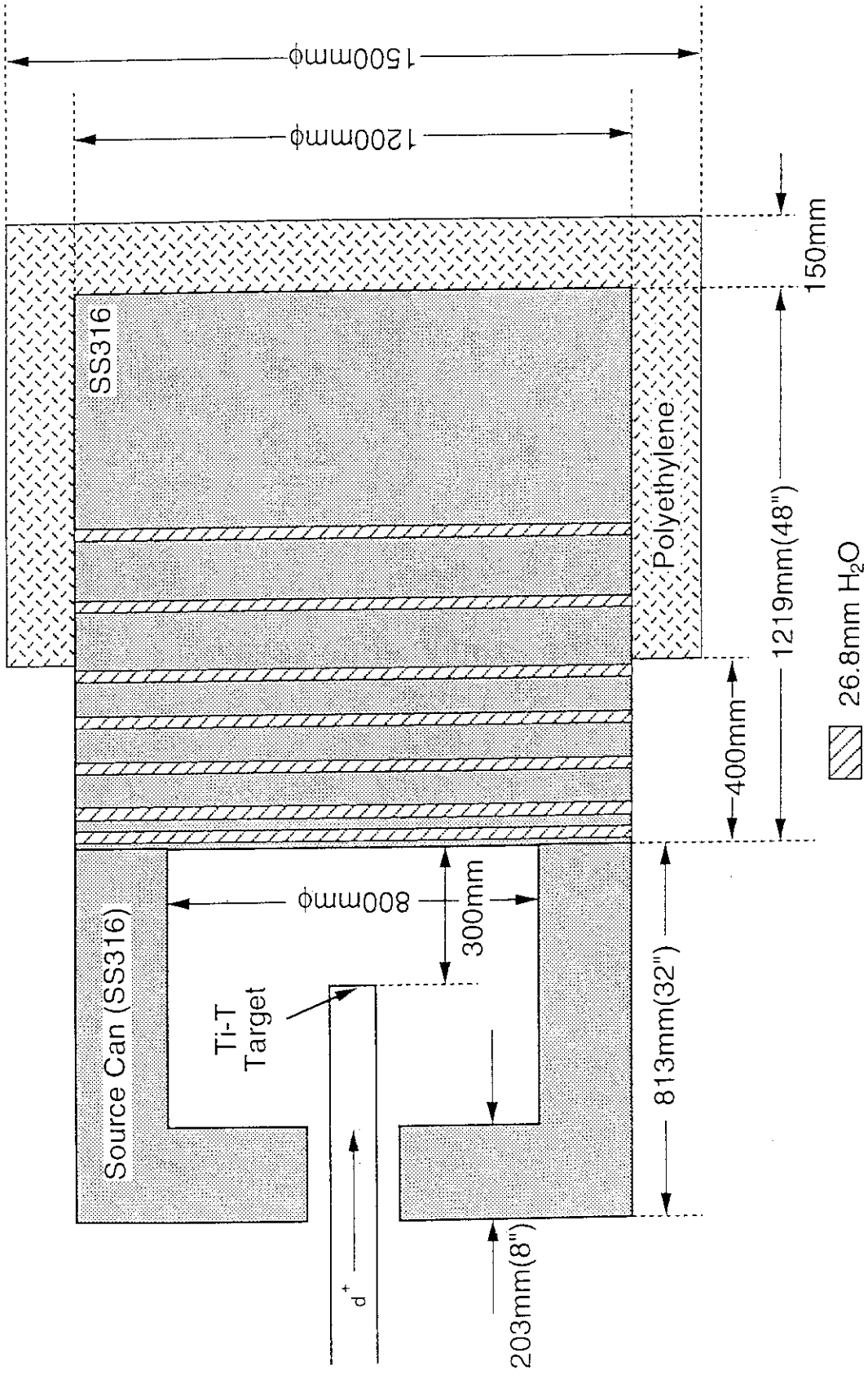

Fig. 2.2.6 Experimental assembly with additional shield determined by pre-analysis.

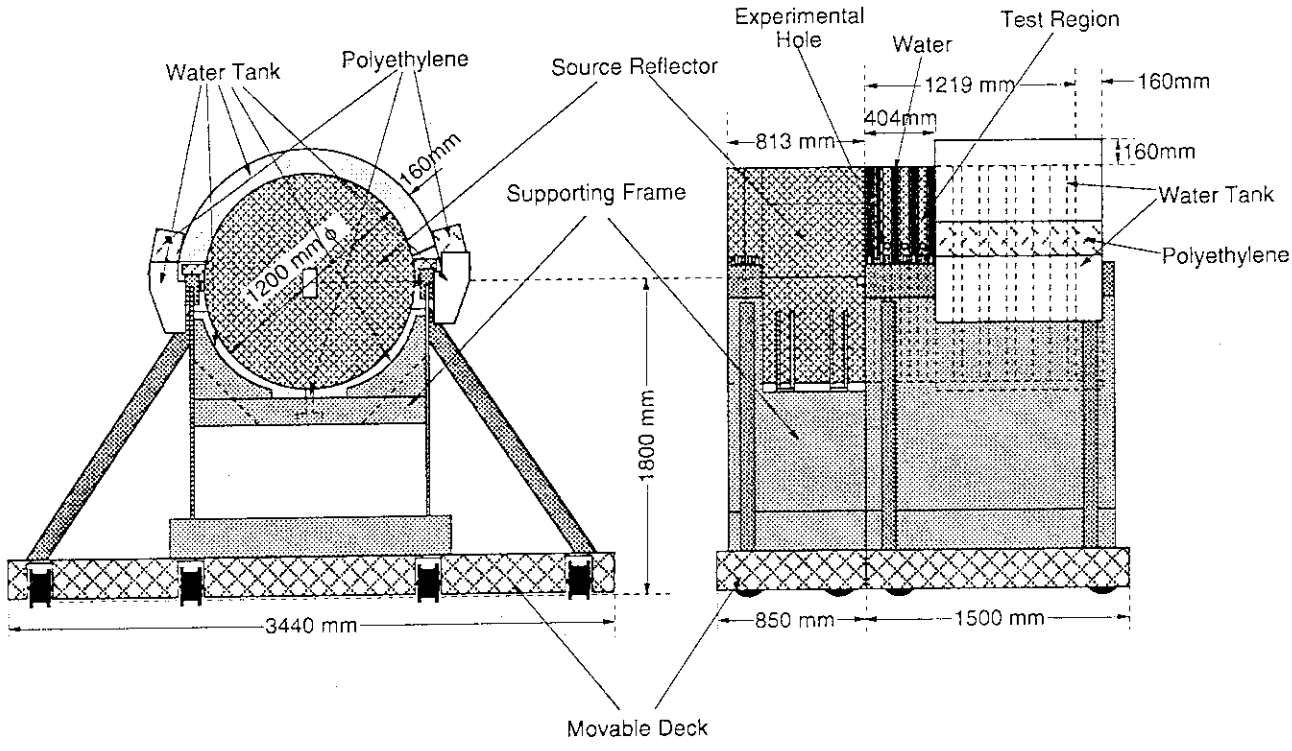

(i) Front View (ii) Side View

(a) Overview of the experimental assembly with the additional shield

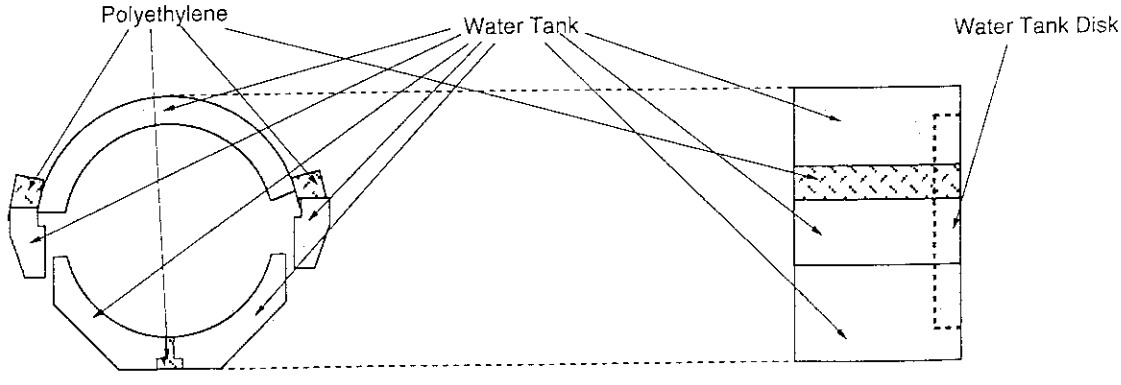

(i) Front View (ii) Side View

(b) Additional shield

Fig. 2.2.7 Overview of the experimental assembly with additional shield.

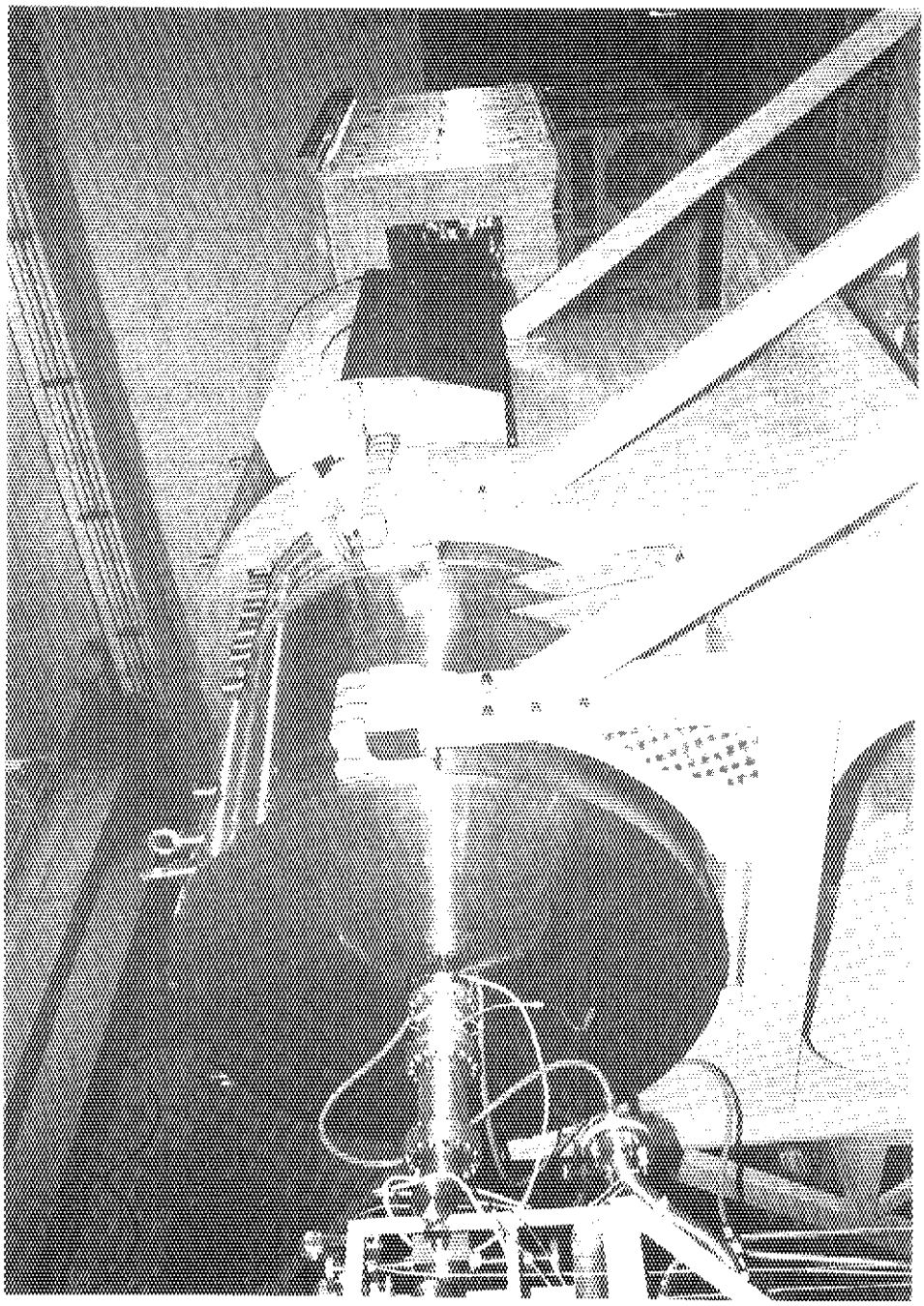

Fig. 2.2.8 Photograph of the experimental assembly with additional shield, supporting frame and movable deck.

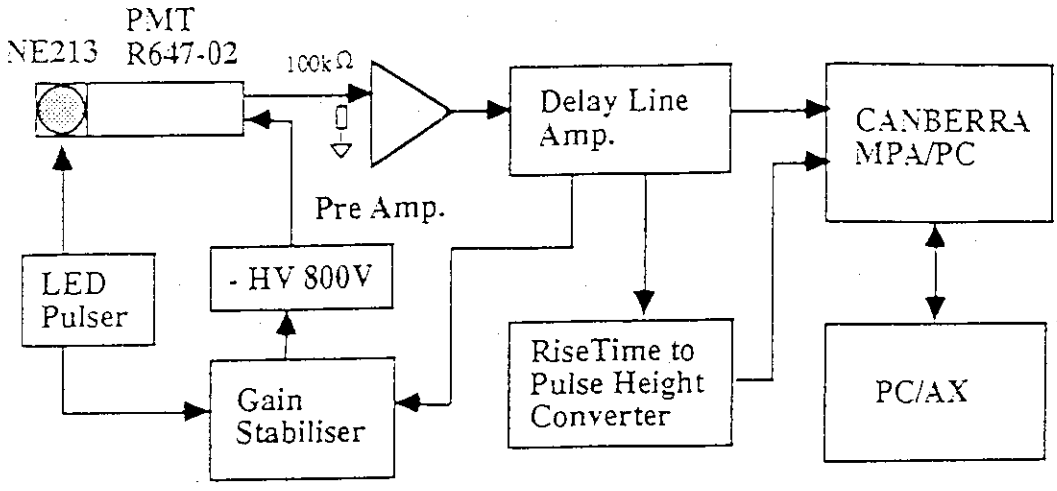

Fig. 3.1.1.1 Block diagram of electronic circuit for small sphere NE213 scintillation detector.

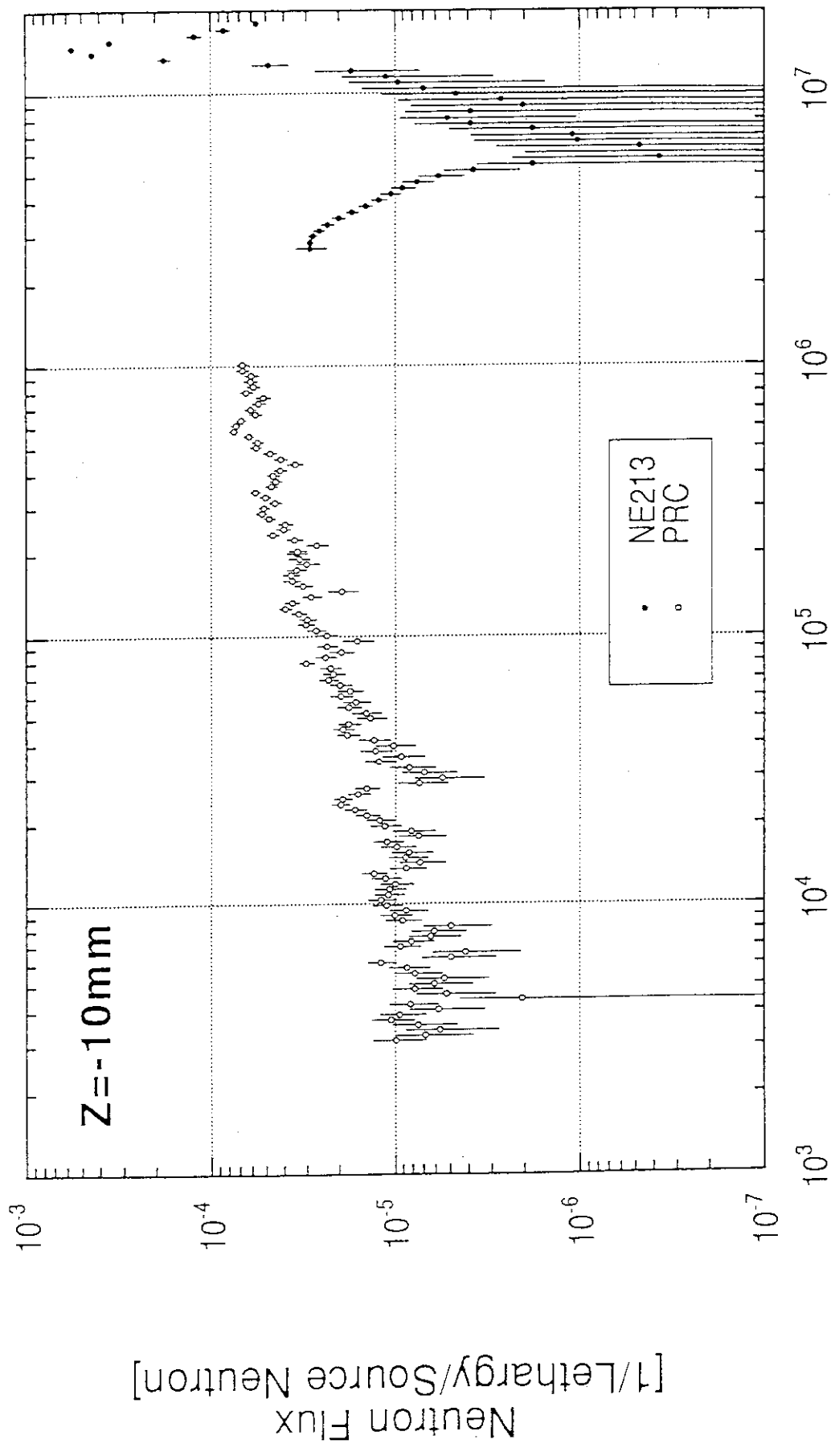

Fig. 3.1.1.2 The measured neutron spectrum at the front surface of the test region.

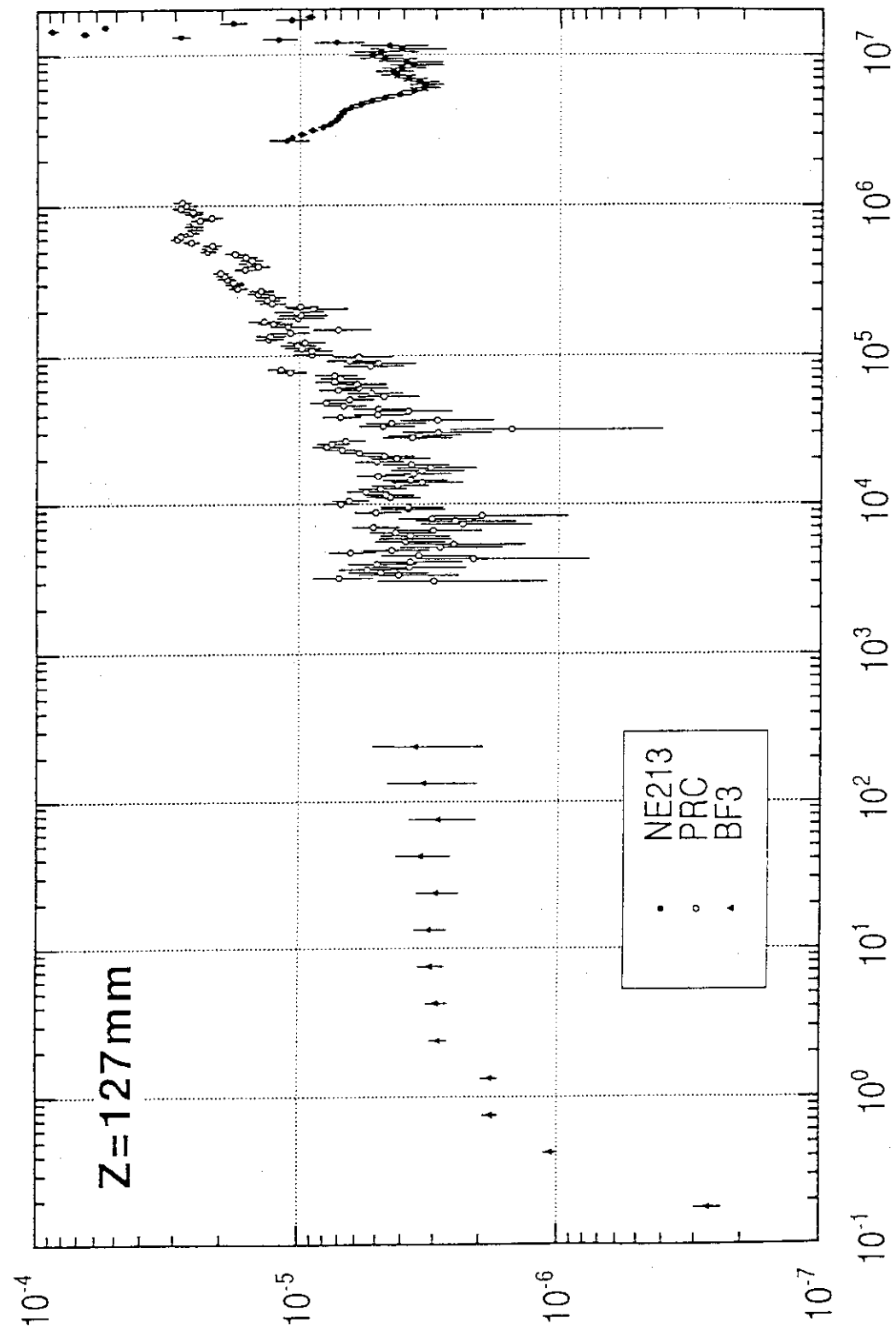

Fig. 3.1.1.3 The measured neutron spectrum at 127 mm from the front surface of the test region.

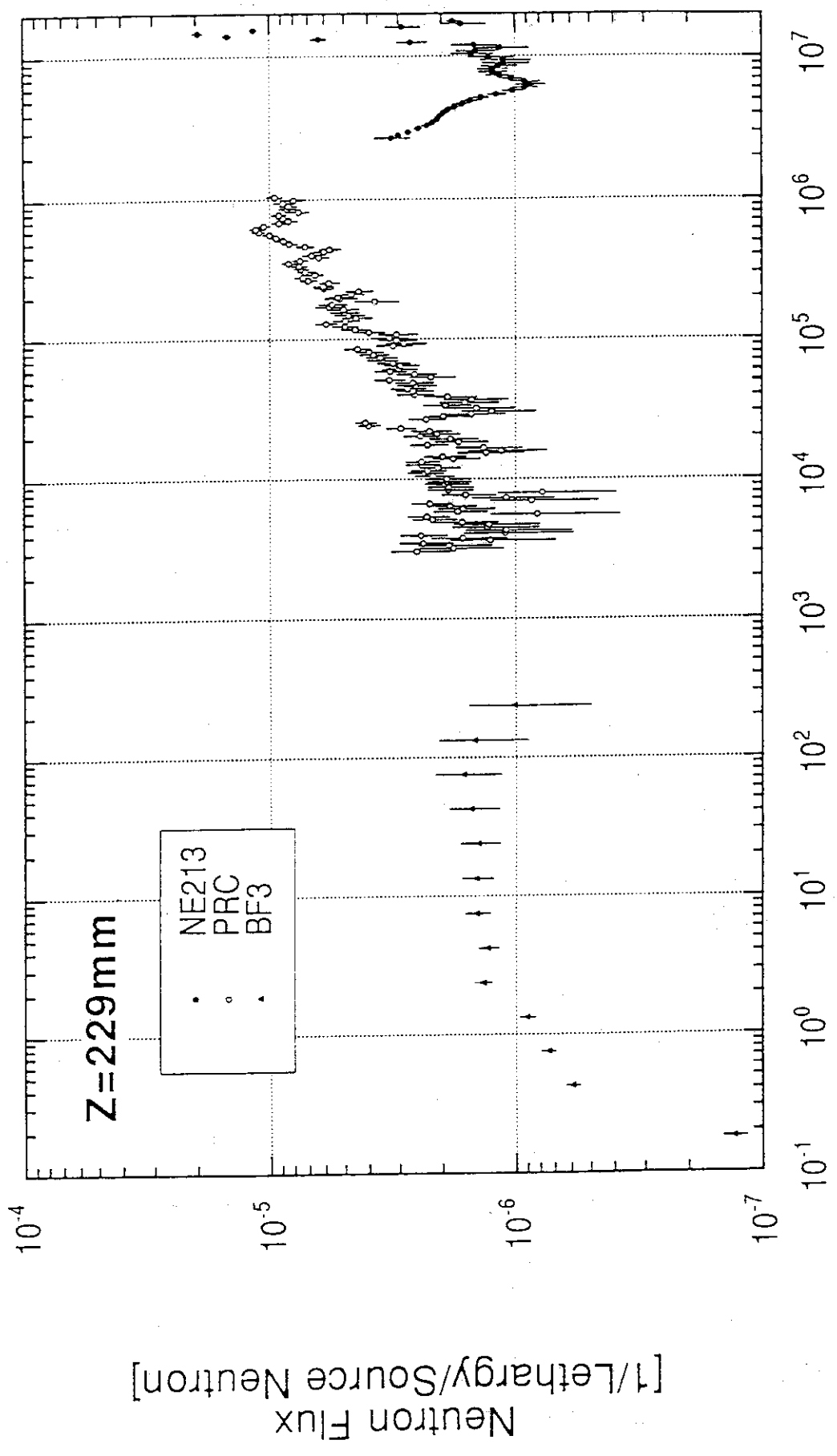

Fig. 3.1.1.4 The measured neutron spectrum at 229 mm from the front surface of the test region.

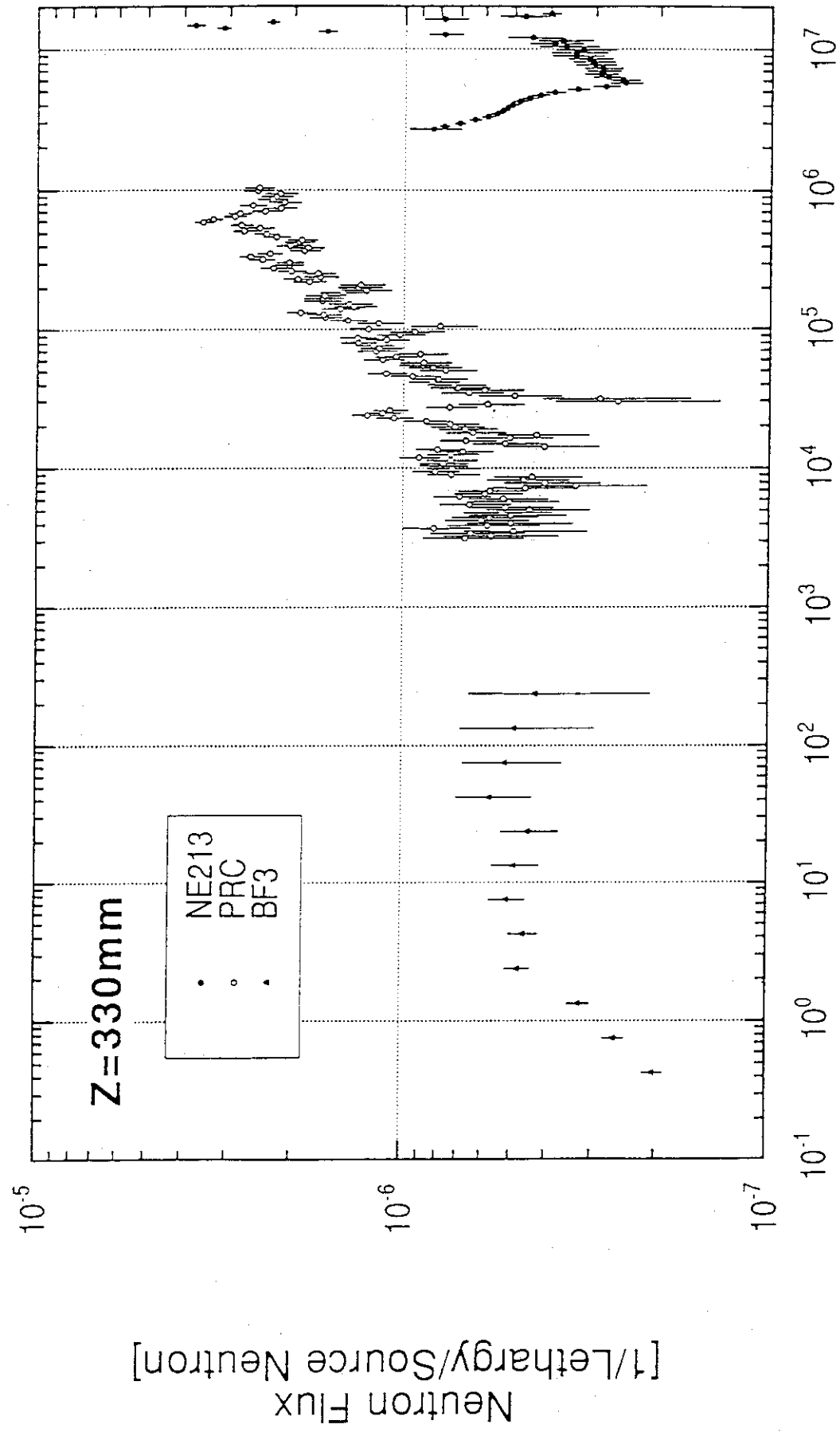

Fig. 3.1.1.5 The measured neutron spectrum at 330 mm from the front surface of the test region.

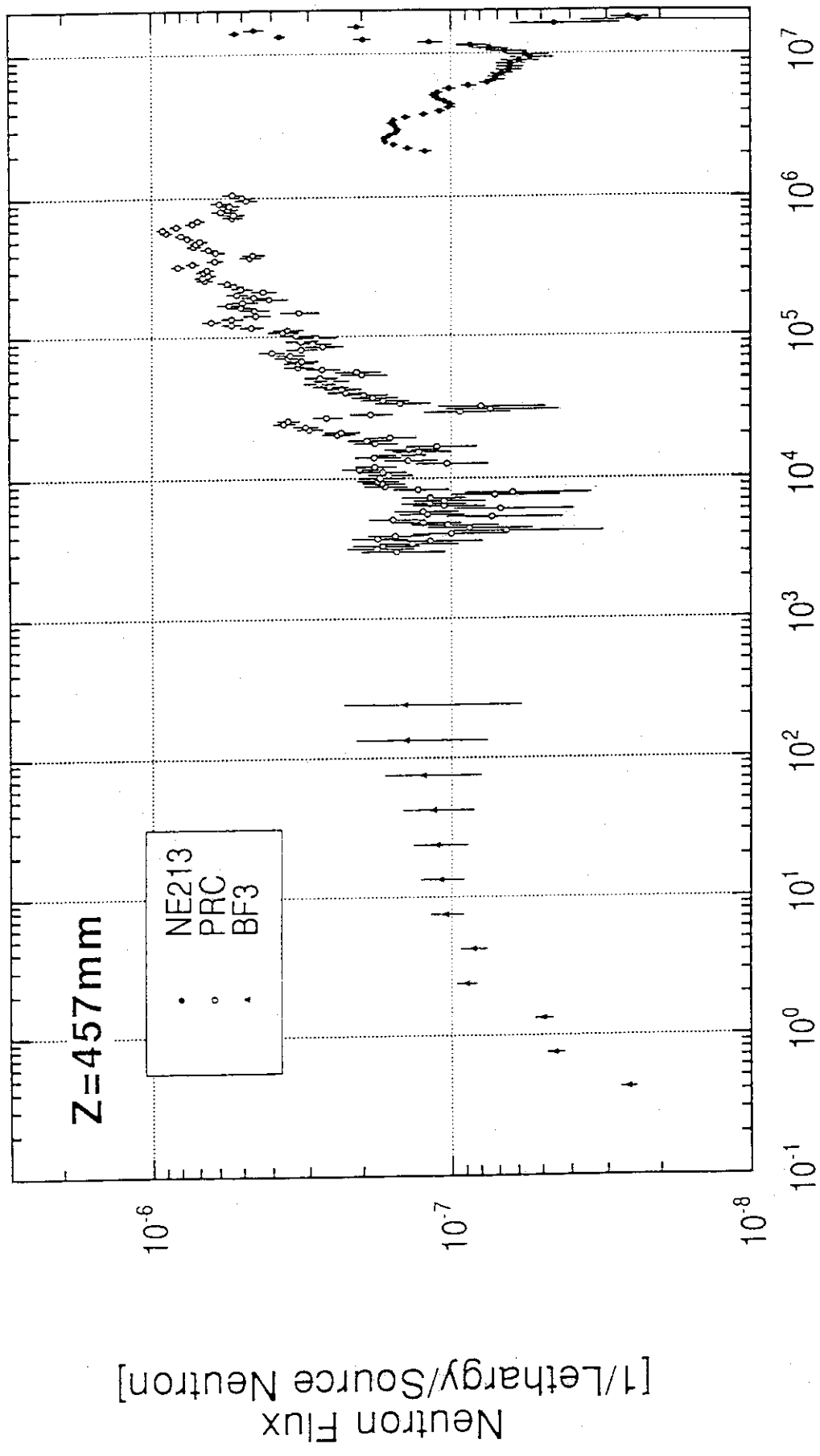

Fig. 3.1.1.6 The measured neutron spectrum at 457 mm from the front surface of the test region.

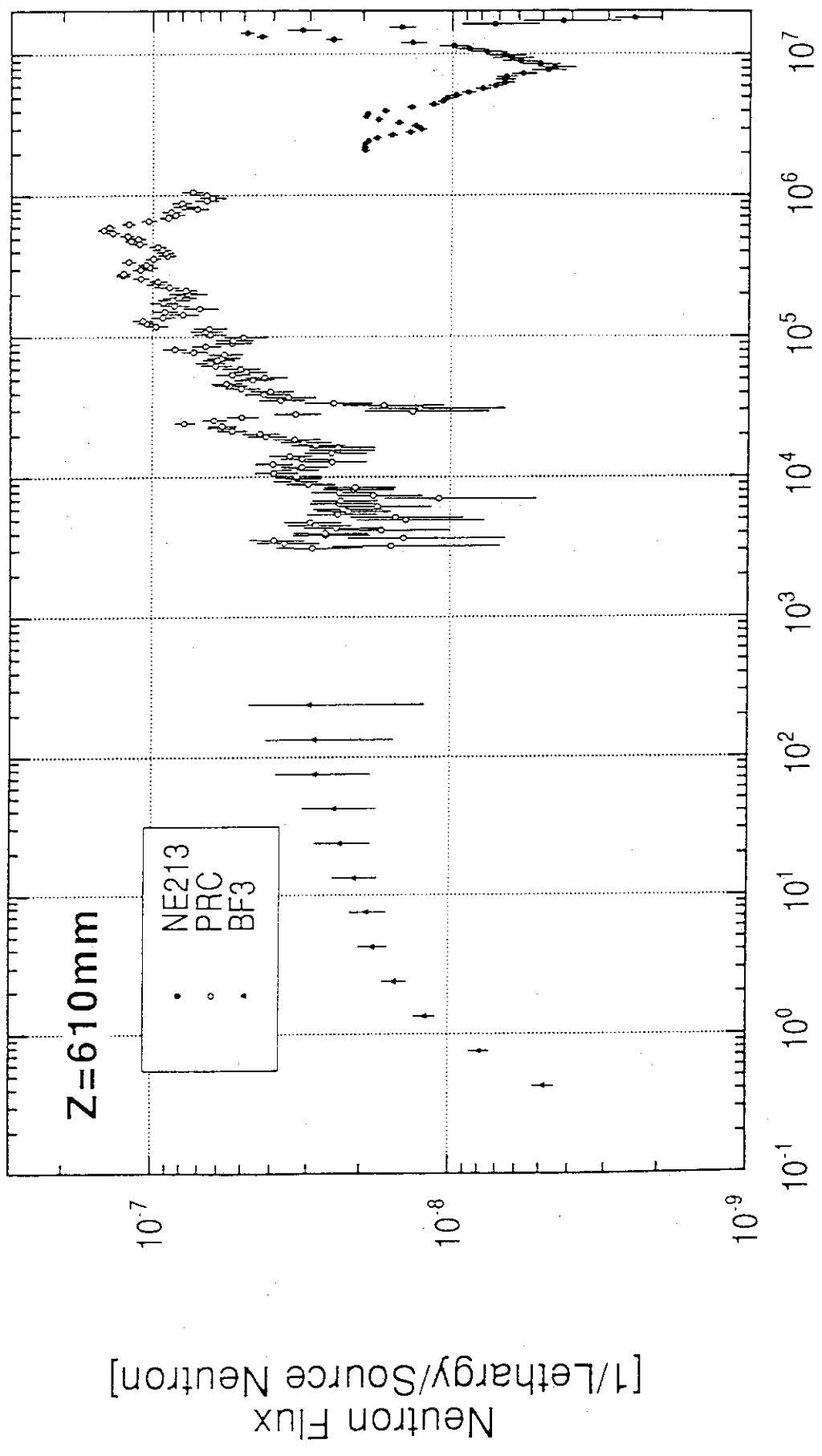

Fig. 3.1.1.7 The measured neutron spectrum at 610 mm from the front surface of the test region.

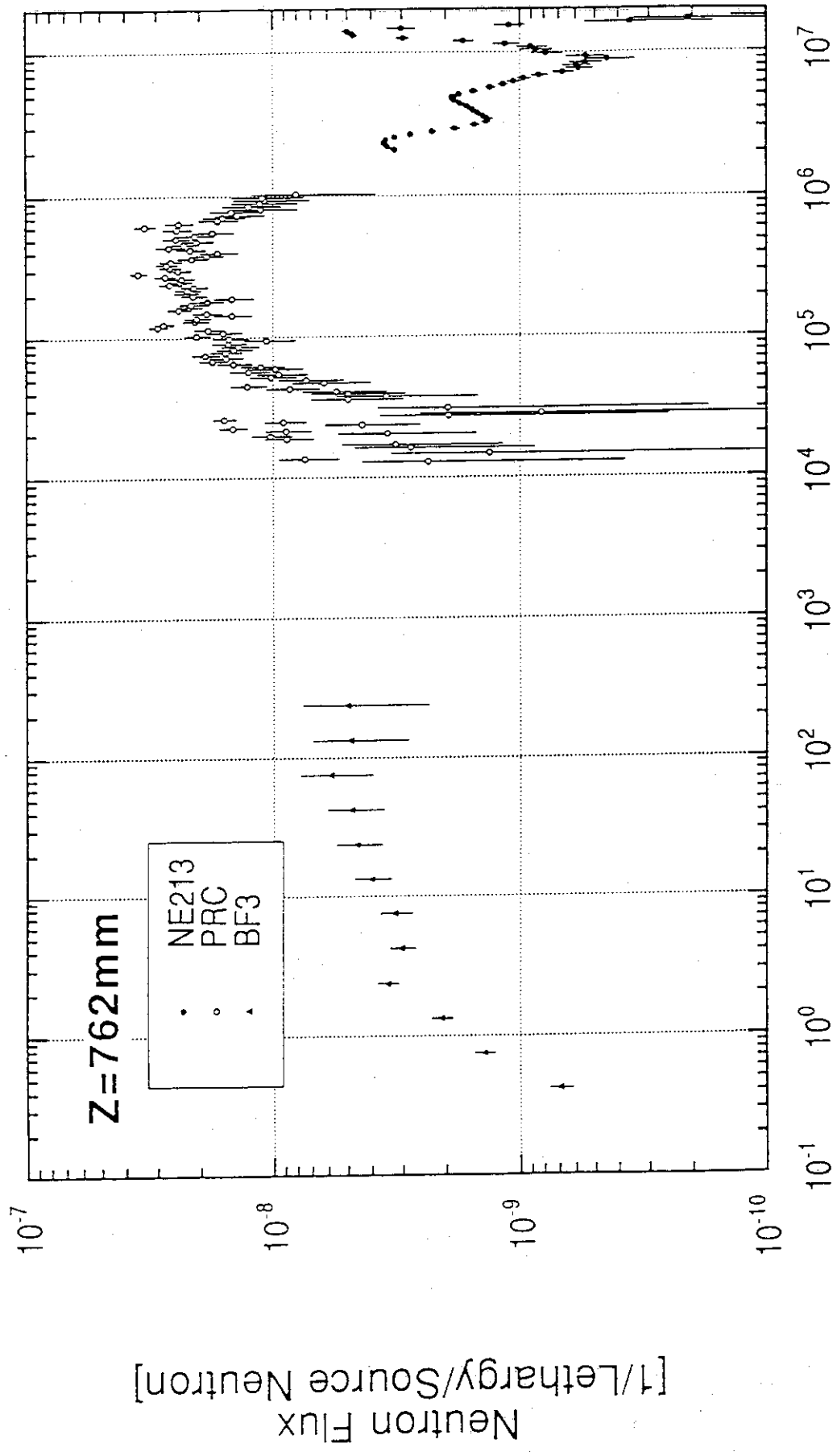

Fig. 3.1.1.8 The measured neutron spectrum at 762 mm from the front surface of the test region.

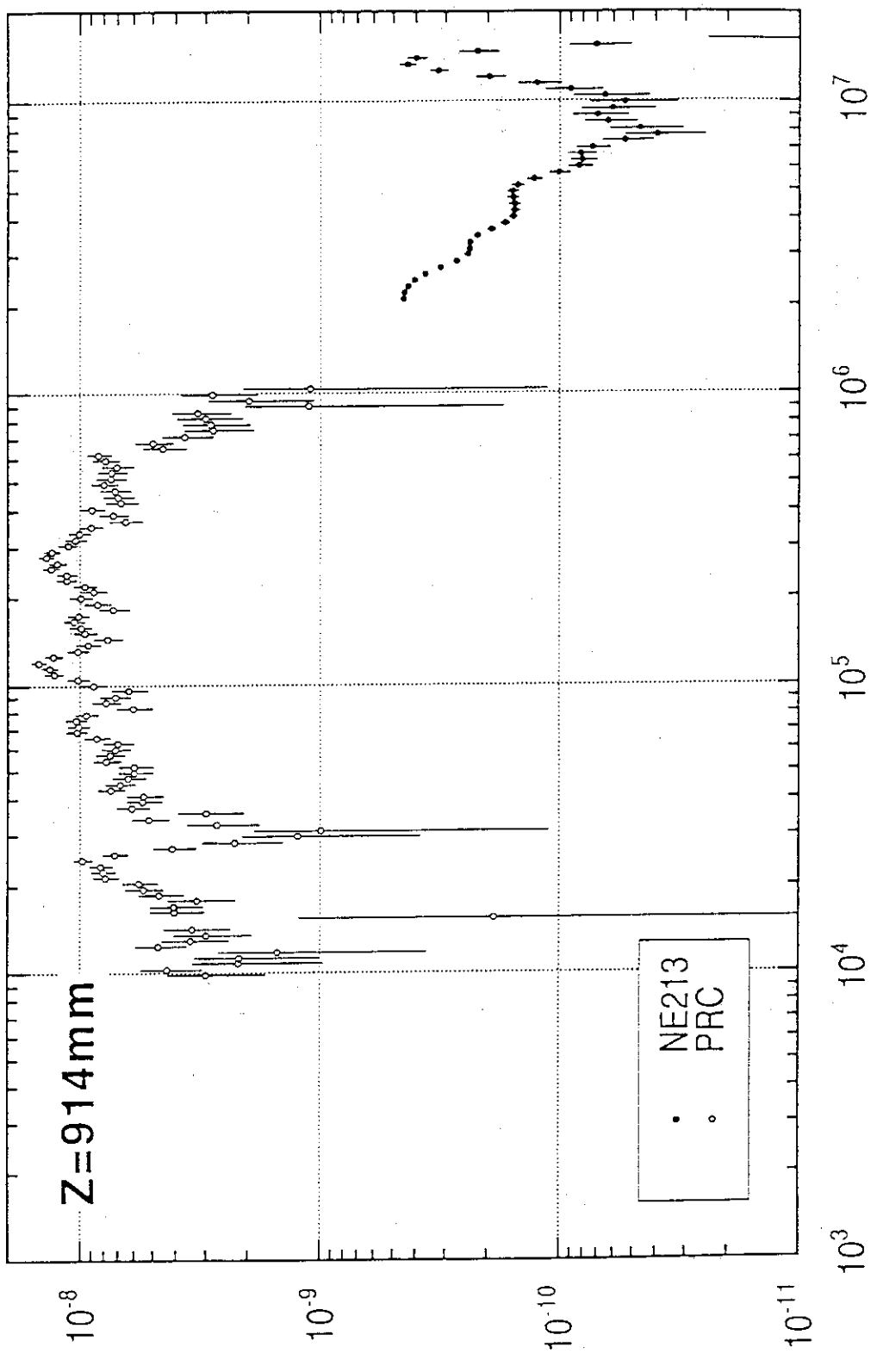

Fig. 3.1.1.9 The measured neutron spectrum at 914 mm from the front surface of the test region.

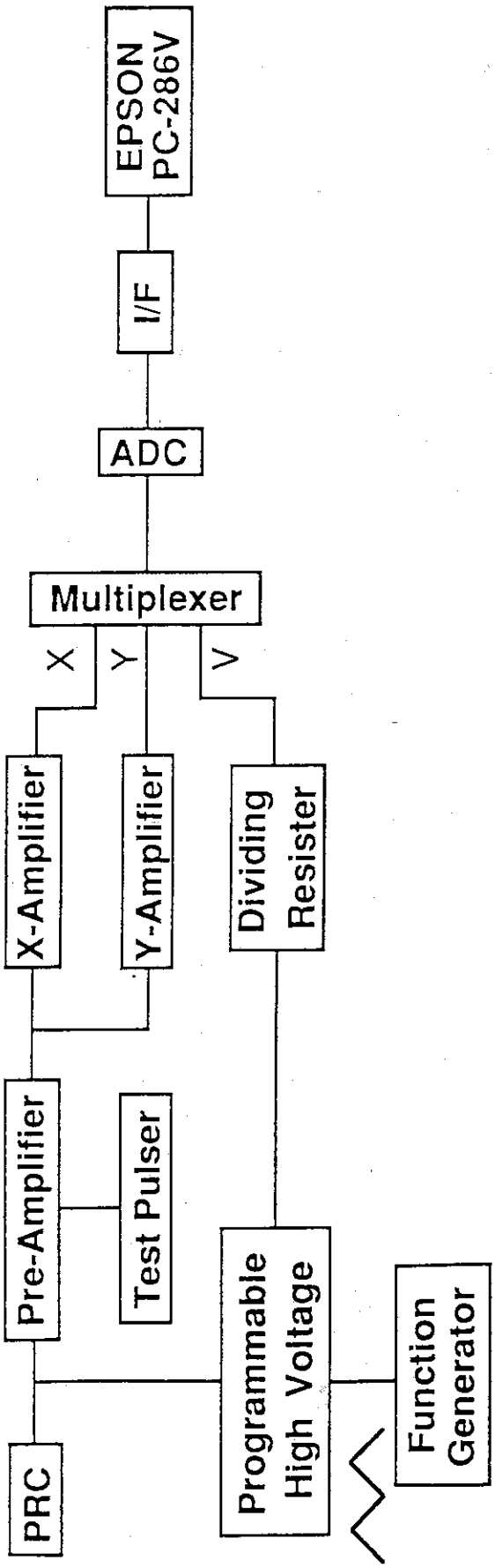

Fig. 3.1.2.1 Block diagram of electronic circuit for the PRC.

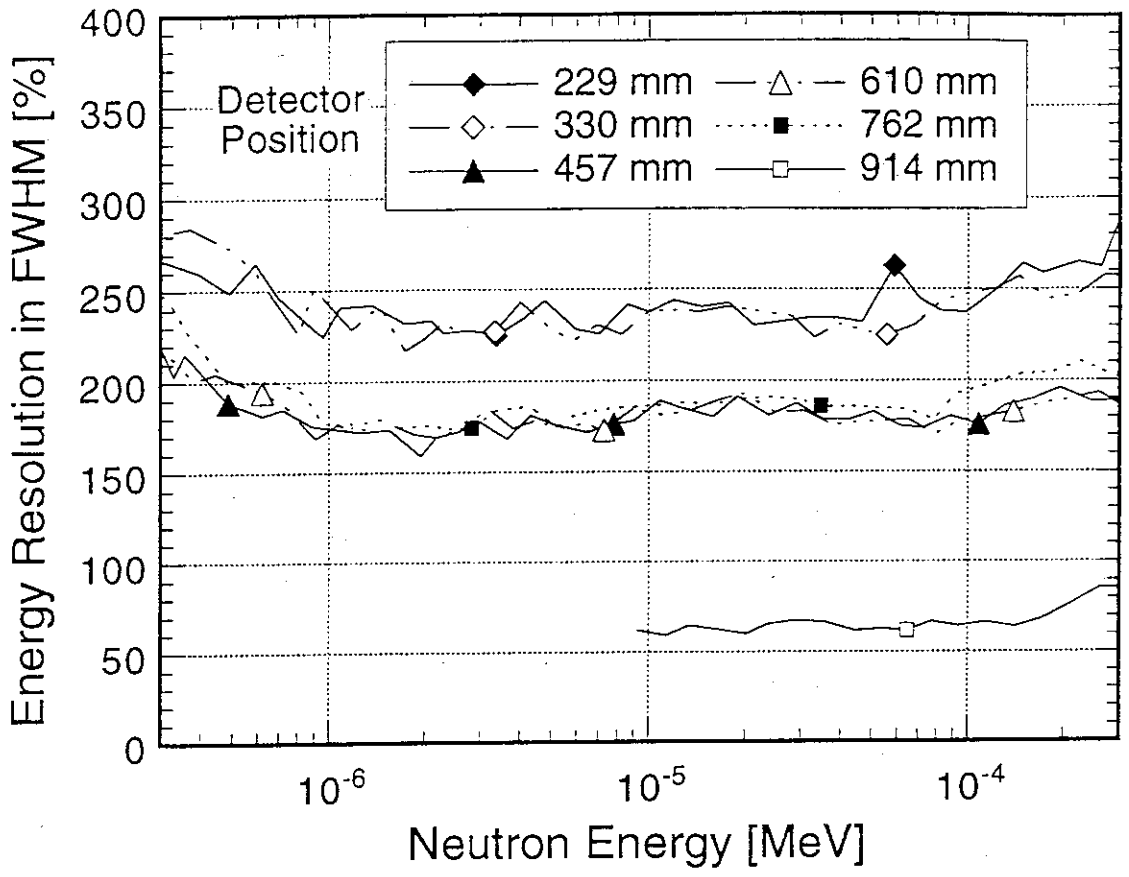

Fig. 3.1.3.1 Expected energy resolution of neutron spectra calculated by MCNP.

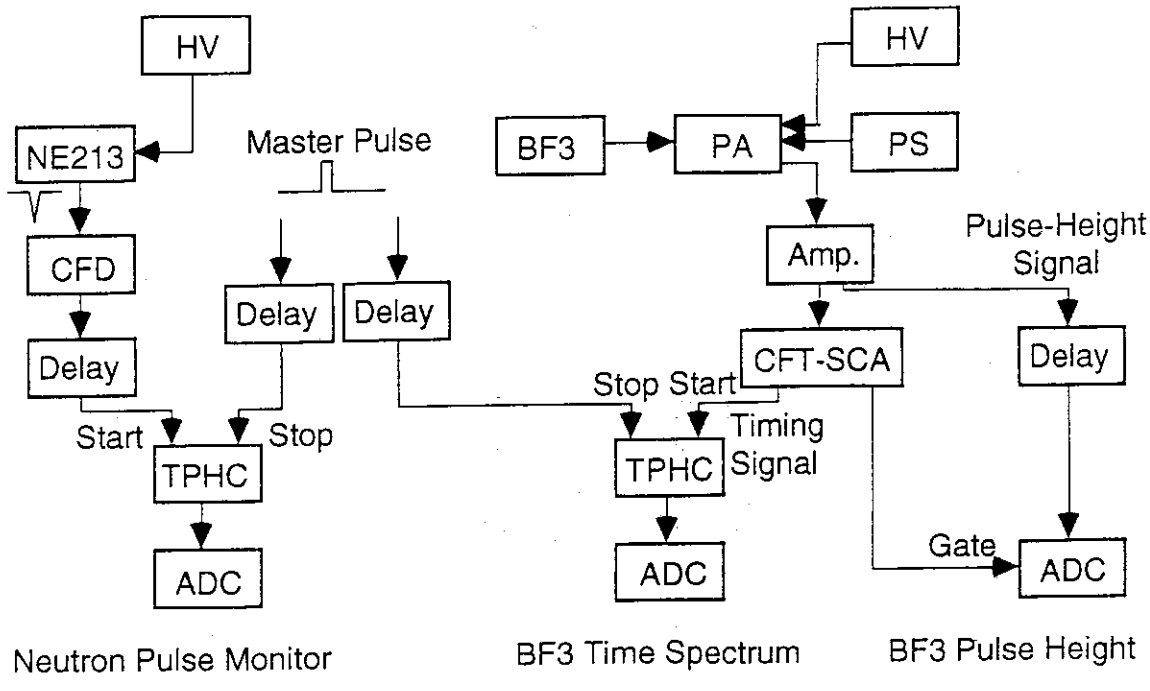

Fig. 3.1.3.2 Electronic circuit used in the slowing down time method.

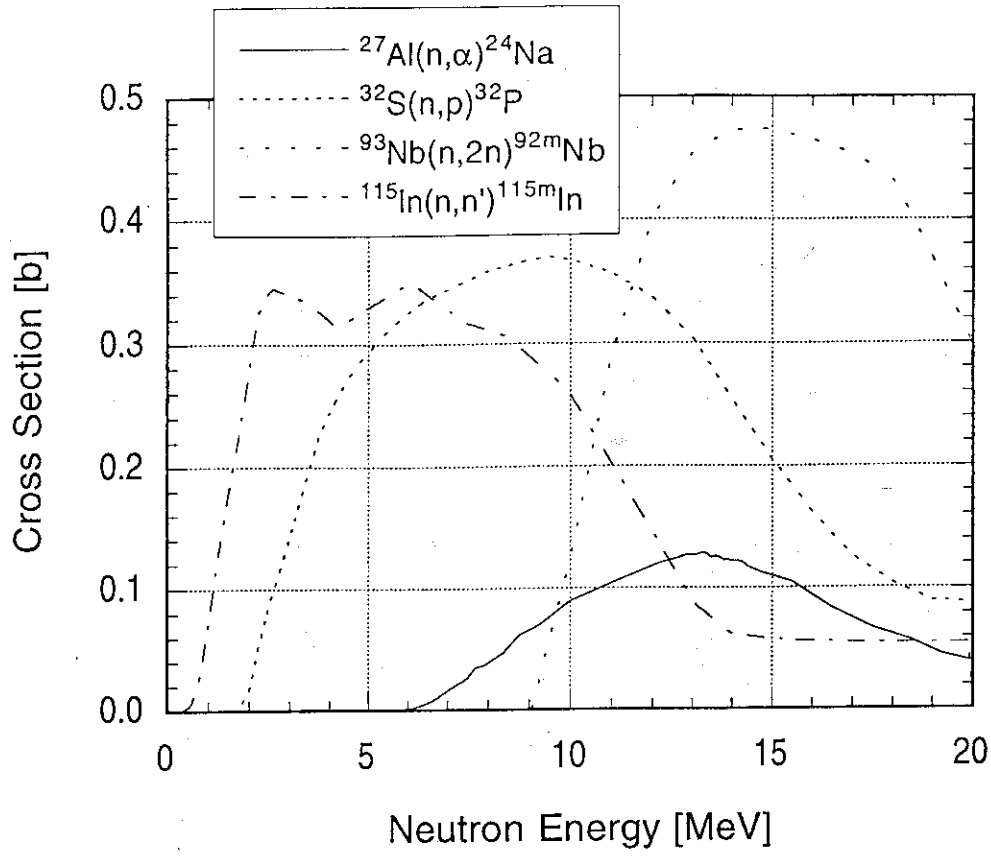

Fig. 3.2.1.1 Cross sections of ^{27}Al(n,α)^{24}Na, ^{32}S(n,p)^{32}P, ^{93}Nb(n,2n)^{92m}Nb and ^{115}In(n,n')^{115m}In reactions taken from JENDL Dosimetry File[22].

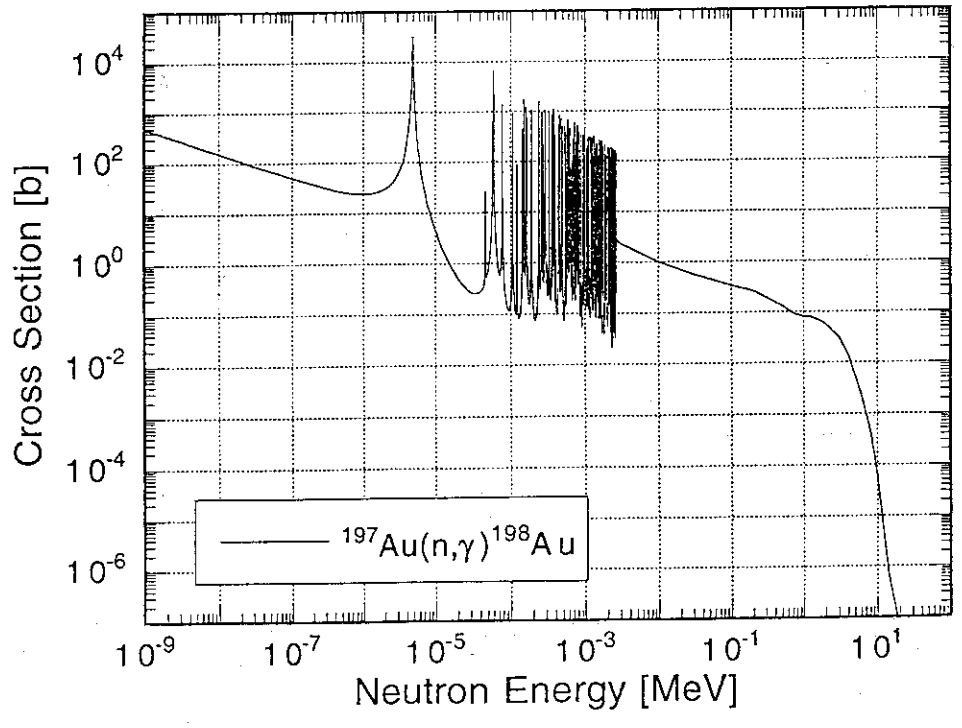

Fig. 3.2.1.2 Cross sections of ^{197}Au(n,γ)^{198}Au reaction taken from JENDL Dosimetry File[22].

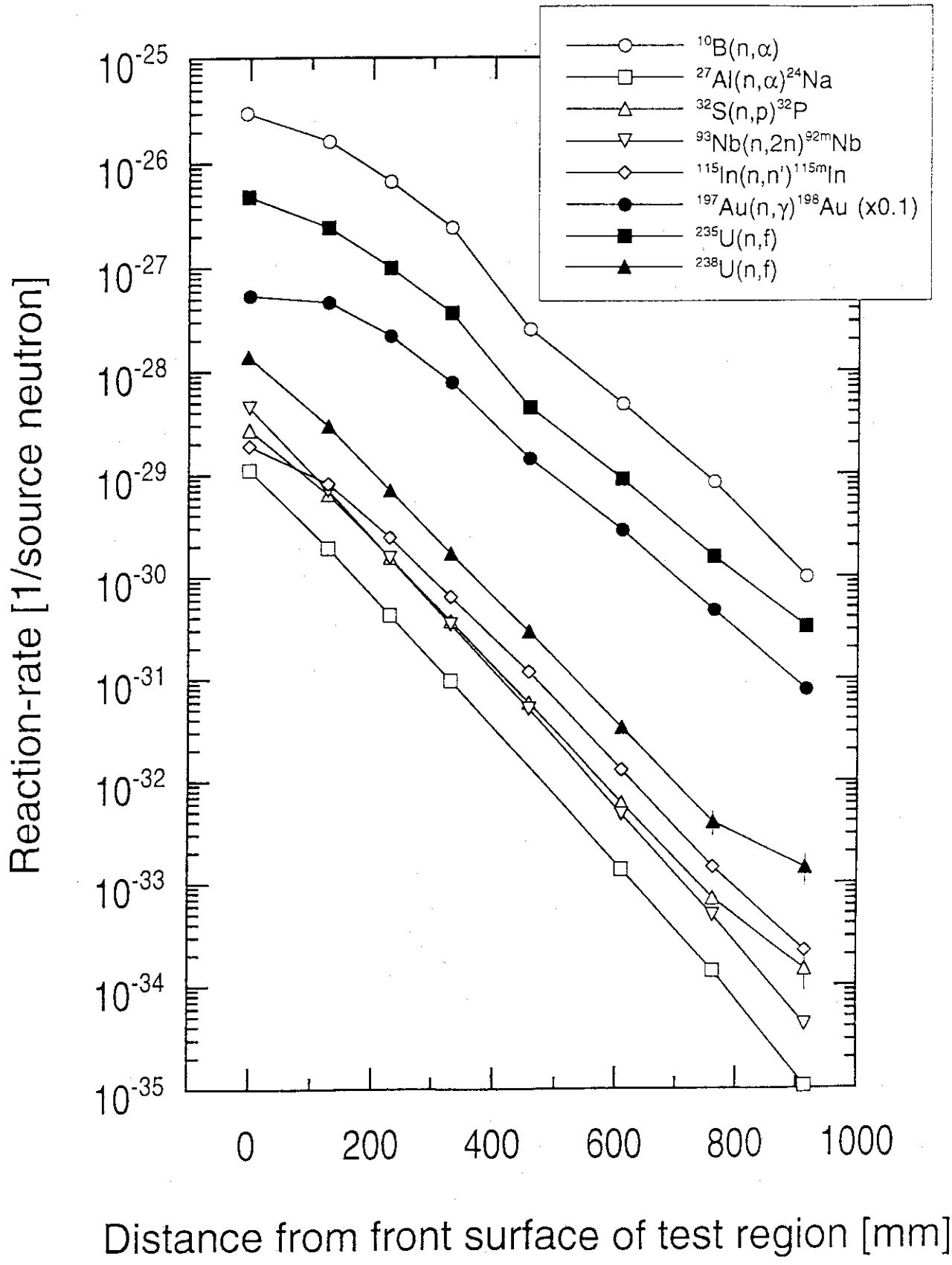

Fig. 3.2.1.3 Measured reaction rates and fission rates.

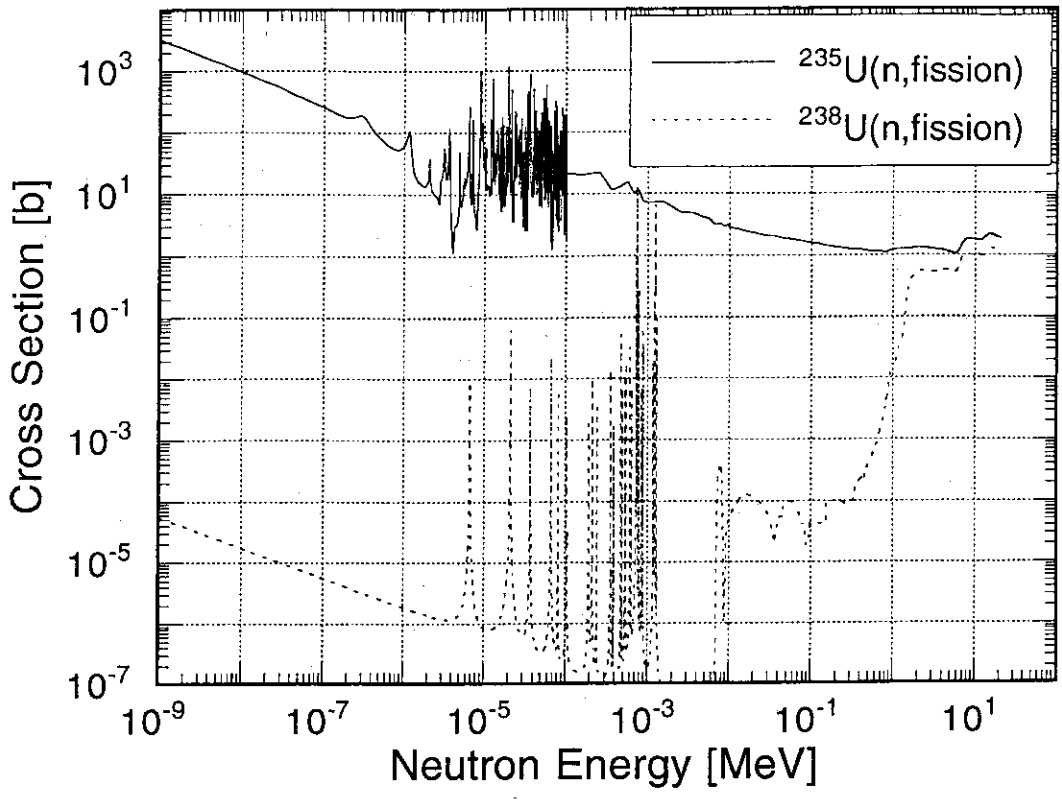

Fig. 3.2.2.1 Cross sections of ^{235}U(n,fission) and ^{238}U(n,fission) reactions taken from JENDL Dosimetry File[22].

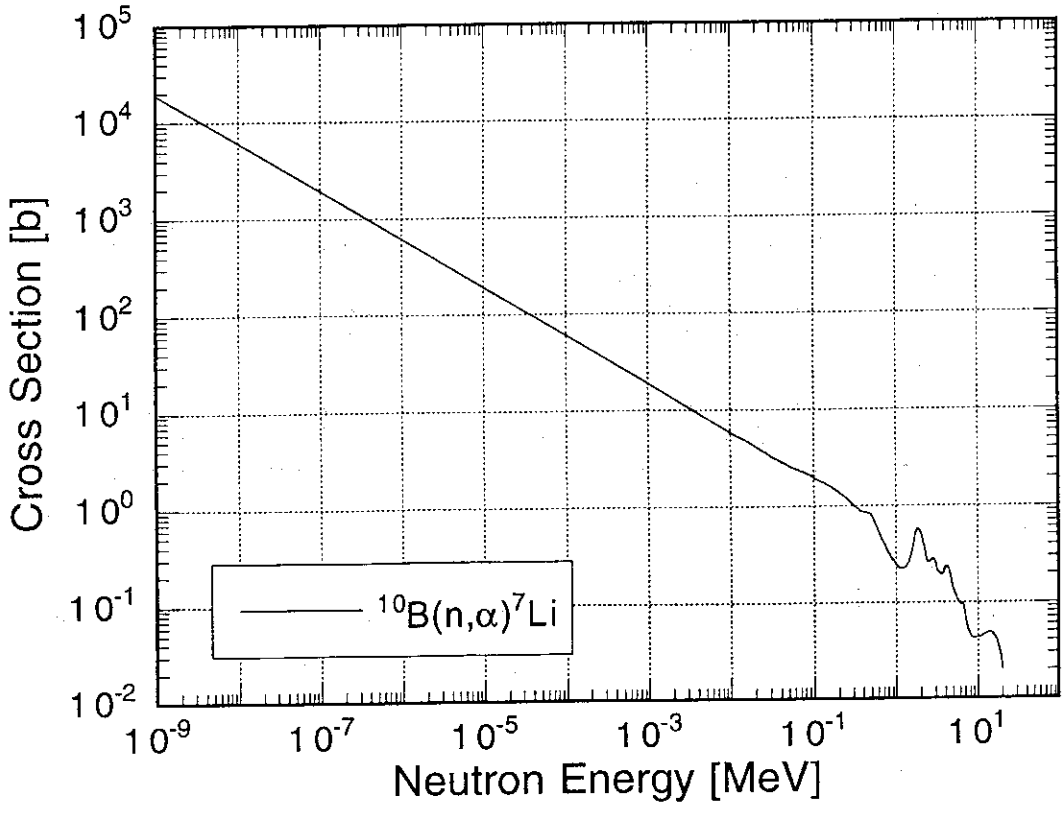

Fig. 3.2.3.1 Cross sections of ^{10}B(n,α)^{7}Li reaction taken from JENDL Dosimetry File[22].

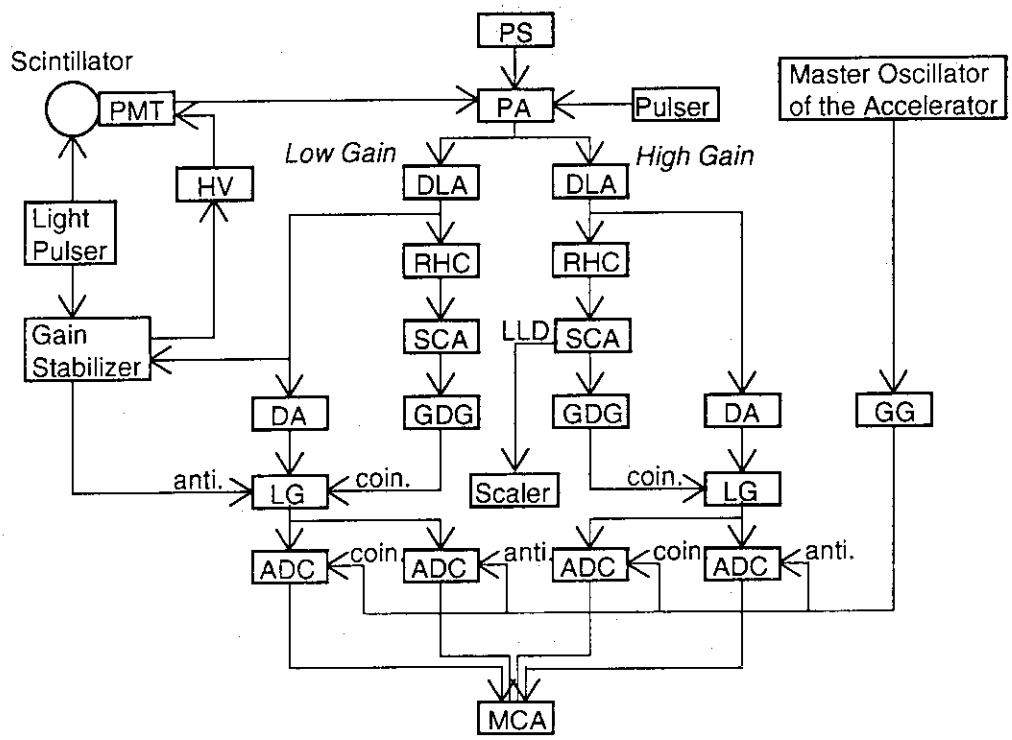

PMT	: Photomultiplier Tube	Hamamatsu	R580
HV	: High Voltage Power Supply	ORTEC	456H
PS	: Power Supply	ORTEC	114
PA	: Preamplifier	ORTEC	113
Pulser	: Research Pulser	ORTEC	448
DLA	: Delay Line Amplifier	ORTEC	460
RHC	: Risetime to Height Convertor	OKEN	723-1
SCA	: Single Channel Analyzer	CANBERRA	2035A
GDG	: Gate & Delay Generator	ORTEC	416A
Scaler	: Timer & Scaler	JAERI	178RA
DA	: Delay Amplifier	CANBERRA	1457
LG	: Linear Gate & Slow Coincidence	OKEN	721-1
GG	: Dual Gate Generator	Le Croy	222
ADC	: Analog to Digital Convertor	CANBERRA	6075
MCA	: Multichannel Analyzer	CANBERRA	MPA/LBB

Fig. 3.3.1 Electronic circuit used in the gamma-ray spectrum measurement.

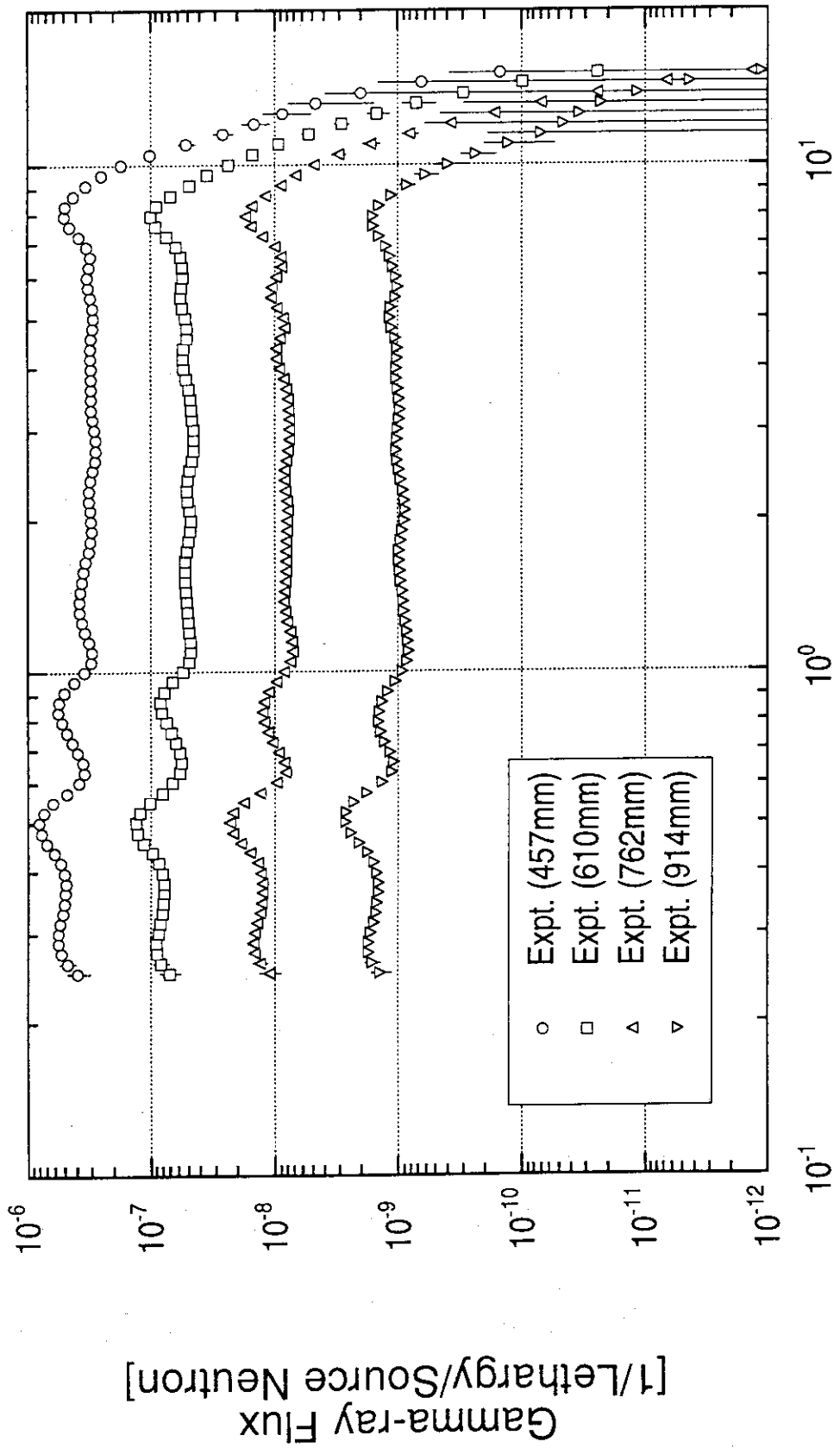

Fig. 3.3.2 Measured gamma-ray spectra.

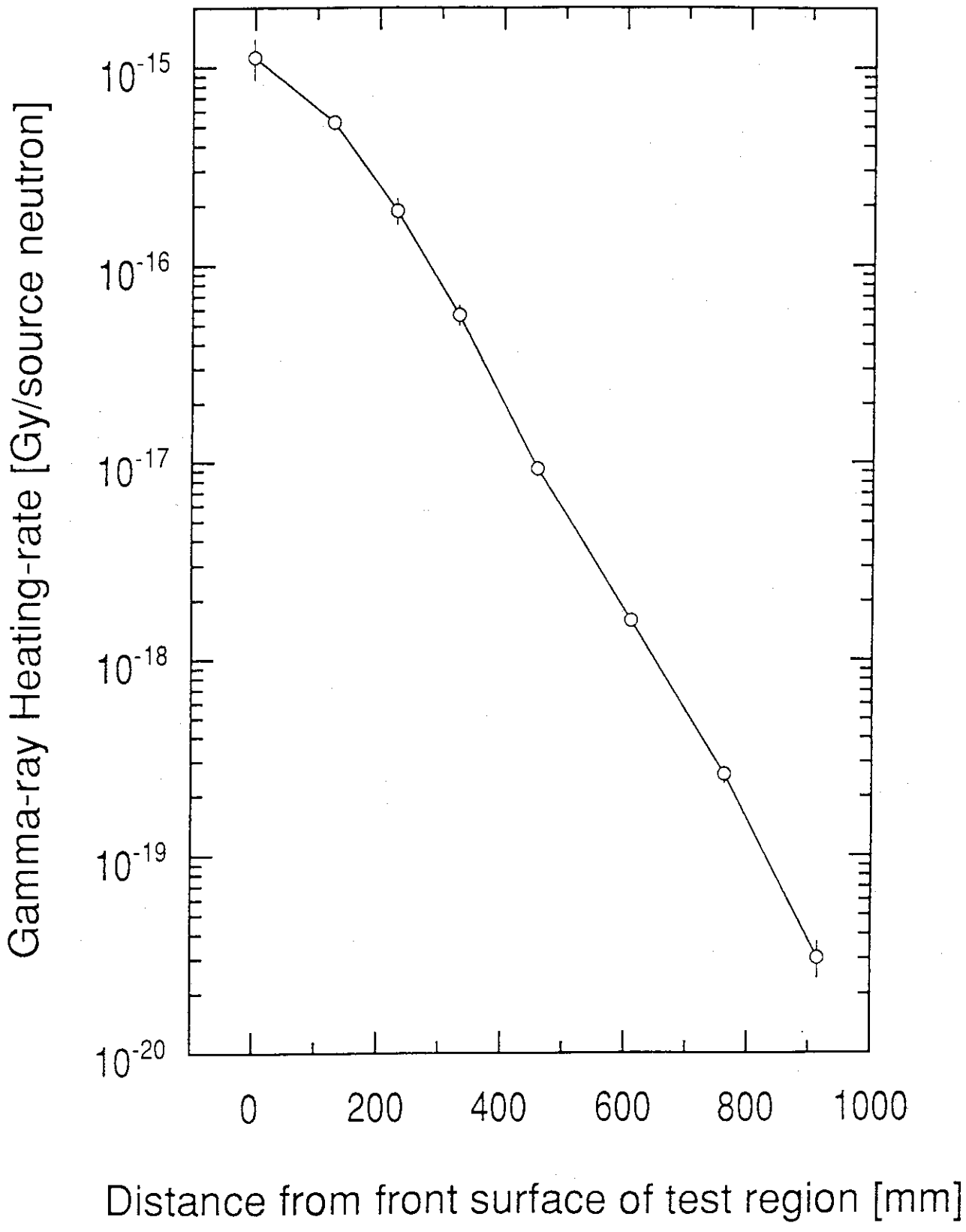

Fig. 3.4.1 Measured gamma-ray heating rates of SS316 by the TLD.

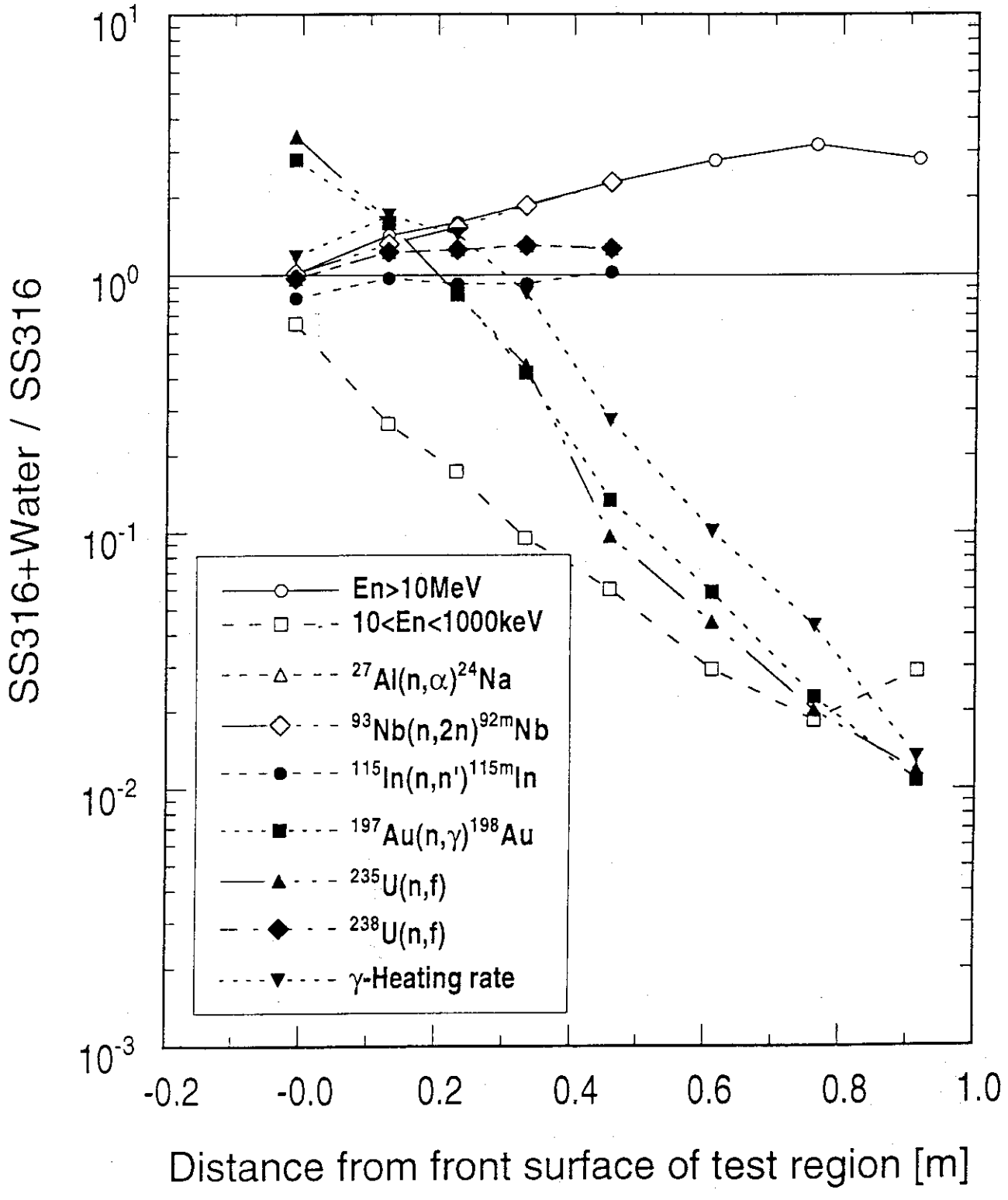

Fig. 4.1 Ratios of the integrated neutron fluxes above 10 MeV and from 10 keV to 1000 keV, reaction-rates of $^{27}Al(n,\alpha)^{24}Na$, $^{93}Nb(n,2n)^{92m}Nb$, $^{115}In(n,n')^{115m}In$ and $^{197}Au(n,\gamma)^{198}Au$, fission-rates of ^{235}U and ^{238}U, and gamma-ray heating rate in the SS316/water assembly to those in the assembly #2 of the previous SS316 experiments.

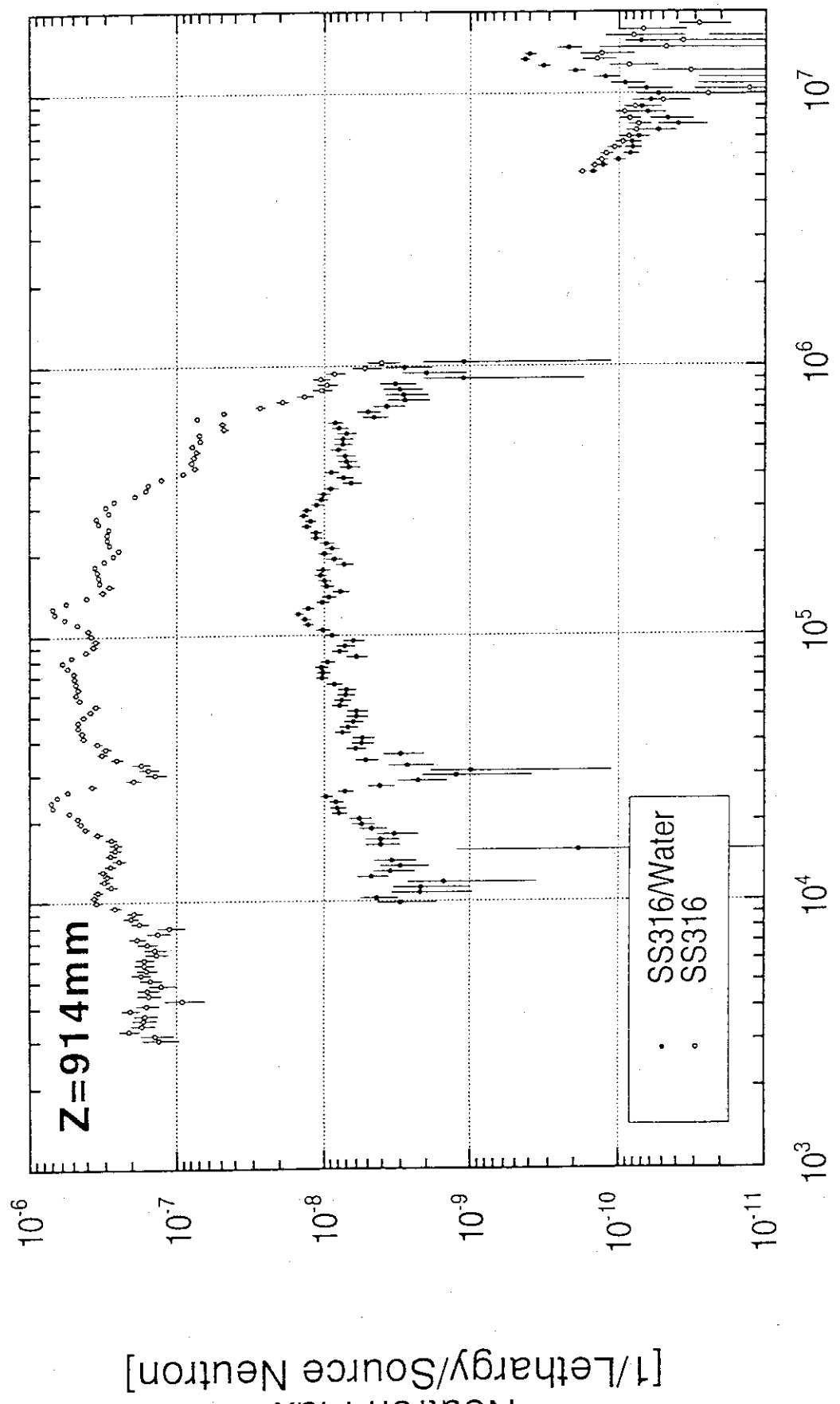

Fig. 4.2 The measured neutron spectra at 914 mm from the front surface of the test region in the SS316/water assembly and the assembly #2 of the previous SS316 experiments.

Appendix 1 Estimation of Background Neutrons with Additional Shield

The fission rate of ^{235}U was adopted for the check of the room-returned background neutrons since the most of room-returned background neutrons are expected to be less than 1 MeV and the response of ^{235}U(n,fission) has large sensitivity to the low energy neutrons. Tungsten blocks were attached on the surface of the test region to reduce the fast neutron flux reaching to the regions of interest. Figure A.1.1 shows the experimental arrangement. The ratio of the measured fission rate with the tungsten blocks to those without the tungsten blocks were shown in Table A.1.1. The ratios in the region between 400 mm and 800 mm are almost the same (the average is 0.266). If there are no background neutrons from outside, the ratio at the depth of 914 mm was also expected to be 0.266. The ratio was, however, 0.321. This means that some contribution of the background neutrons exist at 914 mm. If the fission rate by background neutrons is defined as x, the following equation should be satisfied.

$$\frac{1.030\times10^{-31}-x}{3.214\times10^{-31}-x}=0.266 \qquad \text{(A.1.1).}$$

From this equation, the fission rate x by background neutrons is calculated to be 2.385 x 10^{-32}. The fraction of the background is estimated to be 8 % at 914 mm. As for the position of 756 mm, the effect of background neutrons is considered to be negligibly small. It was concluded that the measured data at the depth of 914 mm, which are high sensitive to lower energy neutrons, might include background by about 10 %, in spite of the additional shield

Table A.1.1 Measured fission rates of ^{235}U with and without tungsten blocks.

Distance from the front surface of the test region [mm]	^{235}U(n,fission) without tungsten [1/source]	^{235}U(n,fission) with tungsten [1/source]	Ratio of ^{235}U(n,fission) with to without tungsten blocks
127	2.40E-27	1.64E-27	0.682
229	9.92E-28	3.85E-28	0.388
330	3.63E-28	1.09E-28	0.299
457	4.39E-29	1.20E-29	0.273
610	8.84E-30	2.25E-30	0.255
762	1.55E-30	4.19E-31	0.271
914	3.21E-31	1.03E-31	0.321

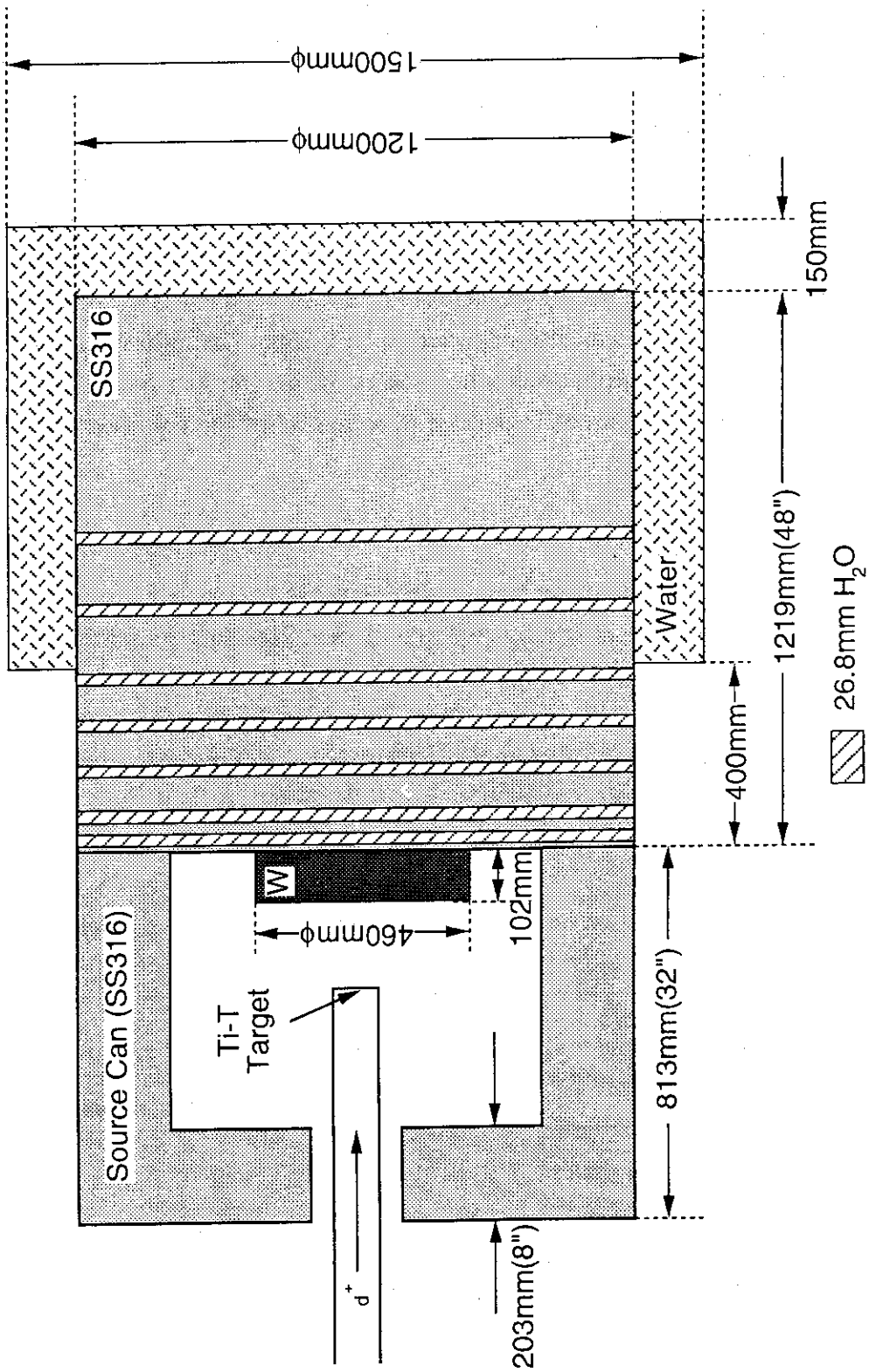

Fig. A.1.1 Experimental assembly with tungsten blocks.

Appendix 2 Influence of the Additional Shield on Neutron Flux

The additional shield of water tanks and polyethylene blocks is required in the measurement at the depths of 762 and 914 mm in order to reduce room returned background neutrons. The data from the test region surface to the depth of 610 mm have been already measured without the additional shield. The analysis of the experiment has been also completed for the assembly without the additional shield. If the additional shield dose not affect neutrons along the central axis of the test region, the measured data up to 610 mm and the results of the analysis without the additional shield are to be valid. In order to assure the validity, the effects was examined by the following procedure.

Neutron fluxes along the central axis of the test region were calculated by two-dimensional discrete ordinate code DOT3.5[12] and nuclear data library FUSION-J3 (neutron 125 groups, gamma 40 groups; Maki et al. JAERI-M 91-72). The calculation conditions are the same as those in the Volume II[9]. Figure A.2.1 shows the calculation models. The additional shield was modeled by assuming that the layer of 150 mm in thickness was filled with water. The ratios of the neutron fluxes with the additional shield to those without are shown in Fig. A.2.2. The ratios deviate from unity by only a few % at maximum at the depths shallower than 1000 mm. This figure suggests that the additional shield does not affect foreground neutrons along central axis of the test region up to the depth of 1000 mm. Thus it is concluded that the data up to 610 mm are valid without consideration of the additional shield. The additional shield and room wall are also not necessary to consider in the analysis.

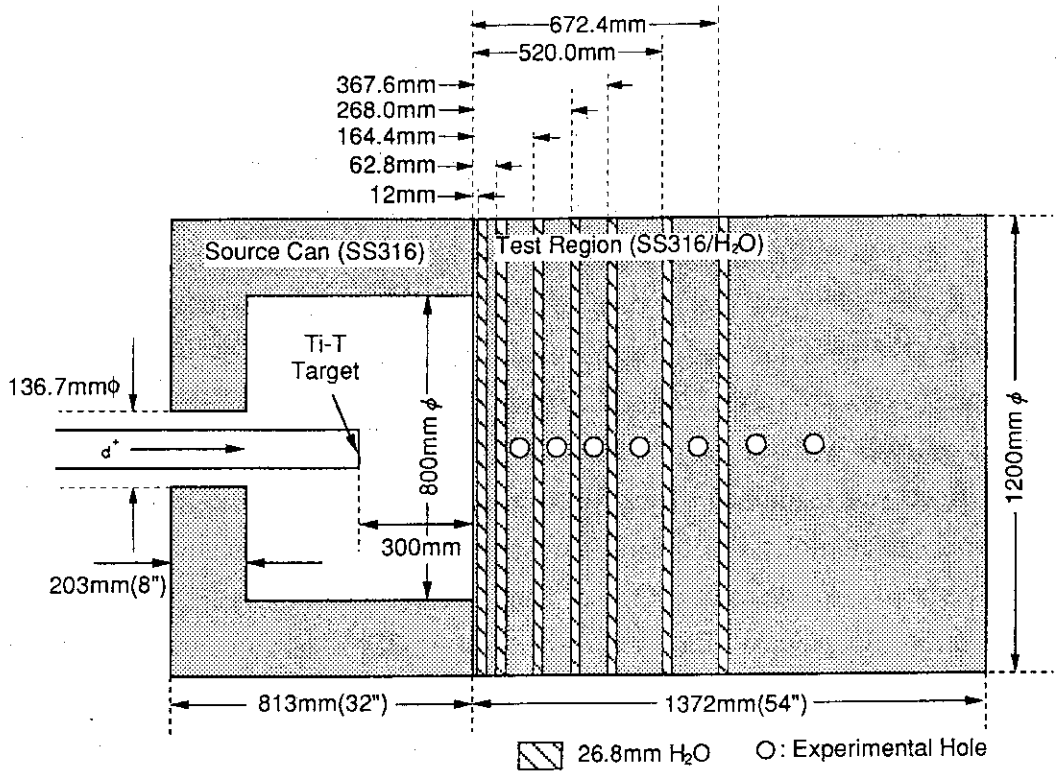

(a) Calculation Model without the additional shield

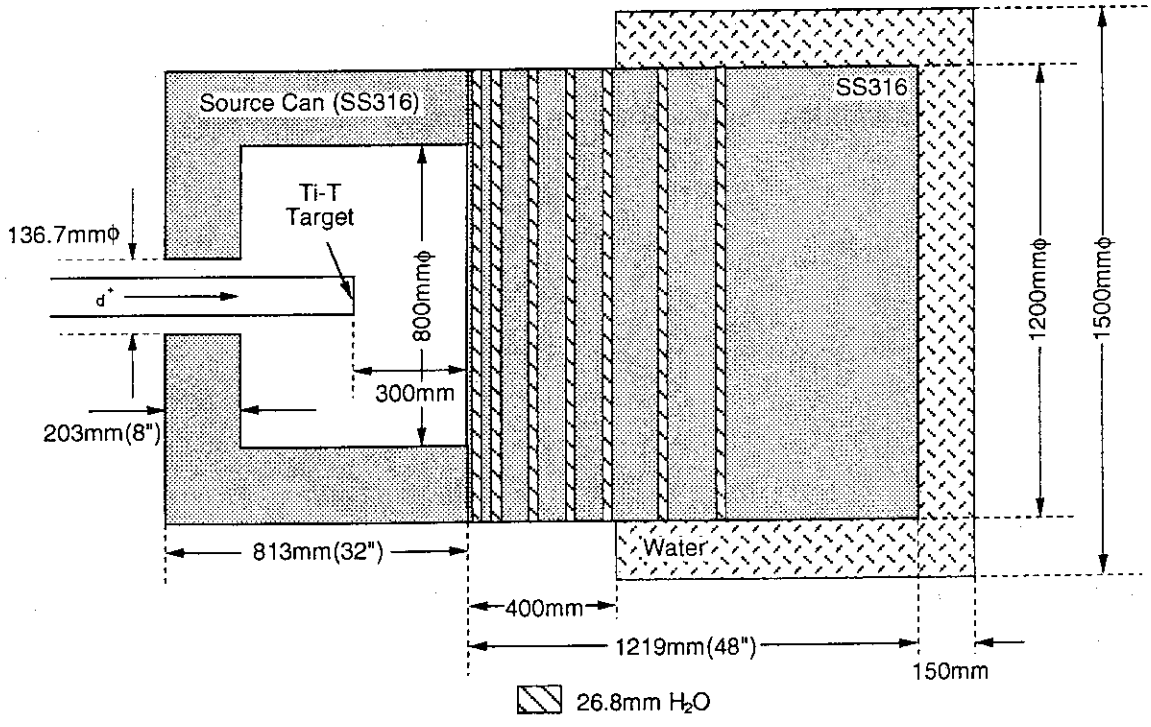

(b) Calculation Model with the additional shield

Fig. A.2.1 Calculation models with and without the additional shield.

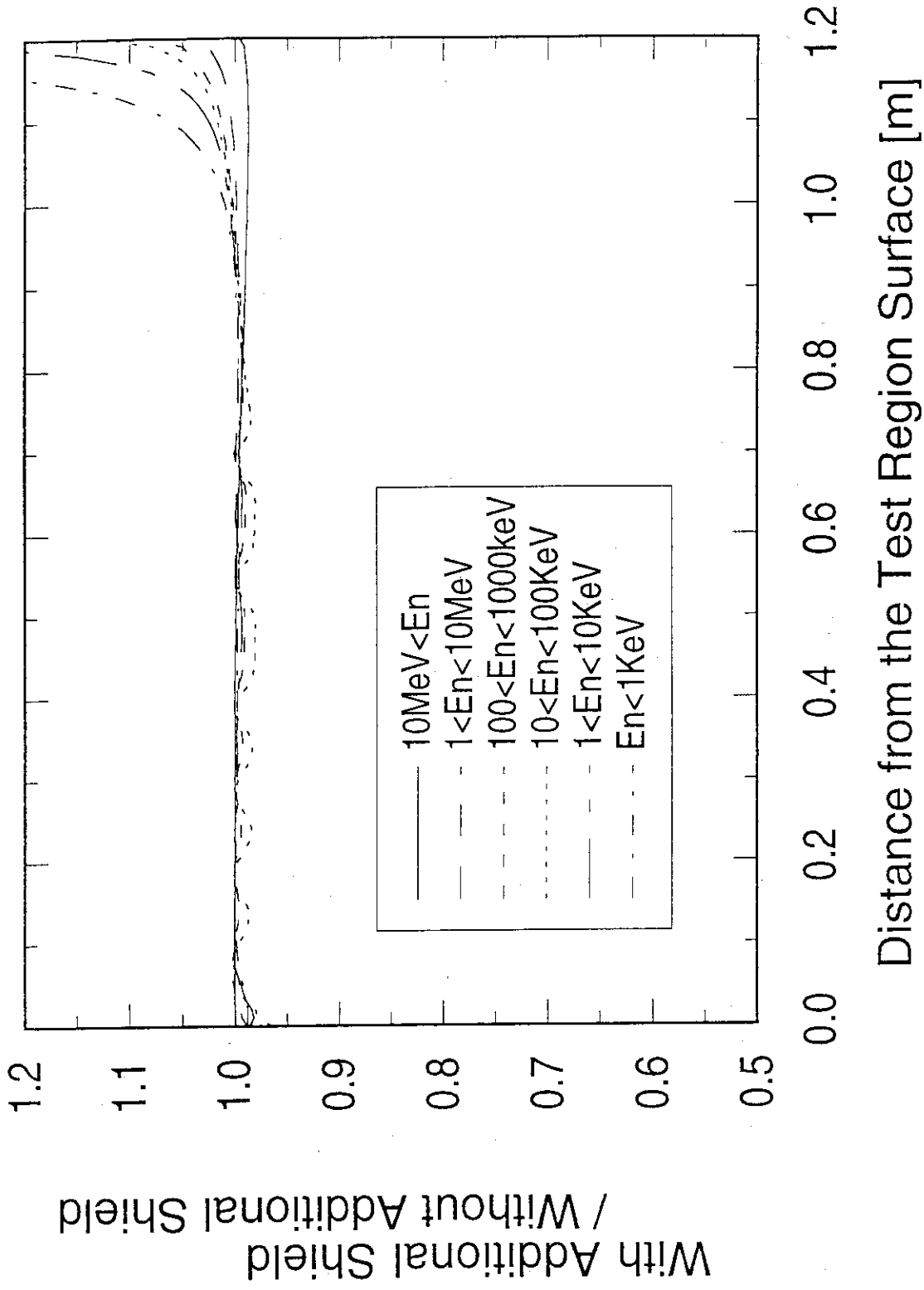

Fig. A.2.2 Ratios of the calculated integrated neutron fluxes at various energy ranges with the additional shield to those without the additional shield.